

Analyzing the role of mucin *O*-glycans in regulating microbial virulence

by

Julie S. Takagi

B.A. Molecular Cell Biology

University of California, Berkeley, 2013

SUBMITTED TO THE BIOLOGY GRADUATE PROGRAM
IN PARTIAL FULFILLMENT OF THE REQUIREMENTS FOR THE DEGREE OF

DOCTOR OF PHILOSOPHY IN BIOLOGY

AT THE

MASSACHUSETTS INSTITUTE OF TECHNOLOGY

MAY 2022

© 2022 Massachusetts Institute of Technology. All rights reserved.

Signature of Author: _____

Julie S. Takagi
Department of Biology
April 14th, 2022

Certified by: _____

Katharina Ribbeck
Professor of Biological Engineering
Thesis Supervisor

Accepted by: _____

Amy Keating
Professor of Biology and Biological Engineering
Co-Director, Biology Graduate Committee

Analyzing the role of mucin *O*-glycans in regulating microbial virulence

by

Julie S. Takagi

Submitted to the Graduate Program in Biology

on May 18th, 2022, in partial fulfillment of the requirement for the degree of
Doctor of Philosophy in Biology at the Massachusetts Institute of Technology

ABSTRACT

Mucus is the principal ecological niche for the human microbiota, acting as an interface between the trillions of microorganisms residing in the mucosal surfaces of the body and the underlying epithelial cells. Here, mucus plays a fundamental role in host defense, maintaining complex communities of microorganisms and preserving host health. Defects in the production or glycosylation of mucins, the gel-forming component of mucus, are associated with microbial dysbiosis and infection; however, owing to the complexity of mucins, an understanding of the molecular motifs and mechanisms underlying mucins' protective functions remains poorly understood. In this thesis, I fill this gap by investigating how mucins and their associated glycans influence microbial physiology in the opportunistic fungal pathogen, *Candida albicans*, and the gram-negative bacterial pathogen, *Vibrio cholerae*. First, I purify and characterize libraries of mucin-attached glycans and establish their role in influencing *C. albicans* pathogenicity, group behavior, and cross-kingdom interactions. Next, I determine the genetic mechanism of the glycan-mediated response and identify individual synthesized glycans that are sufficient for mucins' virulence attenuation. Lastly, I investigate the expression and production of virulence factors in the enteric pathogen, *V. cholerae* and demonstrate that mucin *O*-glycans, specifically Core 2-derived glycans, inhibit the major determinants of infectivity. Collectively, the work presented in my thesis provides a framework for characterizing the biochemical signals underlying mucins' protective function and provides insight for the development of novel therapeutic and diagnostic tools for treating and preventing infection.

Thesis advisor: Katharina Ribbeck

Title: Professor of Biological Engineering

Acknowledgements

First and foremost, I would like to thank my thesis advisor, Katharina Ribbeck, for her scientific mentorship, unwavering support, and invaluable insight throughout my journey. Katharina has a scientific creativity and love for mucus biology that will continue to inspire me throughout my career.

To my committee members, Graham Walker and Becky Lamason, thank you for your guidance, support, and time over the past six years. To my external committee member, Caroline Mitchell, thank you for sharing your expertise.

To the scientific mentors who helped get me to MIT: Jeremy Thorner at the University of California, Berkeley and my undergraduate mentor, Greg Finnigan, thank you for instilling a love for fungal biology and genetics. I would like to thank Sandy Johnson at the University of California, San Francisco for hiring me as a technician and for encouraging me to go to graduate school. I would also like to thank Chiraj Dalal, Matt Lohse, and Sheena Singh-Babak for mentoring me during my time in the Johnson lab.

To the Ribbeck lab: thank you for the encouragement, collaboration, and friendship. In particular I would like to thank Gerardo Cárcamo-Oyarce, Bradley Turner, Tahoura Samad, Jacob Witten, Caroline Wagner and Miri Kurpin for all the advice and help when I first joined the lab; Kelsey Wheeler, Ben Wang, and Caroline Werlang for their scientific feedback and their constant support; Aggi Walsh for helping make the lab run smoothly especially through the pandemic; to Corey Stevens, George Degen, Liubov Yakovlieva, Chloe Wu, Jade Bath, Jeff Hsiao, Michaela Gold, Abigail McShane, and Nicole Bustos for continuing to make the lab a wonderful and welcoming place.

To my MIT Biograds 2016 class: Thank you for the Halloween parties, pit parties, and ice cream trips to Toscanini's that kept me going the first year of graduate school. In particular, I would like to thank my graduate school friends from MIT and Harvard for their friendship: Grace Liu, Justin Roberts, Kwadwo Owusu-Boaiey, Byron Lee, Rachel Soble, Matt Brennan, Joshua Lam and Ted Grunberg. I would also like to thank my high school and college friends who have followed me throughout my graduate school journey: Rory Runser, Lydia Roth, Becca Clapham, Valerie Su, Varun Pemmaraju, Ben Demaree, Erin Colletta, Aisia Azus, Dennis Roth, Lauri Takasci and Emily Moore. I would like to thank the MIT Triathlon Club and MIT Cycling Club for letting me explore the Northeast via biking, running, and swimming for the past six years.

None of this would be possible without the constant love and support from my parents, and my brother, Brian. Thank you for being my safety net throughout my academic journey. I would also like to thank my newly acquired family, Luvleen, Prakash, Vidya, Prateek and Pradnya, for their encouragement.

To my wonderful husband, Vishal Patil, the best part of graduate school was having you by my side through it all. I am forever grateful for your unconditional love, enthusiasm for science, and humor which has kept me smiling these past six years.

TABLE OF CONTENTS

ABSTRACT	2
ACKNOWLEDGEMENTS	3
CHAPTER 1: INTRODUCTION	6
MUCUS BARRIER	6
KEY COMPONENTS OF MUCUS	6
MUCIN GLYCOSYLATION	8
MUCUS AND MICROBES IN HEALTH AND DISEASE	10
MECHANISM OF MUCIN-MICROBE INTERACTIONS	11
RESEARCH FOCUS AND APPROACH	16
REFERENCES	17
CHAPTER 2: MUCIN O-GLYCANS ARE NATURAL INHIBITORS OF <i>CANDIDA ALBICANS</i> PATHOGENICITY	30
ABSTRACT	30
INTRODUCTION	30
RESULTS	32
DISCUSSION	41
MATERIALS AND METHODS	44
REFERENCES	53
ACKNOWLEDGEMENTS	60
FIGURES	61
CHAPTER 3: MUCIN GLYCANS INHIBIT TOXGENIC COVERSION AND VIRULENCE FACTOR PRODUCTION IN <i>VIBRIO CHOLERA</i>E	73
ABSTRACT	73
INTRODUCTION	73
RESULTS	75
DISCUSSION	79
MATERIALS AND METHODS	81
REFERENCES	85
ACKNOWLEDGEMENTS	89

FIGURES	90
CHAPTER 4: CONCLUSIONS	97
CONCLUSIONS	97
FUTURE DIRECTIONS	97
REFERENCES	106
APPENDIX A: SUPPLEMENTARY INFORMATION FOR CHAPTER 2	111
SUPPLEMENTARY FIGURES	112
SUPPLEMENTARY TABLES	120

Chapter 1: Introduction

Mucus barrier

Mucus is a complex viscoelastic secretion that coats the epithelial surfaces of all the organs and glands that are exposed to and communicate with the external environment (Corfield, 2015). This includes the inner linings of organs of the respiratory tract, the gastrointestinal tract, the reproductive tract, and the ocular surfaces of the body (Bansil & Turner, 2018). The mucus barrier canonically functions as a lubricant to protect the underlying host tissue from mechanical and chemical damage associated with processes such as blinking and digestion (Argüeso & Gipson, 2001; Sellers et al., 1988; Taylor Nordgård & Draget, 2015) and as a selective barrier preventing foreign pathogens and harmful molecules from penetrating the mucus barrier, while permitting the passage of gases and nutrients to the underlying epithelial (Bansil & Turner, 2006; Linden et al., 2008). In addition to its protective roles, mucus serves as the major ecological niche for the microbiota accommodating vast and diverse microbial communities (Hansson, 2020; Wang, Wu, et al., 2021).

Key components of mucus

Mucus is primarily composed of water (95%) but also contains salts, lipids, phospholipids and cholesterols, and proteins that serve defensive purposes such as immunoglobulins (Creeth, 1978). However, the major structural component of mucus are mucins, a family of large, glycosylated proteins responsible for the gel-forming and viscoelastic properties of mucus (Bansil & Turner, 2018).

To date, over 21 serotypes of mucin-type glycoproteins, belonging to the MUC gene family, have been identified in the human body and vary both in terms of glycosylation as well as their amino acid sequence (Dekker et al., 2002; Lang et al., 2007; Moniaux et al., 2001). Common to each mucin are the protein backbone composed of a variable number of tandem repeats (VNTR) rich in proline, threonine, and/or serine (PTS domains), as well as cysteine-rich regions at the amino terminal, carboxy terminal, and interspersed between the PTS domains (Bansil & Turner, 2018a). The PTS domains are heavily modified with a diversity of O-linked glycan structures allowing for a large degree of heterogeneity in mucins given their variability in length and the differences in the extent and composition of glycosylation at these sites (Hollingsworth & Swanson, 2004; Perez-

Vilar & Hill, 1999). Mucin glycans are primarily composed of *N*-acetylgalactosamine (GalNAc), *N*-acetylglucosamine (GlcNAc), fucose, galactose and *N*-acetyl neuraminic acid (also known as sialic acid) arranged in linear and moderately branched structures ranging from 2-20 monosaccharides in length assembled on a core serine- or threonine-bound GalNAc (Corfield, 2015; Jin et al., 2017). These mucin-attached glycans extend out radially from the protein backbone leading to a brush polymer architecture, which protects mucins from degradation as well conferring its hydrating properties (Bergstrom & Xia, 2013; Werlang et al., 2019). Mucin glycans are crucial for the structural and functional properties of mucus and have been increasingly appreciated as important regulators in microbial community composition and human health (Belzer, 2022; Bergstrom & Xia, 2013; Hooper & Gordon, 2001).

Broadly, within the mucus family, there are two distinct sub-groups: tethered membrane-bound mucins and secreted mucins (Moniaux et al., 2001). The 11 tethered, or cell-surface, mucins that have been identified so far (MUC1, MUC3A, MUC3B, MUC4, MUC 12, MUC13, MUC15, MUC16, MUC17, MUC20, and MUC21) are typically monomeric and share a short unstructured C-terminal cytoplasmic tail that resides inside of the cell, a transmembrane domain, and an extensive extracellular domain (Bafna et al., 2010; Pelaseyed & Hansson, 2020). Cell-surface mucins are essential contributors of the glycocalyx playing a crucial role in regulating intracellular signaling pathways, facilitating cell adhesion, and immune recognition (Bafna et al., 2010; Carraway et al., 2003). Within the secreted mucins, there exist five oligomeric, gel-forming mucins (MUC2, MUC5AC, MUC5B, MUC6, and MUC19) as well as four nonpolymeric glycoproteins (Hollingsworth & Swanson, 2004; Perez-Vilar & Hill, 1999). Gel-forming mucins, which are entirely extracellular, are extraordinarily long possessing over 5,000 amino acids organized into different domains with varied post-translational modifications, thus they are extremely diverse and complex (Perez-Vilar & Hill, 1999). Gel-forming mucins contain N-terminal and C-terminal cysteine-rich regions that are adapted to crosslink to form an oligomeric mucin gel network (Bansil & Turner, 2018; J. P. Celli et al., 2007; Javitt et al., 2020; Wagner et al., 2018b). Additionally, these long chains can entangle, aggregate, and engage in reversible crosslinking interactions establishing a dynamic mucin gel (Bansil & Turner, 2018; J. P. Celli et al., 2007; Godl et al., 2002). These gel-forming mucins are found throughout the body and are secreted through specialized cells in the surface epithelial known as goblet cells and mucous cells in submucosal glands

(Birchenough et al., 2015; Thornton et al., 2008). The remaining secreted, non-gel forming soluble mucins include MUC7, MUC8, MUC9 and MUC20 (Linden et al., 2008).

In this thesis, I will focus on secreted mucins that when hydrated form the mucosal gel where much of the microbiota resides. In particular, I focus on the secreted gel-forming mucins, MUC2, MUC5B, and MUC5AC which are abundantly located in the gastrointestinal, oral, and respiratory niche, in areas abundantly colonized by rich and diverse microbial communities. Here, the mucus layer provides the first line of defense against invading pathogens and forms a crucial interface between the microbiota and underlying host cells.

Mucin glycosylation

The mucin protein backbone at around 100-500 kDa, is only about 20% of the weight of mucin; the protein's heavy glycosylation brings its total molecular weight up to 0.5-2 MDa. A dense array of over two hundred unique glycan structures are grafted to the mucin backbone, delivering a wealth of biochemical information in a minimum amount of space (Bergstrom & Xia, 2013; Hooper & Gordon, 2001; Jin et. al, 2017). These regions of *O*-glycosylation clustered in the PTS domains confer both protection from proteolysis to the mucin protein core and confer unique rheological properties to mucins (Bansil & Turner, 2018; Fu et al., 2011). While the majority of the mucin-adhered glycans are *O*-glycans, mucins also possess mannose-rich *N*-linked and *C*-linked glycans in other regions of the protein (Corfield, 2015). Mucin-glycans are a promising site for interactions since they may serve as nutrient sources (Koropatkin et al., 2012; Martens et al., 2008), microbial binding sites (Chatterjee et al., 2018; Lindén et al., 2009), and/or signaling molecules, selectin-carbohydrate-mediated cell adhesion (Fukuda, 2002; Tian & Ten Hagen, 2009). Indeed, recent work has shown that defects in glycosylation lead to a breach in the mucosal barrier (Fu et al., 2011) and aberrant glycosylation patterns are associated with various pathologies, such as cancer (An et al., 2007; Barrow et al., 2013; Byrd & Bresalier, 2004; Jiang et al., 2018; Wu et al., 2009), inflammatory bowel disease (Forni et al., 2014; McGovern et al., 2010; Packey & Sartor, 2009), and ulcerative colitis (Kawashima, 2012; Larsson et al., 2011; Tobisawa et al., 2010). However, the underlying mechanism in which glycosylation alters host-microbe interactions under physiologic and pathologic conditions is still poorly understood.

The synthesis of mucin glycans is initiated with the transfer of a GalNac sugar to the hydroxyl group of serine or threonine residues catalyzed by GalNac-transferases (Brockhausen et al., 2009). In

humans, a family of up to 20 distinct polypeptide GalNAc-transferases catalyze the initial step each with unique spatiotemporal expression patterns (Ten Hagen et al., 2003). This GalNAc, in O-linkage to serine or threonine amino acids of the mucin protein backbone, forms the Tn antigen, provides a foundation upon which a set of structurally distinct glycan core types are built (Brockhausen et al., 2009). There are four common O-GalNAc glycan core structures, designated Core 1-8. Core 1-4 are most prevalent in mucins, while Core 5 through 8 occur in extremely restricted conditions (Brockhausen et al., 2009). The Core 1 structure is formed by the addition of the monosaccharide galactose (Gal) in a β 1–3 linkage to an O-linked GalNAc, while the addition of *N*-acetylglucosamine (GlcNAc) in a β 1–3 linkage forms the Core 3 structure. The Core 2 structure occurs upon addition of *N*-acetylglucosamine β 1–6 linkage to an O-linked GalNAc of an unmodified Core 1 structure. These core structures can be further processed to form longer, more complex glycan structures depending on the repertoire of glycosyltransferases expressed in the tissue and species of origin (Corfield, 2015). Common glycan structural features include poly-*N*-acetylglucosamine units which are repeated linear GlcNAc β 1-3Gal β 1-4 sequences that represent the little I antigen, GalNAc β 1-4GlcNAc- (LacdiNAc) and Gal β 1-3GlcNAc- sequences (Cheng & Radhakrishnan, 2011). These units can provide a scaffold for the attachment of additional sugars or functional groups, such as the ABO and other glycan-based blood groups (Corfield, 2015). Sialic acid, fucose, and sulfate are common terminal structures in mucins and are frequently antigenic or represent recognition sites for lectins (Baos et al., 2012; Pinzón Martín et al., 2019). In particular, the sialylated and sulfated Lewis antigens are ligands for selectins (Ley & Kansas, 2004; McEver et al., 1995; Mitoma et al., 2003). Overall, mucin O-glycans are often very heterogeneous, with hundreds of different chains being built providing incredible combinatorial complexity. The tremendous structural heterogeneity shared among mucin glycans suggests that these complex sugars may play multifunctional roles in biological processes.

The dynamic structure of mucin gels lends itself to a diverse array of functions and interactions. The human body produces over a liter of mucus per day and in performing its various functions, mucins are constantly being synthesized, secreted, shed, and cleared (Leal et al., 2017). Upon secretion, mucins form a viscoelastic gel that varies in thickness, viscoelasticity, and composition to perform various protective functions throughout the body (Bansil & Turner, 2006). Mucin gel networks are highly sensitive to changes in pH and to the concentrations of various ions, which can greatly alter their biophysical properties (J. P. Celli et al., 2007). For example, in the eye, at

around neutral pH, a thin layer of viscous mucus provides lubrication and hydration at the ocular surface; meanwhile in the stomach, which is at low pH, mucus forms a stiffer, thicker gel that likely prevents degradation of the epithelial lining of the stomach from its highly acidic gastric juices (Argüeso & Gipson, 2001; Bansil & Turner, 2006; Hansson, 2019). Mucin biosynthesis, glycosylation, and secretion is modulated by various signals, such as microbe-derived factors, inflammatory markers, and neurotransmitters, implying dynamic feedback mechanisms between the host immune system and microbiota that directly influence mucin composition (Bäckhed et al., 2005; Brown et al., 2019; McGuckin et al., 2011; Thai et al., 2008).

Mucus and microbes in health and disease

Much of the microbiome is housed in mucosal tissues where mucus serves as a protective barrier trapping foreign pathogens for ciliary clearance and as a microbial niche mediating host-microbe interaction (Wang, Wu, et al., 2021). The secreted mucus layer accommodates trillions of microbes within the human microbiota most of which reside within the gastrointestinal tract, although diverse and stable communities are also found in the oral and urogenital tract (Hansson, 2020). Many of these microorganisms are essential for human health, mediating diverse beneficial roles including aiding digestion, vitamin synthesis, and shaping the host immune system (Rowland et al., 2018). Mucus forms a habitat in which these rich communities of microorganisms can thrive and benefit within the body, providing a defense against potential invading pathogens (Lozupone et al., 2012). Additionally, mucus traps or aggregates invading bacteria for ciliary clearance contributing to its protective functions (Bansil & Turner, 2006; Linden et al., 2008). Therefore, alterations to the mucosal layer, such as dysregulation of mucin production, can lead to disease and susceptibility to opportunistic infection.

Impaired goblet cell function, synthesis dysregulation, and altered post-translational modifications of mucins lead to alterations in the properties of mucus and are associated in various pathologies across mucosal niches (Devine & McKenzie, 1992; Frenkel & Ribbeck, 2015b; König et al., 2016). Decreased mucus production can lead to a dry and unshielded epithelial barrier, which is prone to infection and microbial dysbiosis, such as in dry eye syndrome or xerostomia (dry mouth) (Chaudhury et al., 2015; Frenkel & Ribbeck, 2015; Stephens & McNamara, 2015). In the gastrointestinal tract, aberrant regulation of mucin synthesis and glycosylation can lead to a discontinuous mucus layer and altered microbiota such as those as observed in Crohn's disease

and ulcerative colitis (Hansson, 2012; Joossens et al., 2011; Larsson et al., 2011). Similar observations occur in a murine model, deletion of Muc2, the dominant mucin in the intestinal tract, in mice leads to spontaneous colonic inflammation, colorectal cancer and increased susceptibility to enteric pathogens (Van der Sluis et al., 2006). In the respiratory tract, individuals with cystic fibrosis and chronic obstructive pulmonary disease are generally more prone to infection in the lungs as ciliary clearance is obstructed from the thick, adherent mucus barrier (Hansson, 2019; Rose & Voynow, 2006). Consistent with these pathologies, Muc5b is required for mucociliary clearance and deletion of the MUC5B gene in a murine model leads to chronic bacterial lung infection and inflammation (Valque et al., 2019). In the female genital tract, cervical mucus forms a thickened plug during pregnancy leading to a strengthening in barrier function which helps prevent microbial ascension in the intrauterine cavity, a well-documented cause for preterm birth (Becher et al., 2009). Experimentally, women at high-risk for preterm birth have mucus plugs with decreased viscoelastic properties and are thus more permeable to infection highlighting the crucial structure and function of the mucus barrier (Critchfield et al., 2013; Smith-Dupont et al., 2017). Overall, loss of functionality of the mucin barrier makes the body more prone to infections and dysbiosis, underscoring the critical role mucins play in regulating microbial physiology.

Mechanism of Mucin-microbe interactions

Mucin-microbe interactions are multifaceted, with both biophysical properties and glycosylation patterns playing important roles in modulating microbial behavior and community structure (Corfield, 2015; Linden et al., 2008; Wagner et al., 2018). Here, I present three mechanisms for how the mucin gels may shape the assembly and behavior of the microbiota. Specifically, mucins impose spatial constraints via selective barrier function, provide a rich and complex nutrient source, and display a source of biochemical signals (Wang, Wu, et al., 2021).

Mucins as a biophysical and spatial barrier

Mucus is a selective barrier acting as a size exclusion barrier to regulate the transport of particles and microorganism to the underlying epithelia (Witten et al., 2018). Mucins are cross-linked both through reversible, hydrophobic interactions and disulfide bonds to form a polymer gel network with a mesh size ranging from 100-2000 nm (Goodrich et al., 2018; Lieleg & Ribbeck, 2011). For particles that are larger than the mesh size, mucus presents a steric filter that physically blocks and hinders diffusion through the gel. While generic small particles diffuse through the gel, binding

interactions with mucin components can slow down or trap particles, thus serving as a selective filter (Witten et al., 2018, 2019). Indeed, mucins display a plethora of glycan structures that mimic those of the epithelia, thus acting as a protective barrier against several microbial pathogens. For example, the bacterium *H. pylori* expresses two adhesions that bind to mucins serving to sterically block adhesion to the cell surface (Skoog et al., 2017). Additionally, mucins can prevent binding to host receptors needed for viral entry including the influenza virus (Delaveris et al., 2020; Kastner et al., 2017), the coronavirus (Wardzala et al., 2022) and cholera toxin-mediated endocytosis in *Vibrio cholerae* (Strombeck & Harrold, 1974). Thus, mucins can serve as a decoy binding molecule trapping these microorganisms or toxins within the gel for mucosal clearance and shielding them from reaching and damaging the underlying epithelium. Similarly, mucins can agglutinate pathogens for mucus clearance; submandibular sublingual mucin is able to agglutinate the oral bacteria *S. sanguinis* and *S. mutans* (Levine et al. 1978) facilitating clearance and MUC5B agglutinates the bacterial pathogen, Group B *Streptococcus* (GBS) in the cervicovaginal mucosa preventing GBS ascension and infection to the uterus (Burcham et al., 2022). By agglutinating these microbes, mucins prevent them from reaching the epithelia and the aggregation facilitates bulk removal by mucus or phagocytosis.

The mucin gel creates a complex 3D matrix that can spatially organize populations of microbes promoting niche specific differentiation in microbial communities (H.-P. Lu et al., 2014; Mark Welch et al., 2016). Moreover, mucins may also be able to affect the diffusion of chemical signals and small molecules, leading to chemical gradients with fluctuating local molecule concentrations (Chen et al., 2017; Gao et al., 2016; Karimi et al., 2014; Li et al., 2013). These chemical signals, including quorum-sensing molecules and small diffusible signaling molecules, play an important role in bacterial physiology effecting various phenotypes, such as biofilm formation, microbial competition, and the exchange of genetic material (Karimi et al., 2014; M. B. Miller & Bassler, 2001). Therefore, by defining spatial gradients of signaling factors, mucins may play an active role in influencing the communication and behavior of microorganisms.

Mucin glycoproteins support a metabolic diverse microbial community

Mucus can regulate the microbiota by serving as a nutrient source for certain microbes, especially in the oral and gastrointestinal niche (Hansson, 2020). For example, *Akkermansia muciniphila*, *Bifidobacterium bifidum*, *Streptococcus mitior*, *Bifidobacterium*

bifidum, *Bacteroides fragilis*, *Ruminococcus gnavus* and *Ruminococcus torques* are prominent species found in the oral cavity and intestinal tract, capable of cleaving complex mucin-derived glycans using a repertoire of glycosidases (Belzer, 2022; Derrien et al., 2010). These glycosidases sequentially cleave sugars off the mucin backbone into smaller oligosaccharides or monosaccharides capable for consumption (Katayama et al., 2005; Tailford et al., 2015). Given that mucins present hundreds of unique glycan structures, linkage and identity-specific glycosidases are required to effectively break down and utilize mucins, likely requiring cooperation between diverse strains of microorganism (Raimondi et al., 2021; Tailford et al., 2015). Interestingly, while some pathogens have evolved mechanisms to consume or cleave mucins for colonization, most pathogenic bacteria do not encode glycosidases capable of degrading mucins and mucin glycans, suggesting that the ability to utilize mucins as a carbon source is largely restricted to commensal microbes (Wang, Wu, et al., 2021). Cooperation and cross-feeding between different mucolytic commensal species can influence microbial composition by selecting for primary mucin degraders and their associated broader communities leading to metabolically diverse communities that prevent pathogen growth by competitive exclusion (Bradshaw et al., 2022.; Martens et al., 2008; Pruss et al., 2021; Sonnenburg et al., 2005).

Although mucins are not the preferred carbon source for many host commensals, the metabolic flexibility in utilizing both host-derived mucin glycans and dietary carbohydrates provides these commensal species with a competitive advantage during the initial colonization and during periods of dietary depletion of polysaccharides (Bergstrom & Xia, 2013). Thus, flexible foraging enables the host to support the growth of commensal microbes with different metabolic capabilities and buffers against large variations in the host diet which broadly contributes to the stability and function diversity of the microbiota. Additionally, while metabolizing these complex glycans, microbes generate short chain fatty acids (SCFAs) as common end-products to carbohydrate-fermentation (Louis & Flint, 2009, 2017). These SCFAs can be absorbed in the epithelium and used as an energy source for the host and help attenuate inflammation (Parada Venegas et al., 2019), illustrating the mutualistic relationship between the microbiota, the mucus layer, and the host.

Mucins as signaling molecules attenuating virulence in opportunistic pathogens

Despite the textbook view of mucus as a simple physical barrier, a growing body of evidence has shown that mucus provides a source of signals that can directly impact microbial physiology and behavior. Recent work has demonstrated that mucins are responsible for suppressing virulence of various cross-kingdom pathogens across mucosal surfaces, including *Streptococcus mutans* (Frenkel & Ribbeck, 2015b), *Candida albicans* (Kavanaugh et al., 2014), and *Pseudomonas aeruginosa* (Wang, Wheeler, et al., 2021; Wheeler et al., 2019).

Streptococcus mutans is a gram-positive bacteria found in the oral niche that can adhere and form biofilms on the surfaces of teeth leading to dental caries. *In vitro* work shows that saliva, particularly the mucin component present in saliva, prevents *S. mutans* biofilm formation without altering its growth. These observations suggest that mucins shift bacteria from a pathogenic biofilm state to planktonic cells (Frenkel & Ribbeck, 2015). Additionally, mucins can decrease competition between *S. mutans* and the oral commensal microbe, *Streptococcus sanguinis* demonstrating that mucins may prevent pathogen overgrowth by preventing microbial antagonism (Frenkel & Ribbeck, 2017). In the respiratory tract, *Pseudomonas aeruginosa* is a bacterial pathogen that is most well-known for causing lethal and chronic respiratory infection in patients with cystic fibrosis or mucus dysfunction. Indeed, mucins can trigger a global downregulation of virulence gene expression in *P. aeruginosa* including pathways involved in iron acquisition, biofilm formation, and type VI secretion (Wheeler et al., 2019). Additionally, mucins were found to reduce cytotoxicity *in vitro* and reduce bacterial burden *in vivo* in a porcine burn wound model, suggesting mucins may actively prevent and clear infection (Wheeler et al., 2019). *Candida albicans* is an opportunistic fungal pathogen that composes the human microbiota, asymptotically colonizing the mucosal niches in most healthy individuals (Nobile & Johnson, 2015). Breaches in the mucosal barrier can lead to *C. albicans* overgrowth and a wide range of infections, from vaginal and oral thrush to life-threatening systemic candidiasis (Ganguly & Mitchell, 2011; Pappas et al., 2018). A key feature that allows *C. albicans* to colonize diverse host environments is its morphological plasticity. One important morphological switch is that from round yeast cells to linear hyphal filaments (Sudbery, 2011). Exposure to mucins suppresses cell-penetrating hyphae and reduces biofilm formation and adhesion to polystyrene and epithelial cells, all hallmarks of infection, demonstrating that mucus is powerful host-produced substance that plays an important role in preventing *C. albicans* virulence (Kavanaugh et al., 2014).

Collectively, these results demonstrate that mucins have evolved a conserved role in regulating microbial physiology. However, owing to the complexity of mucins, the mechanisms and moieties involved in mucin-microbe interaction is still lacking. The large diversity of mucin glycans provides a plethora of potential recognition sites for microbes, which may each have a distinct signaling potential and role in regulating microbial behavior. Indeed, glycosylation patterns drive critical biological functions in host-pathogen interactions, such as bacterial adhesion, immune system activation, and viral infection (Hooper & Gordon, 2001; Sperandio et al., 2009, 2009). For example, in immune cell function, the selectin family of cell adhesion glycoproteins facilitate the trafficking of immune cells to inflamed tissue and sites of infection by recognizing sialylated, fucosylated, and sulfated glycans (Ley & Kansas, 2004; Sperandio et al., 2009). The human immunodeficiency virus exploits the use of glycans to shield the envelope protein (Env) from immune recognition (Crispin et al., 2018) and the bacterial ulcer-causing pathogen *H. pylori* binds to glycan epitopes to facilitate adhesion and colonization (Kobayashi et al., 2009).

Here, I elaborate on three possible mechanisms in which microbes may sense mucin-associated glycans. First, mucin glycans can be directly sensed by microbial receptors, such as the membrane bound histidine kinases or second messenger systems, many of which have carbohydrate binding sites (Bergstrom & Xia, 2013). Recent work has illustrated that in the respiratory pathogen, *Pseudomonas aeruginosa*, mucin glycans activate the two-component system RetS, likely binding to its carbohydrate domain, and triggering downregulation of Type VI secretion (Wang, Wu, et al., 2021). Secondly, mucin glycans may act through dedicated sugar sensing and utilization pathways by modulating metabolic environmental cues. Lastly, mucin glycans may act through sugar-binding proteins, such as adhesins, which may coordinate the expression of virulence factor production.

Given the tremendous complexity and diversity of mucin glycans, it is anticipated that mucin-glycans possess a myriad of specific and multifunctional roles in biological processes. However, investigating the role of mucin glycans on microbial/host physiology has been hindered by technical limitations due to the complexity of glycosylation. Mucin glycosylation is 1) biosynthetically complex with functional redundancies in the family of glycosyltransferase enzymes that synthesize the *O*-glycan structures, confounding single knock-out analysis (Bergstrom & Xia, 2013; Tian & Ten Hagen, 2009) 2) stochastic with the vast majority of glycan structures dictated by temporal and tissue specific expression patterns (Hang & Bertozzi, 2005)

and 3) dynamic with altered glycosylation in response to environmental factors, such as diet (David et al., 2014), resident microbiota (Arike et al., 2017), and disease state (Rose & Voynow, 2006b). A lack of methodologies capable to detect, characterize and track O-glycosylation hinders a mechanistic understanding of *in/ex vivo* mucin-microbe interactions. In this work, we utilize a method that enables isolation and characterization of mucin glycans, generating a highly innovative resource of reagents in bioengineering and chemistry. We purify mucins across major mucosal species, dissociate their glycans from the backbone, and chemically isolate the released glycans to construct a library of annotated glycans from mucins across the body.

Research focus and approach

In this thesis, I seek to understand the ways in which fungal and bacterial pathogens sense and respond to the mucus environment. In Chapter 2, I investigate the role of mucins and their associated glycans, as potent virulence-attenuating molecules in the opportunistic fungal pathogen, *Candida albicans*. I identify the molecular mechanisms and the biochemical structures that underly the glycan-signaling response using *de novo* glycan synthesis and a targeted genetic screen. In Chapter 3, I investigate the role of mucin glycans and synthetic mucin-inspired glycans on the enteric bacterial pathogen *Vibrio cholerae*. I identify glycan-mediated signaling that suppress virulence traits and the evolution of hypervirulent strains. Collectively, these results demonstrate that mucins display an abundance of host-derived regulatory molecules in the form of *O*-glycans that influence microbial behavior and host-microbe interactions. An understanding of the biochemical features underlying mucin-microbe interactions under physiologic and pathologic conditions can inform the development of novel therapeutic candidates for treating infections without disrupting the microbiota.

References

- An, G., Wei, B., Xia, B., McDaniel, J. M., Ju, T., Cummings, R. D., Braun, J., & Xia, L. (2007). Increased susceptibility to colitis and colorectal tumors in mice lacking core 3-derived O-glycans. *The Journal of Experimental Medicine*, *204*(6), 1417–1429. <https://doi.org/10.1084/jem.20061929>
- Argüeso, P., & Gipson, I. K. (2001a). Epithelial mucins of the ocular surface: Structure, biosynthesis and function. *Experimental Eye Research*, *73*(3), 281–289. <https://doi.org/10.1006/exer.2001.1045>
- Argüeso, P., & Gipson, I. K. (2001b). Epithelial mucins of the ocular surface: Structure, biosynthesis and function. *Experimental Eye Research*, *73*(3), 281–289. <https://doi.org/10.1006/exer.2001.1045>
- Arike, L., Holmén-Larsson, J., & Hansson, G. C. (2017). Intestinal Muc2 mucin O-glycosylation is affected by microbiota and regulated by differential expression of glycosyltransferases. *Glycobiology*, *27*(4), 318–328. <https://doi.org/10.1093/glycob/cww134>
- Bäckhed, F., Ley, R. E., Sonnenburg, J. L., Peterson, D. A., & Gordon, J. I. (2005). Host-Bacterial Mutualism in the Human Intestine. *Science*, *307*(5717), 1915–1920. <https://doi.org/10.1126/science.1104816>
- Bafna, S., Kaur, S., & Batra, S. K. (2010). Membrane-bound mucins: The mechanistic basis for alterations in the growth and survival of cancer cells. *Oncogene*, *29*(20), 2893–2904. <https://doi.org/10.1038/onc.2010.87>
- Bansil, R., & Turner, B. S. (2006). Mucin structure, aggregation, physiological functions and biomedical applications. *Current Opinion in Colloid & Interface Science*, *11*(2–3), 164–170. <https://doi.org/10.1016/j.cocis.2005.11.001>
- Bansil, R., & Turner, B. S. (2018). The biology of mucus: Composition, synthesis and organization. *Advanced Drug Delivery Reviews*, *124*, 3–15. <https://doi.org/10.1016/j.addr.2017.09.023>
- Baos, S. C., Phillips, D. B., Wildling, L., McMaster, T. J., & Berry, M. (2012). Distribution of Sialic Acids on Mucins and Gels: A Defense Mechanism. *Biophysical Journal*, *102*(1), 176–184. <https://doi.org/10.1016/j.bpj.2011.08.058>
- Barrow, H., Tam, B., Duckworth, C. A., Rhodes, J. M., & Yu, L.-G. (2013). Suppression of core 1 Gal-transferase is associated with reduction of TF and reciprocal increase of Tn, sialyl-

- Tn and Core 3 glycans in human colon cancer cells. *PloS One*, 8(3), e59792.
<https://doi.org/10.1371/journal.pone.0059792>
- Becher, N., Waldorf, K. A., Hein, M., & Uldbjerg, N. (2009). The cervical mucus plug: Structured review of the literature. *Acta Obstetrica et Gynecologica Scandinavica*, 88(5), 502–513. <https://doi.org/10.1080/00016340902852898>
- Belzer, C. (2022). Nutritional strategies for mucosal health: The interplay between microbes and mucin glycans. *Trends in Microbiology*, 30(1), 13–21.
<https://doi.org/10.1016/j.tim.2021.06.003>
- Bergstrom, K. S. B., & Xia, L. (2013). Mucin-type O-glycans and their roles in intestinal homeostasis. *Glycobiology*, 23(9), 1026–1037. <https://doi.org/10.1093/glycob/cwt045>
- Birchenough, G. M. H., Johansson, M. E., Gustafsson, J. K., Bergström, J. H., & Hansson, G. C. (2015). New developments in goblet cell mucus secretion and function. *Mucosal Immunology*, 8(4), 712–719. <https://doi.org/10.1038/mi.2015.32>
- Bradshaw, D. J., Homer, K. A., Marsh, P. D., & Beighton, D. Y. 1994. (n.d.). Metabolic cooperation in oral microbial communities during growth on mucin. *Microbiology*, 140(12), 3407–3412. <https://doi.org/10.1099/13500872-140-12-3407>
- Brockhausen, I., Schachter, H., & Stanley, P. (2009). O-GalNAc Glycans. In A. Varki, R. D. Cummings, J. D. Esko, H. H. Freeze, P. Stanley, C. R. Bertozzi, G. W. Hart, & M. E. Etzler (Eds.), *Essentials of Glycobiology* (2nd ed.). Cold Spring Harbor Laboratory Press.
<http://www.ncbi.nlm.nih.gov/books/NBK1896/>
- Brown, E. M., Kenny, D. J., & Xavier, R. J. (2019). Gut Microbiota Regulation of T Cells During Inflammation and Autoimmunity. *Annual Review of Immunology*, 37(1), 599–624. <https://doi.org/10.1146/annurev-immunol-042718-041841>
- Burcham, L. R., Bath, J. R., Werlang, C. A., Lyon, L. M., Liu, N., Evans, C., Ribbeck, K., & Doran, K. S. (n.d.). Role of MUC5B during Group B Streptococcal Vaginal Colonization. *MBio*, 0(0), e00039-22. <https://doi.org/10.1128/mbio.00039-22>
- Byrd, J. C., & Bresalier, R. S. (2004). Mucins and mucin binding proteins in colorectal cancer. *Cancer Metastasis Reviews*, 23(1–2), 77–99.
- Carraway, K. L., Ramsauer, V. P., Haq, B., & Carothers Carraway, C. A. (2003). Cell signaling through membrane mucins. *BioEssays*, 25(1), 66–71. <https://doi.org/10.1002/bies.10201>

- Celli, J. P., Turner, B. S., Afdhal, N. H., Ewoldt, R. H., McKinley, G. H., Bansil, R., & Erramilli, S. (2007). Rheology of gastric mucin exhibits a pH-dependent sol-gel transition. *Biomacromolecules*, *8*(5), 1580–1586. <https://doi.org/10.1021/bm0609691>
- Chatterjee, M., Pushkaran, A. C., Vasudevan, A. K., Menon, K. K. N., Biswas, R., & Mohan, C. G. (2018). Understanding the adhesion mechanism of a mucin binding domain from *Lactobacillus fermentum* and its role in enteropathogen exclusion. *International Journal of Biological Macromolecules*, *110*, 598–607. <https://doi.org/10.1016/j.ijbiomac.2017.10.107>
- Chaudhury, N. M. A., Shirlaw, P., Pramanik, R., Carpenter, G. H., & Proctor, G. B. (2015). Changes in Saliva Rheological Properties and Mucin Glycosylation in Dry Mouth. *Journal of Dental Research*, *94*(12), 1660–1667. <https://doi.org/10.1177/0022034515609070>
- Chen, J., Hanke, A., Tegetmeyer, H. E., Kattelman, I., Sharma, R., Hamann, E., Hargesheimer, T., Kraft, B., Lenk, S., Geelhoed, J. S., Hettich, R. L., & Strous, M. (2017). Impacts of chemical gradients on microbial community structure. *The ISME Journal*, *11*(4), 920–931. <https://doi.org/10.1038/ismej.2016.175>
- Cheng, P.-W., & Radhakrishnan, P. (2011). Mucin O-Glycan Branching Enzymes: Structure, Function, and Gene Regulation. *Advances in Experimental Medicine and Biology*, *705*, 465–492. https://doi.org/10.1007/978-1-4419-7877-6_25
- Corfield, A. P. (2015). Mucins: A biologically relevant glycan barrier in mucosal protection. *Biochimica et Biophysica Acta (BBA) - General Subjects*, *1850*(1), 236–252. <https://doi.org/10.1016/j.bbagen.2014.05.003>
- Creeth, J. M. (1978). Constituents of mucus and their separation. *British Medical Bulletin*, *34*(1), 17–24. <https://doi.org/10.1093/oxfordjournals.bmb.a071454>
- Crispin, M., Ward, A. B., & Wilson, I. A. (2018). Structure and Immune Recognition of the HIV Glycan Shield. *Annual Review of Biophysics*, *47*, 499–523. <https://doi.org/10.1146/annurev-biophys-060414-034156>
- Critchfield, A. S., Yao, G., Jaishankar, A., Friedlander, R. S., Lieleg, O., Doyle, P. S., McKinley, G., House, M., & Ribbeck, K. (2013). Cervical Mucus Properties Stratify Risk for Preterm Birth. *PLoS ONE*, *8*(8), e69528. <https://doi.org/10.1371/journal.pone.0069528>

- David, L. A., Maurice, C. F., Carmody, R. N., Gootenberg, D. B., Button, J. E., Wolfe, B. E., Ling, A. V., Devlin, A. S., Varma, Y., Fischbach, M. A., Biddinger, S. B., Dutton, R. J., & Turnbaugh, P. J. (2014). Diet rapidly and reproducibly alters the human gut microbiome. *Nature*, *505*(7484), 559–563. <https://doi.org/10.1038/nature12820>
- Dekker, J., Rossen, J. W. A., Büller, H. A., & Einerhand, A. W. C. (2002). The MUC family: An obituary. *Trends in Biochemical Sciences*, *27*(3), 126–131. [https://doi.org/10.1016/s0968-0004\(01\)02052-7](https://doi.org/10.1016/s0968-0004(01)02052-7)
- Delaveris, C. S., Webster, E. R., Banik, S. M., Boxer, S. G., & Bertozzi, C. R. (2020). Membrane-tethered mucin-like polypeptides sterically inhibit binding and slow fusion kinetics of influenza A virus. *Proceedings of the National Academy of Sciences*, *117*(23), 12643–12650. <https://doi.org/10.1073/pnas.1921962117>
- Derrien, M., van Passel, M. W. J., van de Bovenkamp, J. H. B., Schipper, R., de Vos, W., & Dekker, J. (2010). Mucin-bacterial interactions in the human oral cavity and digestive tract. *Gut Microbes*, *1*(4), 254–268. <https://doi.org/10.4161/gmic.1.4.12778>
- Devine, P. L., & McKenzie, I. F. C. (1992). Mucins: Structure, function, and associations with malignancy. *BioEssays*, *14*(9), 619–625. <https://doi.org/10.1002/bies.950140909>
- Forni, D., Cleynen, I., Ferrante, M., Cassinotti, A., Cagliani, R., Ardizzone, S., Vermeire, S., Fichera, M., Lombardini, M., Maconi, G., de Franchis, R., Asselta, R., Biasin, M., Clerici, M., & Sironi, M. (2014). ABO histo-blood group might modulate predisposition to Crohn's disease and affect disease behavior. *Journal of Crohn's & Colitis*, *8*(6), 489–494. <https://doi.org/10.1016/j.crohns.2013.10.014>
- Frenkel, E. S., & Ribbeck, K. (2015). Salivary Mucins Protect Surfaces from Colonization by Cariogenic Bacteria. *Applied and Environmental Microbiology*, *81*(1), 332–338. <https://doi.org/10.1128/AEM.02573-14>
- Frenkel, E. S., & Ribbeck, K. (2017). Salivary mucins promote the coexistence of competing oral bacterial species. *The ISME Journal*, *11*(5), 1286–1290. <https://doi.org/10.1038/ismej.2016.200>
- Fu, J., Wei, B., Wen, T., Johansson, M. E. V., Liu, X., Bradford, E., Thomsson, K. A., McGee, S., Mansour, L., Tong, M., McDaniel, J. M., Sferra, T. J., Turner, J. R., Chen, H., Hansson, G. C., Braun, J., & Xia, L. (2011). Loss of intestinal core 1–derived O-glycans

- causes spontaneous colitis in mice. *The Journal of Clinical Investigation*, 121(4), 1657–1666. <https://doi.org/10.1172/JCI45538>
- Fukuda, M. (2002). Roles of mucin-type O-glycans in cell adhesion. *Biochimica et Biophysica Acta (BBA) - General Subjects*, 1573(3), 394–405. [https://doi.org/10.1016/S0304-4165\(02\)00409-9](https://doi.org/10.1016/S0304-4165(02)00409-9)
- Ganguly, S., & Mitchell, A. P. (2011). Mucosal biofilms of *Candida albicans*. *Current Opinion in Microbiology*, 14(4), 380–385. <https://doi.org/10.1016/j.mib.2011.06.001>
- Gao, M., Zheng, H., Ren, Y., Lou, R., Wu, F., Yu, W., Liu, X., & Ma, X. (2016). A crucial role for spatial distribution in bacterial quorum sensing. *Scientific Reports*, 6(1), 34695. <https://doi.org/10.1038/srep34695>
- Godl, K., Johansson, M. E. V., Lidell, M. E., Mörgelin, M., Karlsson, H., Olson, F. J., Gum, J. R., Kim, Y. S., & Hansson, G. C. (2002). The N terminus of the MUC2 mucin forms trimers that are held together within a trypsin-resistant core fragment. *The Journal of Biological Chemistry*, 277(49), 47248–47256. <https://doi.org/10.1074/jbc.M208483200>
- Goodrich, C. P., Brenner, M. P., & Ribbeck, K. (2018). Enhanced diffusion by binding to the crosslinks of a polymer gel. *Nature Communications*, 9(1), 4348. <https://doi.org/10.1038/s41467-018-06851-5>
- Hang, H. C., & Bertozzi, C. R. (2005). The chemistry and biology of mucin-type O-linked glycosylation. *Bioorganic & Medicinal Chemistry*, 13(17), 5021–5034. <https://doi.org/10.1016/j.bmc.2005.04.085>
- Hansson, G. C. (2012). Role of mucus layers in gut infection and inflammation. *Current Opinion in Microbiology*, 15(1), 57–62. <https://doi.org/10.1016/j.mib.2011.11.002>
- Hansson, G. C. (2019). Mucus and mucins in diseases of the intestinal and respiratory tracts. *Journal of Internal Medicine*, 285(5), 479–490. <https://doi.org/10.1111/joim.12910>
- Hansson, G. C. (2020). Mucins and the Microbiome. *Annual Review of Biochemistry*, 89(1), 769–793. <https://doi.org/10.1146/annurev-biochem-011520-105053>
- Hollingsworth, M. A., & Swanson, B. J. (2004). Mucins in cancer: Protection and control of the cell surface. *Nature Reviews. Cancer*, 4(1), 45–60. <https://doi.org/10.1038/nrc1251>
- Hooper, L. V., & Gordon, J. I. (2001). Glycans as legislators of host–microbial interactions: Spanning the spectrum from symbiosis to pathogenicity. *Glycobiology*, 11(2), 1R–10R. <https://doi.org/10.1093/glycob/11.2.1R>

- Javitt, G., Khmelnsky, L., Albert, L., Bigman, L. S., Elad, N., Morgenstern, D., Ilani, T., Levy, Y., Diskin, R., & Fass, D. (2020). Assembly Mechanism of Mucin and von Willebrand Factor Polymers. *Cell*, *183*(3), 717-729.e16. <https://doi.org/10.1016/j.cell.2020.09.021>
- Jiang, Y., Liu, Z., Xu, F., Dong, X., Cheng, Y., Hu, Y., Gao, T., Liu, J., Yang, L., Jia, X., Qian, H., Wen, T., & An, G. (2018). Aberrant O-glycosylation contributes to tumorigenesis in human colorectal cancer. *Journal of Cellular and Molecular Medicine*, *22*(10), 4875–4885. <https://doi.org/10.1111/jcmm.13752>
- Jin, C., Kenny, D. T., Skoog, E. C., Padra, M., Adamczyk, B., Vitizeva, V., Thorell, A., Venkatakrishnan, V., Lindén, S. K., & Karlsson, N. G. (2017). Structural Diversity of Human Gastric Mucin Glycans. *Molecular & Cellular Proteomics*, *16*(5), 743–758. <https://doi.org/10.1074/mcp.M117.067983>
- Joossens, M., Huys, G., Cnockaert, M., De Preter, V., Verbeke, K., Rutgeerts, P., Vandamme, P., & Vermeire, S. (2011). Dysbiosis of the faecal microbiota in patients with Crohn's disease and their unaffected relatives. *Gut*, *60*(5), 631–637. <https://doi.org/10.1136/gut.2010.223263>
- Karimi, A., Karig, D., Kumar, A., & Ardekani, A. M. (2014). Interplay of physical mechanisms and biofilm processes: Review of microfluidic methods. *Lab on a Chip*, *15*(1), 23–42. <https://doi.org/10.1039/C4LC01095G>
- Kastner, M., Karner, A., Zhu, R., Huang, Q., Zhang, D., Liu, J., Geissner, A., Sadewasser, A., Lesch, M., Wörmann, X., Karlas, A., Seeberger, P., Wolff, T., Hinterdorfer, P., Herrmann, A., & Sieben, C. (2017). *Relevance of host cell surface glycan structure for cell specificity of influenza A virus* [Preprint]. Microbiology. <https://doi.org/10.1101/203349>
- Katayama, T., Fujita, K., & Yamamoto, K. (2005). Novel bifidobacterial glycosidases acting on sugar chains of mucin glycoproteins. *Journal of Bioscience and Bioengineering*, *99*(5), 457–465. <https://doi.org/10.1263/jbb.99.457>
- Kavanaugh, N. L., Zhang, A. Q., Nobile, C. J., Johnson, A. D., & Ribbeck, K. (2014). Mucins Suppress Virulence Traits of *Candida albicans*. *MBio*, *5*(6), e01911-14. <https://doi.org/10.1128/mBio.01911-14>

- Kawashima, H. (2012). Roles of the gel-forming MUC2 mucin and its O-glycosylation in the protection against colitis and colorectal cancer. *Biological & Pharmaceutical Bulletin*, 35(10), 1637–1641.
- Kobayashi, M., Lee, H., Nakayama, J., & Fukuda, M. (2009). Roles of gastric mucin-type O-glycans in the pathogenesis of *Helicobacter pylori* infection. *Glycobiology*, 19(5), 453–461. <https://doi.org/10.1093/glycob/cwp004>
- König, J., Wells, J., Cani, P. D., García-Ródenas, C. L., MacDonald, T., Mercenier, A., Whyte, J., Troost, F., & Brummer, R.-J. (2016). Human Intestinal Barrier Function in Health and Disease. *Clinical and Translational Gastroenterology*, 7(10), e196. <https://doi.org/10.1038/ctg.2016.54>
- Koropatkin, N. M., Cameron, E. A., & Martens, E. C. (2012). How glycan metabolism shapes the human gut microbiota. *Nature Reviews. Microbiology*, 10(5), 323–335. <https://doi.org/10.1038/nrmicro2746>
- Lang, T., Hansson, G. C., & Samuelsson, T. (2007). Gel-forming mucins appeared early in metazoan evolution. *Proceedings of the National Academy of Sciences*, 104(41), 16209–16214. <https://doi.org/10.1073/pnas.0705984104>
- Larsson, J. M. H., Karlsson, H., Crespo, J. G., Johansson, M. E. V., Eklund, L., Sjövall, H., & Hansson, G. C. (2011). Altered O-glycosylation profile of MUC2 mucin occurs in active ulcerative colitis and is associated with increased inflammation. *Inflammatory Bowel Diseases*, 17(11), 2299–2307. <https://doi.org/10.1002/ibd.21625>
- Leal, J., Smyth, H. D. C., & Ghosh, D. (2017). Physicochemical properties of mucus and their impact on transmucosal drug delivery. *International Journal of Pharmaceutics*, 532(1), 555–572. <https://doi.org/10.1016/j.ijpharm.2017.09.018>
- Ley, K., & Kansas, G. S. (2004). Selectins in T-cell recruitment to non-lymphoid tissues and sites of inflammation. *Nature Reviews Immunology*, 4(5), 325–336. <https://doi.org/10.1038/nri1351>
- Li, L. D., Crouzier, T., Sarkar, A., Dunphy, L., Han, J., & Ribbeck, K. (2013). Spatial configuration and composition of charge modulates transport into a mucin hydrogel barrier. *Biophysical Journal*, 105(6), 1357–1365. <https://doi.org/10.1016/j.bpj.2013.07.050>

- Lieleg, O., & Ribbeck, K. (2011). Biological hydrogels as selective diffusion barriers. *Trends in Cell Biology*, 21(9), 543–551. <https://doi.org/10.1016/j.tcb.2011.06.002>
- Lindén, S. K., Sheng, Y. H., Every, A. L., Miles, K. M., Skoog, E. C., Florin, T. H. J., Sutton, P., & McGuckin, M. A. (2009). MUC1 limits *Helicobacter pylori* infection both by steric hindrance and by acting as a releasable decoy. *PLoS Pathogens*, 5(10), e1000617. <https://doi.org/10.1371/journal.ppat.1000617>
- Linden, S. K., Sutton, P., Karlsson, N. G., Korolik, V., & McGuckin, M. A. (2008). Mucins in the mucosal barrier to infection. *Mucosal Immunology*, 1(3), 183–197. <https://doi.org/10.1038/mi.2008.5>
- Louis, P., & Flint, H. J. (2009). Diversity, metabolism and microbial ecology of butyrate-producing bacteria from the human large intestine. *FEMS Microbiology Letters*, 294(1), 1–8. <https://doi.org/10.1111/j.1574-6968.2009.01514.x>
- Louis, P., & Flint, H. J. (2017). Formation of propionate and butyrate by the human colonic microbiota. *Environmental Microbiology*, 19(1), 29–41. <https://doi.org/10.1111/1462-2920.13589>
- Lozupone, C. A., Stombaugh, J. I., Gordon, J. I., Jansson, J. K., & Knight, R. (2012). Diversity, stability and resilience of the human gut microbiota. *Nature*, 489(7415), 220–230. <https://doi.org/10.1038/nature11550>
- Lu, H.-P., Lai, Y.-C., Huang, S.-W., Chen, H.-C., Hsieh, C., & Yu, H.-T. (2014). Spatial heterogeneity of gut microbiota reveals multiple bacterial communities with distinct characteristics. *Scientific Reports*, 4(1), 6185. <https://doi.org/10.1038/srep06185>
- Mark Welch, J. L., Rossetti, B. J., Rieken, C. W., Dewhirst, F. E., & Borisy, G. G. (2016). Biogeography of a human oral microbiome at the micron scale. *Proceedings of the National Academy of Sciences of the United States of America*, 113(6), E791-800. <https://doi.org/10.1073/pnas.1522149113>
- Martens, E. C., Chiang, H. C., & Gordon, J. I. (2008). Mucosal Glycan Foraging Enhances Fitness and Transmission of a Saccharolytic Human Gut Bacterial Symbiont. *Cell Host & Microbe*, 4(5), 447–457. <https://doi.org/10.1016/j.chom.2008.09.007>
- McEver, R. P., Moore, K. L., & Cummings, R. D. (1995). Leukocyte trafficking mediated by selectin-carbohydrate interactions. *The Journal of Biological Chemistry*, 270(19), 11025–11028. <https://doi.org/10.1074/jbc.270.19.11025>

- McGovern, D. P. B., Jones, M. R., Taylor, K. D., Marciante, K., Yan, X., Dubinsky, M., Ippoliti, A., Vasiliauskas, E., Berel, D., Derkowski, C., Dutridge, D., Fleshner, P., Shih, D. Q., Melmed, G., Mengesha, E., King, L., Pressman, S., Haritunians, T., Guo, X., ... International IBD Genetics Consortium. (2010). Fucosyltransferase 2 (FUT2) non-secretor status is associated with Crohn's disease. *Human Molecular Genetics*, *19*(17), 3468–3476. <https://doi.org/10.1093/hmg/ddq248>
- McGuckin, M. A., Lindén, S. K., Sutton, P., & Florin, T. H. (2011). Mucin dynamics and enteric pathogens. *Nature Reviews Microbiology*, *9*(4), 265–278. <https://doi.org/10.1038/nrmicro2538>
- Miller, M. B., & Bassler, B. L. (2001). Quorum Sensing in Bacteria. *Annual Review of Microbiology*, *55*(1), 165–199. <https://doi.org/10.1146/annurev.micro.55.1.165>
- Mitoma, J., Petryniak, B., Hiraoka, N., Yeh, J.-C., Lowe, J. B., & Fukuda, M. (2003). Extended core 1 and core 2 branched O-glycans differentially modulate sialyl Lewis X-type L-selectin ligand activity. *The Journal of Biological Chemistry*, *278*(11), 9953–9961. <https://doi.org/10.1074/jbc.M212756200>
- Moniaux, N., Escande, F., Porchet, N., Aubert, J. P., & Batra, S. K. (2001). Structural organization and classification of the human mucin genes. *Frontiers in Bioscience: A Journal and Virtual Library*, *6*, D1192-1206. <https://doi.org/10.2741/moniaux>
- Nobile, C. J., & Johnson, A. D. (2015). *Candida albicans* Biofilms and Human Disease. *Annual Review of Microbiology*, *69*, 71–92. <https://doi.org/10.1146/annurev-micro-091014-104330>
- Packey, C. D., & Sartor, R. B. (2009). Commensal bacteria, traditional and opportunistic pathogens, dysbiosis and bacterial killing in inflammatory bowel diseases. *Current Opinion in Infectious Diseases*, *22*(3), 292–301. <https://doi.org/10.1097/QCO.0b013e32832a8a5d>
- Pappas, P. G., Lionakis, M. S., Arendrup, M. C., Ostrosky-Zeichner, L., & Kullberg, B. J. (2018). Invasive candidiasis. *Nature Reviews Disease Primers*, *4*(1), 1–20. <https://doi.org/10.1038/nrdp.2018.26>
- Parada Venegas, D., De la Fuente, M. K., Landskron, G., González, M. J., Quera, R., Dijkstra, G., Harmsen, H. J. M., Faber, K. N., & Hermoso, M. A. (2019). Short Chain Fatty Acids (SCFAs)-Mediated Gut Epithelial and Immune Regulation and Its Relevance for

- Inflammatory Bowel Diseases. *Frontiers in Immunology*, 10.
<https://www.frontiersin.org/article/10.3389/fimmu.2019.00277>
- Pelaseyed, T., & Hansson, G. C. (2020). Membrane mucins of the intestine at a glance. *Journal of Cell Science*, 133(5), jcs240929. <https://doi.org/10.1242/jcs.240929>
- Perez-Vilar, J., & Hill, R. L. (1999). The structure and assembly of secreted mucins. *The Journal of Biological Chemistry*, 274(45), 31751–31754.
<https://doi.org/10.1074/jbc.274.45.31751>
- Pinzón Martín, S., Seeberger, P. H., & Varón Silva, D. (2019). Mucins and Pathogenic Mucin-Like Molecules Are Immunomodulators During Infection and Targets for Diagnostics and Vaccines. *Frontiers in Chemistry*, 7.
<https://www.frontiersin.org/article/10.3389/fchem.2019.00710>
- Pruss, K. M., Marcobal, A., Southwick, A. M., Dahan, D., Smits, S. A., Ferreyra, J. A., Higginbottom, S. K., Sonnenburg, E. D., Kashyap, P. C., Choudhury, B., Bode, L., & Sonnenburg, J. L. (2021). Mucin-derived O-glycans supplemented to diet mitigate diverse microbiota perturbations. *The ISME Journal*, 15(2), 577–591.
<https://doi.org/10.1038/s41396-020-00798-6>
- Raimondi, S., Musmeci, E., Candelieri, F., Amaretti, A., & Rossi, M. (2021). Identification of mucin degraders of the human gut microbiota. *Scientific Reports*, 11(1), 11094.
<https://doi.org/10.1038/s41598-021-90553-4>
- Rose, M. C., & Voynow, J. A. (2006). Respiratory Tract Mucin Genes and Mucin Glycoproteins in Health and Disease. *Physiological Reviews*, 86(1), 245–278.
<https://doi.org/10.1152/physrev.00010.2005>
- Rowland, I., Gibson, G., Heinken, A., Scott, K., Swann, J., Thiele, I., & Tuohy, K. (2018). Gut microbiota functions: Metabolism of nutrients and other food components. *European Journal of Nutrition*, 57(1), 1–24. <https://doi.org/10.1007/s00394-017-1445-8>
- Sellers, L. A., Allen, A., Morris, E. R., & Ross-Murphy, S. B. (1988). Mucus glycoprotein gels. Role of glycoprotein polymeric structure and carbohydrate side-chains in gel-formation. *Carbohydrate Research*, 178(1), 93–110. [https://doi.org/10.1016/0008-6215\(88\)80104-6](https://doi.org/10.1016/0008-6215(88)80104-6)
- Skoog, E. C., Padra, M., Åberg, A., Gideonsson, P., Obi, I., Quintana-Hayashi, M. P., Arnqvist, A., & Lindén, S. K. (2017). BabA dependent binding of *Helicobacter pylori* to human

- gastric mucins cause aggregation that inhibits proliferation and is regulated via ArsS. *Scientific Reports*, 7(1), 40656. <https://doi.org/10.1038/srep40656>
- Smith-Dupont, K. B., Wagner, C. E., Witten, J., Conroy, K., Rudoltz, H., Pagidas, K., Snegovskikh, V., House, M., & Ribbeck, K. (2017). Probing the potential of mucus permeability to signify preterm birth risk. *Scientific Reports*, 7(1), 10302. <https://doi.org/10.1038/s41598-017-08057-z>
- Sonnenburg, J. L., Xu, J., Leip, D. D., Chen, C.-H., Westover, B. P., Weatherford, J., Buhler, J. D., & Gordon, J. I. (2005). Glycan Foraging in Vivo by an Intestine-Adapted Bacterial Symbiont. *Science*, 307(5717), 1955–1959. <https://doi.org/10.1126/science.1109051>
- Sperandio, M., Gleissner, C. A., & Ley, K. (2009). Glycosylation in immune cell trafficking. *Immunological Reviews*, 230(1), 97–113. <https://doi.org/10.1111/j.1600-065X.2009.00795.x>
- Stephens, D. N., & McNamara, N. A. (2015). Altered Mucin and Glycoprotein Expression in Dry Eye Disease. *Optometry and Vision Science: Official Publication of the American Academy of Optometry*, 92(9), 931–938. <https://doi.org/10.1097/OPX.0000000000000664>
- Strombeck, D. R., & Harrold, D. (1974). Binding of Cholera Toxin to Mucins and Inhibition by Gastric Mucin. *Infection and Immunity*, 10(6), 1266–1272.
- Sudbery, P. E. (2011). Growth of *Candida albicans* hyphae. *Nature Reviews Microbiology*, 9(10), 737–748. <https://doi.org/10.1038/nrmicro2636>
- Tailford, L. E., Crost, E. H., Kavanaugh, D., & Juge, N. (2015). Mucin glycan foraging in the human gut microbiome. *Frontiers in Genetics*, 6. <https://doi.org/10.3389/fgene.2015.00081>
- Taylor Nordgård, C., & Draget, K. I. (2015). Dynamic responses in small intestinal mucus: Relevance for the maintenance of an intact barrier. *European Journal of Pharmaceutics and Biopharmaceutics: Official Journal of Arbeitsgemeinschaft Fur Pharmazeutische Verfahrenstechnik e.V.*, 95(Pt A), 144–150. <https://doi.org/10.1016/j.ejpb.2015.01.024>
- Ten Hagen, K. G., Fritz, T. A., & Tabak, L. A. (2003). All in the family: The UDP-GalNAc:polypeptide N-acetylgalactosaminyltransferases. *Glycobiology*, 13(1), 1R-16R. <https://doi.org/10.1093/glycob/cwg007>

- Thai, P., Loukoianov, A., Wachi, S., & Wu, R. (2008). Regulation of Airway Mucin Gene Expression. *Annual Review of Physiology*, 70(1), 405–429. <https://doi.org/10.1146/annurev.physiol.70.113006.100441>
- Thornton, D. J., Rousseau, K., & McGuckin, M. A. (2008). Structure and Function of the Polymeric Mucins in Airways Mucus. *Annual Review of Physiology*, 70(1), 459–486. <https://doi.org/10.1146/annurev.physiol.70.113006.100702>
- Tian, E., & Ten Hagen, K. G. (2009). Recent insights into the biological roles of mucin-type O-glycosylation. *Glycoconjugate Journal*, 26(3), 325–334. <https://doi.org/10.1007/s10719-008-9162-4>
- Tobisawa, Y., Imai, Y., Fukuda, M., & Kawashima, H. (2010). Sulfation of colonic mucins by N-acetylglucosamine 6-O-sulfotransferase-2 and its protective function in experimental colitis in mice. *The Journal of Biological Chemistry*, 285(9), 6750–6760. <https://doi.org/10.1074/jbc.M109.067082>
- Valque, H., Gouyer, V., Duez, C., Leboeuf, C., Marquillies, P., Le Bert, M., Plet, S., Ryffel, B., Janin, A., Gottrand, F., & Desseyn, J.-L. (2019). Muc5b-deficient mice develop early histological lung abnormalities. *Biology Open*, 8(11), bio046359. <https://doi.org/10.1242/bio.046359>
- Van der Sluis, M., De Koning, B. A. E., De Bruijn, A. C. J. M., Velcich, A., Meijerink, J. P. P., Van Goudoever, J. B., Büller, H. A., Dekker, J., Van Seuningen, I., Renes, I. B., & Einerhand, A. W. C. (2006). Muc2-Deficient Mice Spontaneously Develop Colitis, Indicating That MUC2 Is Critical for Colonic Protection. *Gastroenterology*, 131(1), 117–129. <https://doi.org/10.1053/j.gastro.2006.04.020>
- Wagner, C. E., Wheeler, K. M., & Ribbeck, K. (2018). Mucins and Their Role in Shaping the Functions of Mucus Barriers. *Annual Review of Cell and Developmental Biology*, 34(1), 189–215. <https://doi.org/10.1146/annurev-cellbio-100617-062818>
- Wang, B. X., Wheeler, K. M., Cady, K. C., Lehoux, S., Cummings, R. D., Laub, M. T., & Ribbeck, K. (2021). Mucin Glycans Signal through the Sensor Kinase RetS to Inhibit Virulence-Associated Traits in *Pseudomonas aeruginosa*. *Current Biology*, 31(1), 90–102.e7. <https://doi.org/10.1016/j.cub.2020.09.088>

- Wang, B. X., Wu, C. M., & Ribbeck, K. (2021). Home, sweet home: How mucus accommodates our microbiota. *The FEBS Journal*, 288(6), 1789–1799. <https://doi.org/10.1111/febs.15504>
- Wardzala, C. L., Wood, A. M., Belnap, D. M., & Kramer, J. R. (2022). Mucins Inhibit Coronavirus Infection in a Glycan-Dependent Manner. *ACS Central Science*, 8(3), 351–360. <https://doi.org/10.1021/acscentsci.1c01369>
- Werlang, C., Cárcarmo-Oyarce, G., & Ribbeck, K. (2019). Engineering mucus to study and influence the microbiome. *Nature Reviews Materials*, 4(2), 134–145. <https://doi.org/10.1038/s41578-018-0079-7>
- Wheeler, K. M., Cárcamo-Oyarce, G., Turner, B. S., Dellos-Nolan, S., Co, J. Y., Lehoux, S., Cummings, R. D., Wozniak, D. J., & Ribbeck, K. (2019). Mucin glycans attenuate the virulence of *Pseudomonas aeruginosa* in infection. *Nature Microbiology*, 4(12), 2146–2154. <https://doi.org/10.1038/s41564-019-0581-8>
- Witten, J., Samad, T., & Ribbeck, K. (2018). Selective permeability of mucus barriers. *Current Opinion in Biotechnology*, 52, 124–133. <https://doi.org/10.1016/j.copbio.2018.03.010>
- Witten, J., Samad, T., & Ribbeck, K. (2019). Molecular Characterization of Mucus Binding. *Biomacromolecules*, 20(4), 1505–1513. <https://doi.org/10.1021/acs.biomac.8b01467>
- Wu, Y.-M., Nowack, D. D., Omenn, G. S., & Haab, B. B. (2009). Mucin Glycosylation Is Altered by Pro-Inflammatory Signaling in Pancreatic-Cancer Cells. *Journal of Proteome Research*, 8(4), 1876–1886. <https://doi.org/10.1021/pr8008379>

Chapter 2: Mucin *O*-glycans are natural inhibitors of *Candida albicans* pathogenicity

Work presented in this Chapter is published in:

Takagi J, Aoki K, Turner BS, Lamont S, Lehoux S, Kavanaugh N, Gulati M, Valle Arevalo A, Lawrence TJ, Kim CY, Bakshi B, Ishihara M, Nobile CJ, Cummings RD, Wozniak DJ, Tiemeyer M, Hevey R, Ribbeck K. Mucin *O*-glycans are natural inhibitors of *Candida albicans* pathogenicity. *Nature Chemical Biology*. (2022).

Supplementary information is provided in Appendix A

Abstract

Mucins are large gel-forming polymers inside the mucus barrier that inhibit the yeast to hyphal transition of *Candida albicans*, a key virulence trait of this important human fungal pathogen. However, the molecular motifs in mucins that inhibit filamentation remain unclear, despite their potential for therapeutic interventions. Here, we determined that mucins display an abundance of virulence-attenuating molecules in the form of mucin *O*-glycans. We isolated and catalogued >100 mucin *O*-glycans from three major mucosal surfaces and established that they suppress filamentation and related phenotypes relevant to infection, including surface adhesion, biofilm formation, and cross-kingdom competition between *C. albicans* and the bacterium *Pseudomonas aeruginosa*. Using synthetic *O*-glycans we identified three structures (Core 1, Core 1+fucose, and Core 2+galactose) that are sufficient to inhibit filamentation with potency comparable to the complex *O*-glycan pool. Overall, this work identifies mucin *O*-glycans as host molecules with untapped therapeutic potential to manage fungal pathogens.

Introduction

Candida albicans is an opportunistic fungal pathogen that asymptotically colonizes the mucosal surfaces of most healthy humans (Ganguly & Mitchell, 2011; Valle Arevalo & Nobile, 2020). Alterations to the mucus barrier and microbiota can lead to *C. albicans* overgrowth and infection, causing conditions such as oral thrush, vulvovaginal candidiasis, and life-threatening systemic candidiasis (Ganguly & Mitchell, 2011; Pappas et al., 2018). The scarcity of antifungal drug classes, their limited efficacy, toxicity, and the development of resistance (Perlin, 2015) contribute

to a mortality rate of ~40% in deep-seated candidiasis (Pappas et al., 2018), highlighting an urgent need for alternative treatments to fungal infections.

Targeting pathogenic mechanisms rather than growth represents an attractive approach for developing novel antimicrobial agents. The infection of diverse host niches is supported by a wide range of *C. albicans* virulence and fitness attributes, including the morphological yeast-to-hyphal transition (filamentation), adhesin expression, biofilm formation, and the secretion of hydrolytic enzymes that damage the underlying epithelium (Calderone & Fonzi, 2001). The yeast-to-hyphal transition is a major virulence factor (Calderone & Fonzi, 2001) and is integral for robust biofilms, which are intrinsically resistant to treatment, posing a significant clinical challenge (Nobile & Johnson, 2015). Strikingly, despite its potential for pathogenicity, *C. albicans* is accommodated in healthy mucus (Kennedy & Volz, 1985), suggesting that mucus may underpin novel strategies for preventing *C. albicans* virulence.

Mucus is a complex viscoelastic secretion that coats all non-keratinized epithelial surfaces in the body that are exposed to and communicate with the external environment (Corfield, 2015). Much of the microbiota is housed in the mucus layer, serving as a protective barrier and microbial niche (Corfield, 2015; Wang et al., 2021). Mucins are the main structural component of mucus and play an integral role in attenuating virulence traits in various cross-kingdom pathogens, including *C. albicans* (Kavanaugh et al., 2014; Valle Arevalo & Nobile, 2020). Mucin exposure suppresses *C. albicans* virulence phenotypes, including the formation of host-cell-penetrating hyphae (Kavanaugh et al., 2014). However, the mechanisms through which mucins attenuate virulence in *C. albicans* remain unknown, impeding their application for therapeutic intervention.

To close this gap, we characterized the mechanism and biochemical motifs of mucins that suppress *C. albicans* virulence gene expression and phenotypes. By isolating and characterizing mucin-derived glycans across major mucosal surfaces, we determined that mucin glycans repress *C. albicans* virulence traits including filamentation, adhesion, and biofilm formation and alter fungal–bacterial dynamics. We identified that specific Core-1- and Core-2-modified glycan structures within the mucin polymer suppress filamentation and downregulate filamentation-associated genes in *C. albicans*. These results elucidate the mechanisms by which healthy mucins attenuate *C. albicans* pathogenicity, suggesting therapeutic candidates for treating *C. albicans* infection

without disrupting the microbiota (and potential evolution of antifungal resistance) that normally accompanies the killing of cells.

Results

Mucins share a conserved function in attenuating *C. albicans* virulence

While previous studies identified mucin polymers as candidates for managing *C. albicans* virulence *in vitro* (Kavanaugh et al., 2014), it is unclear whether mucin activity persists in native and complex mucus or in the context of an intact immune system, which may indicate whether mucins are viable candidates for therapeutic intervention on mucosal surfaces. Here, we investigated mucus from three distinct sources (Supplementary Fig. 2.1a)—porcine intestinal mucus, porcine gastric mucus, and human saliva—representing model systems (Celli et al., 2005; Krupa et al., 2020; Turner et al., 1999) for mucosal niches colonized by *C. albicans* (Fig. 2.1a). We quantified *C. albicans* adhesion to a polystyrene surface using fluorescence microscopy in medium with or without mucus. All three mucus types significantly decreased *C. albicans* adhesion *in vitro* (Supplementary Fig. 2.1b). Cell growth was similar with or without mucus (Supplementary Fig. 2.1c); thus, mucus shifts *C. albicans* to a planktonic state without affecting viability.

One candidate for mediating this function is mucin polymers, which suppress *C. albicans* adhesion *in vitro* (Kavanaugh et al., 2014). To determine whether mucins are the dominant adhesion-suppressing factor in mucus, we removed high-molecular-weight components from porcine intestinal mucus using a centrifugal filter with a 100-kDa cutoff. The filtrate was less effective in preventing adhesion than whole mucus (Fig. 2.1b). Re-introducing the filtrate with 0.5% w/v MUC2, the predominant mucin in the intestinal tract, restored this effect and significantly decreased adhesion; similar results were observed for all three mucin types (Fig. 2.1b, Supplementary Fig. 2.1d,e). Thus, mucins from these mucosal surfaces are both necessary and sufficient to recapitulate the adhesion-suppressing effects of mucus.

To clarify how mucins regulate *C. albicans* physiology, we performed RNA sequencing on cells grown in RPMI medium with or without (0.5% w/v) MUC2 (intestinal mucin), MUC5B (salivary mucin), or MUC5AC (gastric/respiratory mucin), representing mucins secreted on mucosal surfaces abundantly colonized by *C. albicans* (Supplementary Fig. 2.1a). Each mucin type elicited a specific gene-expression profile (Fig. 1c,d), with 262 downregulated and 343 upregulated genes

($P < 0.05$) shared among the three transcriptional profiles (Fig. 2.1e). Filamentation- and adhesion-regulating pathways were enriched in the shared downregulated genes (Supplementary Data 2.1). Notably, all three mucins caused the downregulation of various virulence-associated genes (Fig. 2.1f). Consistent with previous observations (Kavanaugh et al., 2014), inoculation of *C. albicans* in RPMI medium caused the formation of extensive hyphae, while mucin-exposed cells were predominantly in the round yeast form or formed short chains resembling pseudohyphae (Fig. 2.1g, Supplementary Fig. 2.2a). The upregulated pathways were enriched in genes encoding cellular amino-acid and small-molecule biosynthetic and metabolic processes (Supplementary Data 2.1). *C. albicans* metabolism plays a central role in biofilm formation and hyphal morphogenesis (Han et al., 2011); thus, metabolic changes may correlate with virulence suppression. Together, these data indicate that mucins across various mucosal surfaces downregulate virulence-associated gene expression and phenotypes, providing rich sources of bioactive molecules for regulating *C. albicans*.

To investigate the roles of mucins in the context of an intact immune system (Fig. 1h), we infected murine puncture wounds with *C. albicans*, topically treated the wounds with 0.5% MUC2, and quantified the fungal burden over time in colony-forming units (CFUs). While the fungal burden on day 5 and 7 did not differ between MUC2 and mucin-free treatment, exposure to MUC2, but not mucin-free mock treatment, caused a significant CFU reduction 7 days post-infection compared to day 5 of infection (Fig. 2.1i). This enhanced *C. albicans* clearance is likely not due to direct killing by MUC2 because mucins do not alter growth (Fig. 2.1j) (Kavanaugh et al., 2014). Rather, mucins may facilitate fungal clearance by attenuating *C. albicans* pathogenicity, thus supporting host defense mechanisms to reduce the fungal burden in the wound.

Mucin glycans act via Nrg1 to prevent filamentation

Mucin glycans are promising molecules for regulating host–microbe interactions: they serve as nutrients (Tailford et al., 2015), microbial binding sites (Corfield, 2015), and signaling molecules (Bergstrom & Xia, 2013; Wheeler et al., 2019). To determine whether mucin glycans mediate virulence suppression, we isolated glycans via non-reductive, alkaline β -elimination, which preserved the structural heterogeneity of glycan chains, yielding a library of glycans released from MUC5AC (Fig. 2.2a). We analyzed the released glycans as permethylated derivatives using nanospray-ionization multi-dimensional mass spectrometry (NSI-MSn, ThermoFisher Orbitrap

Discovery) to characterize structural topology features beyond simple monosaccharide composition (Fig. 2.2b, Supplementary Table 2.1). We identified >80 glycan structures, including isobaric glycans with distinct structural characteristics. Negative-mode NSI-MSⁿ indicated sulfation on 34 of these glycans. The MUC5AC glycan pool was dominated by Core-1- and Core-2-type O-glycan structures that were partially modified by fucose, possessed multiple LacNAc repeats, and were only sparsely capped by sialic acid (Fig. 2.2c). Sulfation was most abundant on non-sialylated Core-2-type O-glycans with a single fucose (Supplementary Table 2.2).

To determine whether the mucin glycan pool can replicate mucin-induced virulence suppression, we performed RNA sequencing of *C. albicans* in medium with or without 0.1% w/v MUC5AC glycans. A pooled library of MUC5AC glycans triggered global gene expression changes, with 233 and 308 genes significantly upregulated and downregulated, respectively, compared with cells grown in medium alone ($P < 0.05$; Fig. 2.2d). Similar to intact mucins, MUC5AC glycans upregulated the transcription of amino-acid biosynthetic and metabolic processes (Supplementary Data 2.2) and downregulated pathways associated with filamentation, biofilm formation, and interspecies interactions (Fig. 2.2e).

Over 20% of the downregulated genes were associated with filamentous growth, which was suppressed by intact mucins (Supplementary Data 2.2). We found that isolated MUC5AC glycans suppressed filamentation across the three medium conditions without altering growth, while medium alone supported the formation of extensive hyphae (Fig. 2.2f,g, Supplementary Fig. 2.2b). Addition of the monosaccharides found in mucins did not suppress filamentation or alter the expression of signature hyphal-specific (*UME6*, *HGCI*) (Banerjee et al., 2008; Zheng et al., 2004) or yeast-specific (*YWPI*) (Granger et al., 2005) genes relative to medium alone (Fig. 2.2h). We detected gene expression changes 30 min after exposure to MUC5AC glycans, which intensified over 4 h (Fig. 2.2i). Filamentation suppression was visualized 4 h after hyphal induction (Supplementary Fig. 2.2b) and the round yeast morphology was maintained over 8 h (Fig. 2.2f), suggesting a prolonged glycan response. Further, we detected a dose-dependent effect of mucin glycans, with potent filamentation suppression occurring at concentrations below those of mucosal surfaces (Fig. 2.2j, Supplementary Fig. 2.3). Together, these data demonstrate that complex glycan structures are critical for retaining *C. albicans* in a host-compatible yeast state and may signal a healthy mucosal environment.

Hyphal morphogenesis in *C. albicans* is induced by environmental signals acting via multiple signaling cascades, including a cAMP-dependent pathway and a MAPK pathway (Fig. 2.3a) (Sudbery, 2011). Our RNA-sequencing data revealed that the transcription of many filamentation activators and key outputs of these pathways (including hyphal-specific proteins Ume6, Eed1, and Hgc1 (Lu et al., 2014)) were significantly downregulated in the presence of mucin glycans (Fig. 3a, Supplementary Fig. 2.4a). Hyphal-specific gene expression is negatively regulated by a protein complex consisting of the general transcriptional corepressor Tup1 and DNA-binding proteins Nrg1 or Rfg1 (Lu et al., 2014). The transcription of *NRG1*, a major transcriptional repressor of filamentation, increased in the presence of mucin glycans (Fig. 2.3a). Thus, mucin glycans may inhibit filamentation by regulating transcriptional activators and/or repressors, which play prominent roles in the yeast-to-hyphal transition (Sudbery, 2011).

To assess whether mucin glycans suppress hyphal formation by preventing activation of the major transcriptional activators of filamentation, we screened mutants that constitutively activate major positive filamentation regulators (Ras1, Cph1, and Efg1) for the filamentation-suppression response to mucin glycans. Ras1 cycles between inactive and active states. The *RASI^{G13V}* strain is locked in an active state, leading to hyperfilamentation (Feng et al., 1999). If mucin glycans act upstream or directly via Ras1 activation, the dominant active *RASI^{G13V}* strain should remain filamentous in the presence of mucin glycans, being unable to respond to mucin glycans. However, in the presence of mucin glycans, cells from both the *RASI^{G13V}* strain and wild-type strain retained the yeast morphology (Fig. 2.3b, Supplementary Fig. 2.2c,d), suggesting that this function does not depend on Ras1 activation.

To determine whether mucin glycans act via the cAMP-PKA pathway, we tested whether mucin glycans suppress filamentation in a strain with a phosphomimetic mutation controlled by the glucose-repressible *PCK1* promoter (Bockmühl & Ernst, 2001; Leuker et al., 1997) (*PCKpr-efg1-T206E*), which simulates constitutive signaling of Efg1, a downstream transcription factor in the cAMP-PKA pathway (Sudbery, 2011). In the presence of mucin glycans, cells from a constitutively expressed Efg1 transcription factor transitioned to a yeast morphology, as observed for the wild-type strain in Spider medium (Fig. 2.3b, Supplementary Fig. 2.2c,e), suggesting that the filamentation suppression of mucin glycans is independent of the cAMP-PKA pathway. To determine whether mucin glycans act via the MAPK pathway, we tested filamentation suppression in a strain overexpressing Cph1 (*prADHI-CPHI*). In the presence of mucin glycans, cells

overexpressing Cph1 remained in the yeast form (Fig. 2.3b) at levels comparable to those of the wild-type strain (Supplementary Fig. 2.2c,d), indicating that mucin glycans suppress filamentation independently of the MAPK pathway. Thus, mucin glycans do not act directly via the major transcriptional activators of hyphal induction to suppress filamentation; instead, they likely act downstream of Cph1 and Efg1 or via alternate pathways.

To explore alternate regulation pathways, we examined whether mucin glycans act via transcriptional repressors of filamentation, which inhibit the yeast-to-hyphal transition (Sudbery, 2011). We focused on *NRG1* and *TUPI*, as their loss leads to constitutive filamentation and upregulation of hyphal genes, even in non-inducing conditions (Shapiro et al., 2011). Specifically, 30 min after exposure to mucin glycans (Fig. 2.3c), expression of Nrg1 was upregulated, which continued throughout an 8-h time course (Fig. 2.3a). If filamentation suppression depends on Nrg1 or Tup1, those mutant strains should remain filamentous in the presence of mucin glycans. Indeed, opposed to the wild-type strain (Supplementary Fig. 2.2c), upon exposure to mucin glycans, cells lacking *NRG1* or *TUPI* were constitutively filamentous in the presence or absence of mucin glycans (Fig. 2.3d), suggesting that mucin glycans block hyphal formation in an Nrg1/Tup1-dependent manner.

To further explore this function of mucin glycans, we performed RNA sequencing of the wild-type strain and $\Delta/\Delta nrg1$ mutant strain after 2 h in the presence or absence of mucin glycans to detect early transcriptional changes during hyphal morphogenesis. In the wild-type strain, mucin glycans downregulated 45 and upregulated 64 genes ($P < 0.05$) after 2 h (Fig. 2.3e, Supplementary Data 2.3). The transcription of several hyphal-specific genes (*ALS3*, *HWPI*, *EFG1*, and *HGC1*) was downregulated; further, *YWPI*, a marker for yeast cells, was upregulated (Fig. 2.3e). We also detected downregulation of genes involved in ion regulation, white–opaque regulation, and amino-peptidase activity (Fig. 2.3e). However, in the $\Delta/\Delta nrg1$ mutant strain, only 22 genes were differentially expressed (Fig. 2.3e, Supplementary Data 2.4). Several genes involved in ion homeostasis were differentially downregulated in the $\Delta/\Delta nrg1$ mutant strain and wild-type strain (Fig. 2.3e), suggesting that these changes constitute general responses to mucin glycans, independent of morphology. The hyphal-associated genes that were downregulated in the wild-type strain were unchanged in the $\Delta/\Delta nrg1$ mutant strain (Fig. 2.3f), consistent with the observation that the $\Delta/\Delta nrg1$ mutant strain remains filamentous in the presence of mucin glycans

(Fig. 2.3d). These observations imply that mucin glycans act via Nrg1 to downregulate the expression of hyphal-specific and other virulence-associated genes.

Mucin glycans regulate group-level behavior

A major virulence attribute of *C. albicans* is its ability to form robust biofilms (Nobile & Johnson, 2015). Biofilm cells are highly resistant to conventional antifungal therapeutics and the host immune system, making them highly pathogenic (Nobile & Johnson, 2015). In *C. albicans*, biofilm development requires six master transcriptional regulators (Efg1, Tec1, Bcr1, Ndt80, Brg1, and Rob1) (Nobile et al., 2012). The first step in biofilm formation involves cell adherence to a surface, mediated by the master regulator Bcr1 and its downstream target genes (Lohse et al., 2018).

We observed that MUC5AC glycans significantly downregulated the transcription of several genes involved in adherence and biofilm initiation, while equivalent amounts of monosaccharides had no effect (Fig. 2.4a, Supplementary Data 2.2). By inoculating yeast cells into medium with or without (0.1% w/v) mucin glycans and visualizing surface adherence, we found that mucin glycans significantly reduced cell attachment, while equivalent amounts of monosaccharides had no effect (Fig. 2.4b,c).

After initial adherence and biofilm initiation, the next step in biofilm formation is biofilm maturation, where hyphal cells grow and all cells become encased in extracellular matrix (Nobile et al., 2012). Our RNA-sequencing data revealed significant downregulation of several transcriptional regulators of biofilm maturation, including genes encoding Efg1, Tec1, Brg1, and Rob1 (Supplementary Fig. 2.4a,b) (Lohse et al., 2018). To investigate *C. albicans* biofilm formation, we visualized biofilms formed on the bottom of polystyrene plates after 24 h of growth. *C. albicans* typically forms biofilms consisting of yeast, hyphae, and pseudohyphae cells; however, in the presence of MUC5AC glycans, only a layer of yeast-form cells was present on the plate surface (Fig. 2.4d), with more cells remaining in the yeast non-adhered (planktonic) state compared with the results observed for medium only (Fig. 4d,e, Supplementary Fig. 4c).

In a host, *C. albicans* is generally part of a larger multispecies microbial community (Morales & Hogan, 2010; Nobile & Johnson, 2015). We found that genes involved in microbial interspecies interactions are differentially regulated by mucin glycans (Supplementary Data 2.2), suggesting that mucins influence microbial community dynamics. *C. albicans* is often found in the presence of the bacterial pathogen *Pseudomonas aeruginosa*, both as part of the normal microbiota and

during infection (Morales & Hogan, 2010). *In vitro* work has shown that these two microbes have an antagonistic relationship when grown together in *C. albicans* filamentation-inducing conditions (Hogan & Kolter, 2002), where *P. aeruginosa* forms biofilms on *C. albicans* hyphal cells and secretes small molecules that result in fungal cell death (Fig. 2.4f). Consistent with previous work, *P. aeruginosa* does not adhere to or kill *C. albicans* yeast cells when these species are grown together in non-filamentation-inducing conditions (Fig. 2.4f) (Brand et al., 2008).

Because mucins suppress filamentation (Fig. 2.1g) (Kavanaugh et al., 2014), we hypothesized that in filamentation-inducing conditions, mucin glycans would increase the viability of *C. albicans* in coculture with *P. aeruginosa*. As previously reported (Hogan & Kolter, 2002), cocultures grown under filamentation-inducing conditions in the absence of mucin glycans showed reduced *C. albicans* CFUs and eventual eradication of *C. albicans* cells (Fig. 2.4g). Addition of mucin glycans delayed *C. albicans* eradication (Fig. 2.4g), indicating that mucin glycans protect *C. albicans* against *P. aeruginosa*. Therefore, mucin glycans may influence microbial population dynamics by modulating *C. albicans* morphogenesis.

To determine whether filamentation suppression is the dominant factor promoting microbial coexistence, we cocultured the *C. albicans* $\Delta/\Delta nrg1$ mutant strain, which remains filamentous in the presence of mucin glycans (Fig. 2.3d, Supplementary Fig. 2.4d,e), with *P. aeruginosa* in the presence or absence of mucin glycans. The increased viability of *C. albicans* in the presence of mucin glycans was eliminated in the $\Delta/\Delta nrg1$ mutant strain (Fig. 2.4h), indicating that filamentation-suppression effects confer protection from *P. aeruginosa*. These results suggest that mucin glycans may influence microbial communities and inhibit a range of virulence behaviors.

Mucins display a plethora of glycans with regulatory potential

To determine the glycan structures regulating *C. albicans* physiology and the therapeutic potential of novel glycan-based drugs for *C. albicans* infection, we screened mucin glycan libraries for filamentation suppression. Glycans isolated from human saliva (MUC5B), porcine gastrointestinal mucus (MUC2), and porcine gastric mucin (MUC5AC) all suppressed filamentation (Fig. 2.5a), suggesting that these mucin-derived glycans are sufficient to recapitulate the filamentation-suppression response in *C. albicans*.

To distinguish unique and shared structural features, we used NSI-MSn to analyze released, permethylated glycans from these three mucin pools (Methods). We identified glycans at 83

distinct mass/charge (m/z) ratios, approximately 1/3rd of which produced MS fragmentation, indicating the presence of 2–3 isomeric glycan structures (Fig. 2.5b, Supplementary Table 2.1). Thus, the full glycan diversity of these mucin pools exceeds the number of discrete m/z values detected by NSI-MSn. These glycans are predominantly characterized by the presence of a HexNAc (GalNAc) at their reducing terminal. This GalNAc, in O-linkage to serine or threonine amino acids of the mucin protein backbone, provides a foundation upon which a set of structurally distinct glycan core types are built; the core structures are extended to longer, more complex glycan structures depending on the repertoire of glycosyltransferases expressed in the tissue and species of origin. The majority of all three glycan pools consisted of glycans built on Core 1 (Gal β 1-3GalNAc α 1-Ser/Thr) or Core 2 (Gal β 1-3(GlcNAc β 1-6)GalNAc α 1-Ser/Thr) structures, while the Tn antigen (GalNAc α 1-Ser/Thr) or glycans built on Core 3 (GlcNAc β 1-6GalNAc α 1-Ser/Thr) and Core 4 (GlcNAc β 1-3(GlcNAc β 1-6)GalNAc α 1-Ser/Thr) structures contributed <10% for each glycan pool (Fig. 2.5c). Of these 83 glycan compositions, 51 were monosulfated and 20 were disulfated; the most abundant sulfated O-glycans of MUC2 and MUC5AC were Core-2-type, while the most abundant sulfated O-glycans of MUC5B were Core-1- and O-Man-type (Supplementary Table 2.2). MUC5AC and MUC5B glycans were more complex than MUC2 glycans (Fig. 2.5b, Supplementary Table 2.1). Specifically, >60% of MUC2 glycans were detected as the Core-1 disaccharide (glycan #2; Fig. 2.5b, Supplementary Table 2.1) or Core 1 modified with a single additional monosaccharide (Fuc or sialic acid; glycans #3 and 4, respectively), compared with <35% for MUC5AC and MUC5B.

Beyond the core structures, 23% and 15% of MUC5AC and MUC5B glycans, respectively, were more than seven sugars long, versus <3% of MUC2 glycans (Supplementary Table 2.1). The shortened length of MUC2 glycans may result from degradation through microbial feeding or differences in endogenous glycosyltransferase expression levels in the intestinal tract (Tailford et al., 2015). Consistent with previous reports (Jin et al., 2017; Wheeler et al., 2019), mucin glycans from all three sources were heavily fucosylated, with >35% of structures containing at least one fucose, with minimal sialylation (Fig. 2.5d). MUC5AC yielded the highest abundance of non-fucosylated and asialo glycans (i.e., uncapped glycans), while MUC5B and MUC2 glycans were the most fucosylated and most sialylated, respectively. These capping residues (Fuc and sialic acid) can block the extension of core structures by limiting the addition of *N*-acetylglucosamine (LacNAc) units. Thus, the glycan collection prepared from MUC5AC had the highest abundance

of LacNAc repeats. We detected several glycan structural elements or motifs with known roles in immunorecognition (e.g., LacNAc, LacdiNAc, Lewis X, GalGal)(Amon et al., 2014) or cell adhesion (e.g., O-Man) as minor components of all three preparations (Fig. 2.5e); thus, these structures may contribute to immunomodulatory activities. Despite substantial overlap in the glycan structures among the three mucin glycan pools (Fig. 2.5b, Supplementary Table 2.1), differences in mucin glycan identity and length likely arise from niche-specific selective preferences that have coevolved to influence the structural and functional properties of the mucus barrier.

Synthetic Core-1 and Core-2 structures suppress filamentation

Because glycan structure compositions vary across mucin types, we focused on glycan structures that were highly abundant across the mucin species examined here. In total, six glycan structures (Fig. 2.5f, Supplementary Table 2.1) were shared among all three mucin glycan pools and together represented >40% of the total glycan profile in each sample (Fig. 2.5f), highlighting them as candidates for virulence-attenuating activity. To date, most known mucin glycan structures have not been associated with clearly delineated functions.

Rather than fractionating glycan pools down to the single-glycan level, which poses technical challenges (Cummings & Pierce, 2014), we developed a synthetic approach to obtain these six highly abundant mucin glycans (Fig. 2.6a, Methods). We first focused on Core 1 (#1) and Core 2 (#2), which constitute 40% of total mucin glycans (Supplementary Table 2.1). Neither Core 1 nor Core 2 showed toxic effects, as measured by *C. albicans* growth at a concentration of 0.1% (w/v), an effective concentration for filamentation suppression in the mucin glycan pool (Fig. 6b). To determine whether Core 1 and Core 2 have a similar regulatory capacity as the complex glycan pool, we tested their ability to regulate two signature proteins, the yeast-wall protein Ywp1 and the filamentation-associated cytotoxin Ece1, whose genes were strongly up- and downregulated, respectively, by the native mucin glycan pool (see Fig. 2.2). RT-qPCR revealed that Core 1 and Core 2 individually upregulated *YWPI* expression at 0.1% (w/v) to a similar degree as the intact mucin pool, and a concentration increase to 0.4% (w/v) did not significantly alter *YWPI* expression (Fig. 2.6c). Moreover, Core 1 and Core 2 both suppressed *ECE1* expression at 0.1% and 0.4%, albeit less strongly than the mucin glycan pool (Fig. 2.6c). By contrast, an equal-parts mixture of the mucin monosaccharide components did not change gene expression at corresponding

concentrations (Fig. 2.6c). Thus, both Core 1 and Core 2 regulate these two genes with similar potency as the native glycan pool.

To elucidate the role of glycan composition, we tested the effects of four modified Core structures: Core 1+fucose (#3), Core 1+sialic acid (#4), Core 2+fucose (#5), and Core 2+galactose (#6) (Fig. 2.6a). These four glycans all transcriptionally upregulated *YWPI* while downregulating *ECEL*, similar to their unmodified Core counterparts (Fig. 2.,e). The addition of fucose to Core 1 and Core 2 did not measurably alter the ability of these structures to up- or downregulate the two signature genes (Fig. 2.6d,e); the addition of galactose did not significantly alter Core 2 activity (Fig. 2.6e). However, the addition of sialic acid dampened the gene regulatory response of Core 1 (Fig. 2.6d). Exploring a broader range of filamentation-associated genes, we observed that all six synthetic glycans possessed a sliding range of bioactivity, rather than an on/off response: Core 1, Core 1+fucose, and Core 2+galactose showed the strongest suppression of filamentation-associated genes, while Core 1+sialic acid exhibited the weakest effect (Fig. 2.6f).

The phenotypic filamentation assay confirmed this conclusion: while medium alone supported the formation of extensive hyphal filaments, Core 1, Core 1+fucose, and Core 2+galactose most potently blocked filamentation, as evidenced by the predominance of yeast cells in culture with these structures compared with the monosaccharide pool and medium alone (Fig. 2.6g, Supplementary Fig. 2.2f). Core 1+sialic acid was less effective at suppressing filamentation, despite partially downregulating the transcription of filamentation-associated genes (Fig. 2.6d,g).

Discussion

Research on mucus has traditionally focused on the role of mucins as scaffolding polymers. Here, we show that mucin *O*-glycans potently inhibit a range of virulence behaviors, which could be leveraged for therapeutic applications. Specifically, we show that mucin glycans across three major niches are potent regulators of *C. albicans* filamentation (Fig. 2.2) that block hyphal formation through Nrg1 (Fig. 2.3) and regulate community behavior (Fig. 2.4). These insights demonstrate the wealth of biochemical information and regulatory power housed within mucus and may inform diagnostic strategies for treating and preventing infection.

By characterizing bioactive glycans across mucin types, we identified and synthesized prominent Core-1- and Core-2-modified structures commonly found across mucosal surfaces. We demonstrated that Core 1, Core 2+galactose, and Core 1+fucose individually suppress

filamentation at potencies comparable to those of native mucins. Our findings highlight that *O*-glycans can control virulence traits (Fig. 6) without killing the microbe, which may prevent the evolution of drug resistance. Many well-known small-molecule drugs, such as antibiotics and anticancer agents (Dube & Bertozzi, 2005), naturally contain glycans as part of their core structure and/or sugar side chain. Therefore, the discovery of *O*-glycans that attenuate *C. albicans* virulence may lead to novel glycan-based or glycan-mimetic therapeutics that enhance, or even replace, current antifungals. Native glycans, which are unconjugated to larger macromolecules, are generally ineffective as small-molecule pharmaceuticals due to their inherently poor pharmacokinetic properties (Hevey, 2019a). By identifying the most bioactive mucin *O*-glycans, we can establish the precise glycan epitopes required for activity to design glycomimetic structures that retain activity while exhibiting improved drug-like properties. For example, glycan hydroxyl groups or post-synthetic modifications that are not necessary for activity can be chemically modified or eliminated to improve overall drug-likeness (Hevey, 2019b). Additionally, smaller glycan epitopes should be more amenable to larger-scale production. Frequently, small glycans with biological activity gain potency when presented as multivalent conjugates on a defined backbone. Identifying minimal functional epitopes of mucin glycans may lead to conjugates with enhanced efficacies, which may mimic the multivalent glycan presentation offered by endogenous mucin proteins.

Given the complexity and diversity of mucin glycans (Jin et al., 2017; Wheeler et al., 2019) and dynamic glycosylation changes based on cell type (Brockhausen, 2006), developmental stage (Tabak, 2010), and disease state (Kudelka et al., 2015), structural changes in host signals may activate or inhibit the function of specific *O*-glycans. Accordingly, we determined that Core 1, Core 1+fucose, and Core 2+galactose effectively suppress filamentation, while Core 1+sialic acid significantly dampens this response. Hence, sialic acid, which is ubiquitously expressed on host cells (Giancetti et al., 2021), may have an unappreciated role in modulating virulence. We posit that changes in glycosylation in disease states may mask or eliminate mucins' protective functions. We conclude that the presentation of complex glycan structures in mucus contributes to a healthy mucosal environment, while degradation or modification of mucin glycans may trigger *C. albicans* to transition from commensal to pathogenic.

The receptors involved in sensing mucin glycans, leading to *NRG1* upregulation, remain unknown. *Nrg1* regulation is temporally coordinated by two central signaling pathways mediating cell

growth, leading to transient *NRG1* downregulation and degradation of Nrg1 protein followed by occlusion of Nrg1 from hyphal-specific promoters that sustain hyphal development (Lu et al., 2014). Mucin glycans may potentially function as ligands to mimic nutrient signaling pathways or may bind directly to *C. albicans* adhesins, thus modulating morphogenesis (Donohue et al., 2011). Uncovering the receptors involved in sensing mucin glycans and the pathways regulated by glycans will elucidate how *C. albicans* senses its host environment and how these cues regulate microbial antagonism, microbial community composition, and pathogenesis.

Methods

C. albicans strains and media

Strains were maintained on YPD agar (2% Bacto peptone, 2% glucose, 1% yeast extract, 2% agar) and grown at 30 °C. Single colonies were inoculated into YPD broth and grown with shaking overnight at 30 °C prior to each experiment. Experiments were performed with Gibco RPMI 1640 medium (catalog number 31800-089; Life Technologies) buffered with 165 mM 3-(*N*-morpholino)propanesulfonic acid (MOPS) and supplemented with 0.2% NaHCO₃ and 2% glucose; YPD medium with 10% fetal bovine serum; GlcNAc medium (0.5% *N*-acetylglucosamine, 0.5% peptone, 0.3% KH₂PO₄); Spider medium (1% nutrient broth, 1% D-mannitol, 2 g K₂HPO₄, 50 mg/mL arginine, 10 mg/mL histidine, and 50 mg/mL tryptophan); or Lee's medium (Lee et al., 1975). Growth curves were performed in Synthetic Defined (SD) + 0.004% (w/v) L-Arginine + 0.0025% (w/v) L-Leucine media with 2% glucose.

The *C. albicans* reference strains used in this study were SC5314 and HGFP3. Strain HGFP3 was constructed by inserting the *GFP* gene next to the promoter of *HWPI1*, a gene encoding a hyphal cell wall protein, in SC5314; this strain was provided by E. Mylonakis (Massachusetts General Hospital, Boston, MA) with the permission of P. Sundstrom. Homozygous deletion strains were obtained from the transcriptional factor deletion collection and were provided by the Fungal Genome Stock Center (<http://www.fgsc.net/>).

The following *C. albicans* strains used for pathway analyses were gifts from Paul Kauman (University of Massachusetts, Medical School): AV55 (*ura3::λimm434/ura3::λimm 434; LEU2::pCK1-efg1- T206E::URA3*); DH409 (*ura3::λimm434/ura3; ras1-G13V*); and CDH72-1 (*ura3/ura3 cph1Δ::hisG/cph1Δ::hisG; ADH1prCPH1*).

Collection of human saliva

Submandibular saliva was collected from healthy human volunteers using a custom vacuum pump, pooled, centrifuged at 2,500 x g for 5 min, and 1 mM of phenylmethylsulfonyl fluoride was added. Samples of human saliva were collected after obtaining informed consent, and receiving approval from the institutional review board and Massachusetts Institute of Technology's Committee on the Use of Humans as Experimental Subjects under protocol no. 1312006096.

Mucin purification

This study used native porcine gastric mucins (MUC5AC), porcine intestinal mucins (MUC2), and human salivary mucins (MUC5B), which differ from industrially purified mucins in their rheological properties and bioactivities (Kavanaugh et al., 2014; Wagner et al., 2017). Native mucins were purified as described previously (Kavanaugh et al., 2014; Wheeler et al., 2019). In brief, mucus was scraped from fresh pig stomachs and intestines and solubilized in sodium chloride buffer containing protease inhibitors. Insoluble material was removed via low speed centrifugation at 8,000g for 1 h and ultracentrifugation at 190,000 x g for 1 h at 4 °C (Beckman 50.2 Ti rotor with polycarbonate bottles). Submandibular saliva was collected from human volunteers as described above using a custom vacuum pump, pooled, centrifuged, and protease inhibitors were added (Kavanaugh et al., 2014). Mucins were purified using size-exclusion chromatography on separate Sepharose CL-2B columns. Mucin fractions were then desalted, concentrated, and lyophilized for storage at -80 °C. The desired medium was added to the lyophilized mucins and reconstituted by shaking them gently at 4 °C overnight.

Mass spectrometry is routinely used to monitor the composition of purified mucin extracts. This type of analysis has shown that mucin extracts purified from porcine stomach mucus, for example, are composed predominantly of MUC5AC, with small quantities of MUC2, MUC5B, and MUC6, as well as histones, actin, and albumin (Lieg et al., 2012).

Isolation of mucin oligosaccharides

We applied non-reductive alkaline β -elimination ammonolysis to dissociate non-reduced glycans from mucins as described previously (Huang et al., 2001; Wheeler et al., 2019). Purified mucins were dissolved in ammonium hydroxide saturated with ammonium carbonate and incubated at 60 °C for 40 h to release oligosaccharide glycosylamines and partially deglycosylated mucins. Volatile salts were removed using repeated centrifugal evaporation. The oligosaccharide glycosylamines were separated from residual deglycosylated mucins via centrifugal filtration through 10 kDa molecular weight cut-off membranes (Amicon Ultracel) in accordance with the manufacturer's instructions. The resulting oligosaccharide glycosylamines were converted to reducing oligosaccharide hemiacetals via treatment with 0.5 M boric acid at 37 °C for 1 h. The samples were washed with methanol and residual solvents were removed via repeated centrifugal evaporation. Oligosaccharides were further purified using solid-phase extraction using Hypercarb

mini-columns (ThermoFisher) and residual solvents were removed through centrifugal evaporation.

Analysis of mucin O-glycan profiles

Glycans released from MUC2, MUC5B, and MUC5AC were permethylated and analyzed by nanospray ionization tandem mass spectrometry (NSI-MS) following direct infusion into a linear/orbital hybrid ion trap instrument (Orbitrap-LTQ Discovery, ThermoFisher) operated in positive ion mode for non-sulfated glycans or in negative mode for the detection of sulfated glycans. The permethylated O-glycans were dissolved in 1 mM sodium hydroxide in methanol/water (1:1) for infusion at a syringe flow rate of 0.60 $\mu\text{l}/\text{min}$ and capillary temperature set to 210 $^{\circ}\text{C}$ (Aoki et al., 2007). For fragmentation by collision-induced dissociation (CID) in MS/MS and MSⁿ, a normalized collision energy of 35-40% was applied. Detection and relative quantification of the prevalence of individual glycans was accomplished using the total ion mapping (TIM) functionality of the Xcalibur software package version 2.0 (ThermoFisher) as previously described (Aoki et al., 2007). For TIM, the m/z range from 600 to 2000 was automatically scanned in successive 2.8 mass unit windows with a window-to-window overlap of 0.8 mass units, which allowed the naturally occurring isotopes of each glycan species to be summed into a single response, thereby increasing detection sensitivity. Most glycan components were identified as singly, doubly, and/or triply charged, sodiated species (M + Na) in positive mode or as singly or doubly charged (M – H) species in negative mode. Charge states for each glycan were deconvoluted manually and summed for quantification. Structural representations of mucin glycans were based on topologic features detected upon CID fragmentation and knowledge of O-glycan biosynthetic pathways. Approximately 33% of the m/z values reported here were associated with 2 or 3 isomeric glycan structures. NSI-MS/MS and MSⁿ were used as needed to assign isomeric heterogeneity at each of these m/z values. For purposes of representing and comparing the heterogeneity of the glycan profile associated with each mucin, the signal intensity associated with an m/z value comprised of more than one glycan was assigned to the most abundant glycan structure among the isomers. Graphic representations of glycan monosaccharide residues are consistent with the Symbol Nomenclature For Glycans (SNFG) as adopted by the glycomics and glycobiology communities. Glycomics data and metadata were obtained and are presented in accordance with MIRAGE standards and the Athens Guidelines (Liu et al., 2017). GlyTouCan accessions were retrieved from the GlyTouCan repository through GlyGen for glycan instances in

which accessions already existed. If new accessions were required for glycans not previously placed in the repository, the desired structural representations were generated in GlycoGlyph and submitted directly to GlyTouCan for registration (Mehta & Cummings, 2020). All raw mass spectrometric data related to mucin glycan profiles were deposited at GlycoPost (Watanabe et al., 2021). Heatmap and other data analysis was performed on extracted signal intensities using Prism GraphPad and Excel software.

Filamentation assay

Hyphal growth of *C. albicans* was induced by diluting cells to $OD_{600}=0.05$ into pre-warmed hyphae-inducing medium as indicated and incubating at 37 °C (200 rpm) in a glass-bottom, 96-well plate. Cells were grown in hyphae-inducing medium for several hours, as described in the figure legends. Images were acquired with a confocal laser scanning microscope (LSM 800; Zeiss) equipped with a $\times 63/1.4$ NA oil-immersion or a 25x objective. Images were analyzed using Zeiss ZEN v.2.1. Representative micrographs are shown.

RNA extraction

For the extraction of the RNA of *C. albicans* grown in the presence or absence of mucins, 1 mL of RPMI or 0.5% w/v MUC2, MUC5AC, or MUC5B in RPMI was inoculated with 10 μ L of an overnight culture of strain SC5314 and incubated in a culture tube at 37 °C with shaking (180 rpm) for 8 h. Total RNA was extracted using the Epicentre MasterPure Yeast RNA Purification Kit and treated with Sigma-Aldrich AMPD1 amplification-grade DNase I.

For RNA extraction from *C. albicans* grown in the presence or absence of mucin glycans, 100 μ L of RPMI or 0.1% w/v MUC5AC glycans in RPMI were inoculated with a 1:50 dilution of an overnight culture of strain SC5314 and incubated at 37 °C for the time indicated. Total RNA was extracted with the MasterPure RNA Purification Kit (Lucigen) and residual DNA was removed using the Turbo DNA-free kit (Ambion). The integrity of the total RNA was assessed using an Agilent 2100 Bioanalyzer (Agilent Technologies). rRNA was removed using the Ribo-Zero rRNA Removal Kit (Yeast; Epicentre).

RNA sequencing

For RNA sequencing of *C. albicans* grown in mucins, poly(A) RNA was isolated from total RNA via two rounds of purification. Samples were run on a MiSeq with a paired-end protocol and read lengths of 150 bp.

For RNA sequencing of *C. albicans* grown in mucin glycans, Illumina RNA-seq was used. Libraries were produced using the KAPA RNA HyperPrep kit (Kapa Biosystems) and sequenced using the Illumina HiSeq platform with a single-end protocol and read lengths of 40 or 50 nucleotides.

RT-qPCR analysis

A list of the primers used in this study is provided in Supplementary Table 3. qPCR with reverse transcription (RT-qPCR) was performed using a two-step method. First-strand cDNA was synthesized from total RNA using the ProtoScript IV First Strand cDNA Synthesis kit (NEB). The cDNA was used as template for RT-qPCR using a SYBR PowerUp Master Mix kit (Applied Biosystems by Life Technologies) on a Roche LightCycler 480 real-time PCR system. Primers for RT-qPCR were designed on the basis of the published literature or using the NCBI Primer-BLAST tool (<https://www.ncbi.nlm.nih.gov/libproxy.mit.edu/tools/primer-blast/>). The *ACT1* and *18S* rRNA genes were used as endogenous controls as specified. The elimination of contaminating DNA was confirmed using qPCR amplification of *ACT1* and *18S* rRNA genes on control samples that did not have reverse transcriptase added during cDNA synthesis. Changes in gene expression were calculated on the basis of mean change in qPCR cycle threshold (ΔC_t) using the $\Delta\Delta C_t$ method (fold change = $2^{-\Delta\Delta C_t}$).

Analysis of RNA sequencing data

For mucins RNA sequencing experiments, reads were mapped to the *C. albicans* SC5314 haplotype A genome, version A22-s05-m05-r03, retrieved from the *Candida* Genome Database (www.candidagenome.org) using Rsubread v1.28.1 (Liao et al., 2013). Read summarization was performed on the gene level using featureCounts (Liao et al., 2014) using annotations from a modified version of *C. albicans* SC5314 haplotype A, which only contained protein coding genes. Multimapping read pairs, read pairs mapping across more than one gene, and read pairs in which ends mapped to different chromosomes were removed from downstream analyses. Genes that had <10 counts per million in at least two samples were discarded. Remaining gene counts were normalized using trimmed mean of M-values (Robinson & Oshlack, 2010). Differential expression

analysis was performed using limma v3.34.9 (Ritchie et al., 2015) with voom-transformed read counts (Law et al., 2014). Genes were considered differentially expressed when $P < 0.05$ after the false-discovery rate was controlled using Benjamini–Hochberg correction.

For mucin glycans RNA sequencing experiments, reads were mapped to the *C. albicans* SC5314 haplotype A genome, version A22-s05-m05-r03, retrieved from the *Candida* Genome Database (www.candidagenome.org) using the Galaxy Server (Afgan et al., 2018). Read summarization was performed on the gene level with annotations from a modified version of *C. albicans* SC5314 haplotype A. Multimapping read pairs, read pairs mapping across more than one gene, and read pairs in which ends mapped to different chromosomes were removed from downstream analyses. Differential expression analysis was performed using DESEQ2 (Love et al., 2014). Genes were considered differentially expressed when $P < 0.05$ after the false-discovery rate was controlled using Benjamini–Hochberg correction.

Functional category (pathway) assignments were obtained from *Candida* Genome Database Gene Ontology annotations and assessed using PANTHER (Mi et al., 2019). Over-representation of biological pathways in mucin was assessed using Fisher’s exact test followed by a Benjamini-Hochberg procedure for multiple corrections, for differentially expressed genes from $n=3$ replicates. Enrichment of pathways in MUC5AC glycans was determined based on mean \log_2 -transformed fold changes from $n=3$ replicates and calculated with the Mann-Whitney U -test followed by a Benjamini-Hochberg procedure for multiple corrections. Heat maps and scatter plots of gene expression data were constructed using GraphPad Prism.

Murine Wound C. albicans Protocol

Female, 8-week old, SKH-1 mice were anesthetized with isoflurane and given buprenorphine (0.05mg/kg) before wounding with a 6-mm punch biopsy to generate two identical full-thickness dermal wounds on the dorsal side of the mouse. Wounds were kept covered with an occlusive dressing (Opsite Flexifix) throughout the duration of the experiment. After a 24 h recovery period, wounds were inoculated with 30 ul volume of PBS containing 10^8 SC513 Eno1-mCherry yeast. Topical treatments of 30 ul of 0.5% MUC2, or PBS were administered to each wound on Day 1, 3, and 5 post-infection. Wounds were gently washed with 500 ul of sterile PBS and bandages changed prior to each treatment. Wound fluorescence was imaged daily with IVIS Lumina II

optical imaging system to assess fungal burden. At Day 5 and Day 7, wound biopsy specimens were collected and CFUs were calculated per gram of tissue.

The mice used in this experiment were housed at 72°F at 30% humidity with a 12-hour light/dark cycle. All care of laboratory animals was in accordance with institutional guidelines and approved by the Ohio State University Institutional Animal Care and Use Committee (IACUC) under 2017A00000033-R1.

Polystyrene attachment assay

Strain HGFP3 was pregrown overnight in YPD medium at 30 °C, diluted to $OD_{600}=0.1$, added into prewarmed RPMI medium in a polystyrene 96-well plate, and incubated at 37 °C for the time indicated in the figure legend. Medium was decanted and plates were washed three times with phosphate-buffered saline. Images were acquired with a confocal laser scanning microscope (LSM 800, Zeiss) equipped with a $\times 20/1.4$ NA objective. The excitation wavelength for GFP was 488 nm. Four images were recorded for each well and for at least three independent wells. Images were analyzed in Fiji as follows: each image was converted to 8-bit and the contrast was enhanced (0.4% saturated pixels), then thresholded to create a binary image. Each image was analyzed using the Analyze Particles tool to measure the surface area covered by cells as described previously (Kavanaugh et al., 2014). The mean surface area measurements of the images for each condition were calculated.

Biofilm formation assays and visualization

In vitro biofilm growth assays were carried out in RPMI medium by growing the biofilm directly on a 96-well polystyrene plate. Briefly, strain SC5314 was grown overnight in YPD at 30 °C, washed twice with phosphate-buffered saline, then diluted to $OD_{600}=0.5$ in 100 μ L of RPMI in a 96-well polystyrene plate. The inoculated plate was incubated at 37 °C for 90 min to facilitate attachment of yeast cells to the surface. Nonadherent cells were washed twice with phosphate-buffered saline, and samples were subsequently submerged in fresh RPMI. Biofilms were grown for 24 h at 37 °C. For CFU enumeration, the medium containing the planktonic cells was removed and plated on YPD plates. Biofilms were resuspended with phosphate-buffered saline, disrupted by pipetting, serially diluted in phosphate-buffered saline, and plated on YPD plates. Biofilms and planktonic cells were imaged using a Zeiss wide-field fluorescence microscope.

Coculture viability assays

An overnight SC5314 culture grown in YPD was diluted 1:100 into RPMI in a 96-well plate (Mattek) with or without 0.1% MUC5AC glycans and grown for 4 h with shaking at 37 °C. A control well without *C. albicans* was included. Concurrently, 2 mL of LB were inoculated with 40 µL *Pseudomonas aeruginosa* strain PA14 and grown for 4 h with shaking at 37 °C. RPMI was then removed from *C. albicans* and replaced with 200 µL SLB. *P. aeruginosa* was added to a final OD₆₀₀=0.25. At 0 h, 24 h, 48 h, and 72 h, the contents of the wells were homogenized and a 5-µL aliquot was serially diluted in phosphate-buffered saline. Dilutions were plated on YPD agar + Gm³⁰ + Tet⁶⁰ (to select for *C. albicans*) and Ceftrimide agar (to select for *P. aeruginosa*) and incubated overnight at 30 °C and 37 °C, respectively. Colonies were counted after incubation.

Confocal imaging of coculture

Images were acquired with a confocal laser scanning microscope (LSM 800; Zeiss) equipped with a ×63/1.4 NA oil-immersion objective. Images were analyzed using Zeiss ZEN v.2.1. *C. albicans* was stained with 20 µg/mL calcofluor white. The excitation and emission wavelengths for calcofluor white were 365 nm and 445 nm, respectively; the excitation and emission wavelengths for mCherry were 587 nm and 610 nm, respectively.

Glycan synthesis and analysis

All commercial reagents were used as supplied unless otherwise stated, and solvents were dried and distilled using standard techniques. Thin layer chromatography was performed on silica-coated glass plates (TLC Silica Gel 60 F₂₅₄, Merck) with detection via fluorescence, charring with 5% H₂SO_{4(aq)}, or staining with a ceric ammonium molybdate solution. Organic solutions were concentrated and/or evaporated to dry under vacuum in a water bath (<50 °C). Molecular sieves were dried at 400 °C under vacuum for 20-30 min prior to use. Amberlite IR-120H resin was washed extensively with MeOH and dried under vacuum prior to use. Medium-pressure liquid chromatography was performed using a CombiFlash Companion equipped with RediSep normal-phase flash columns, and solvent gradients refer to sloped gradients with concentrations reported as % v/v. Nuclear magnetic resonance spectra were recorded on a Bruker Avance DMX-500 (500 MHz) spectrometer, and assignments achieved with the assistance of 2D gCOSY, 2D gTOCSY, 2D gHSQC, and 2D gHMBC; chemical shifts are expressed in ppm and referenced to either Si(CH₃)₄ (for CDCl₃), residual CHD₂OD (for CD₃OD), or a MeOH internal standard (for D₂O).

Low-resolution electron-spray ionization mass spectrometry was performed with a Waters micromass ZQ. High-resolution mass spectrometry was performed with an Agilent 1100 LC equipped with a photodiode array detector, and a Micromass QTOF I equipped with a 4 GHz digital-time converter. Optical rotation was determined in a 10-cm cell at 20 °C using a Perkin-Elmer Model 341 polarimeter. High-performance liquid chromatography was performed with an Agilent 1100 LC equipped with an Atlantis T3 (3 mm, 2.1x100 mm) C18 column and ELSD detection.

References

- Afgan, E., Baker, D., Batut, B., van den Beek, M., Bouvier, D., Cech, M., Chilton, J., Clements, D., Coraor, N., Grüning, B. A., Guerler, A., Hillman-Jackson, J., Hiltemann, S., Jalili, V., Rasche, H., Soranzo, N., Goecks, J., Taylor, J., Nekrutenko, A., & Blankenberg, D. (2018). The Galaxy platform for accessible, reproducible and collaborative biomedical analyses: 2018 update. *Nucleic Acids Research*, *46*(W1), W537–W544. <https://doi.org/10.1093/nar/gky379>
- Amon, R., Reuven, E. M., Leviatan Ben-Arye, S., & Padler-Karavani, V. (2014). Glycans in immune recognition and response. *Carbohydrate Research*, *389*, 115–122. <https://doi.org/10.1016/j.carres.2014.02.004>
- Aoki, K., Perlman, M., Lim, J.-M., Cantu, R., Wells, L., & Tiemeyer, M. (2007). Dynamic developmental elaboration of N-linked glycan complexity in the *Drosophila melanogaster* embryo. *The Journal of Biological Chemistry*, *282*(12), 9127–9142. <https://doi.org/10.1074/jbc.M606711200>
- Banerjee, M., Thompson, D. S., Lazzell, A., Carlisle, P. L., Pierce, C., Monteagudo, C., López-Ribot, J. L., & Kadosh, D. (2008). UME6, a Novel Filament-specific Regulator of *Candida albicans* Hyphal Extension and Virulence. *Molecular Biology of the Cell*, *19*(4), 1354–1365. <https://doi.org/10.1091/mbc.E07-11-1110>
- Bergstrom, K. S. B., & Xia, L. (2013). Mucin-type O-glycans and their roles in intestinal homeostasis. *Glycobiology*, *23*(9), 1026–1037. <https://doi.org/10.1093/glycob/cwt045>
- Bockmühl, D. P., & Ernst, J. F. (2001). A Potential Phosphorylation Site for an A-Type Kinase in the Efg1 Regulator Protein Contributes to Hyphal Morphogenesis of *Candida albicans*. *Genetics*, *157*(4), 1523–1530. <https://doi.org/10.1093/genetics/157.4.1523>
- Brand, A., Barnes, J. D., Mackenzie, K. S., Odds, F. C., & Gow, N. A. R. (2008). Cell wall glycans and soluble factors determine the interactions between the hyphae of *Candida albicans* and *Pseudomonas aeruginosa*. *FEMS Microbiology Letters*, *287*(1), 48–55. <https://doi.org/10.1111/j.1574-6968.2008.01301.x>
- Brockhausen, I. (2006). Mucin-type O-glycans in human colon and breast cancer: Glycodynamics and functions. *EMBO Reports*, *7*(6), 599–604. <https://doi.org/10.1038/sj.embor.7400705>

- Calderone, R. A., & Fonzi, W. A. (2001). Virulence factors of *Candida albicans*. *Trends in Microbiology*, *9*(7), 327–335. [https://doi.org/10.1016/S0966-842X\(01\)02094-7](https://doi.org/10.1016/S0966-842X(01)02094-7)
- Celli, J., Gregor, B., Turner, B., Afdhal, N. H., Bansil, R., & Erramilli, S. (2005). Viscoelastic Properties and Dynamics of Porcine Gastric Mucin. *Biomacromolecules*, *6*(3), 1329–1333. <https://doi.org/10.1021/bm0493990>
- Chatterjee, M., Pushkaran, A. C., Vasudevan, A. K., Menon, K. K. N., Biswas, R., & Mohan, C. G. (2018). Understanding the adhesion mechanism of a mucin binding domain from *Lactobacillus fermentum* and its role in enteropathogen exclusion. *International Journal of Biological Macromolecules*, *110*, 598–607. <https://doi.org/10.1016/j.ijbiomac.2017.10.107>
- Corfield, A. P. (2015). Mucins: A biologically relevant glycan barrier in mucosal protection. *Biochimica et Biophysica Acta (BBA) - General Subjects*, *1850*(1), 236–252. <https://doi.org/10.1016/j.bbagen.2014.05.003>
- Cummings, R. D., & Pierce, J. M. (2014). The Challenge and Promise of Glycomics. *Chemistry & Biology*, *21*(1), 1–15. <https://doi.org/10.1016/j.chembiol.2013.12.010>
- Donohue, D. S., Ielasi, F. S., Goossens, K. V. Y., & Willaert, R. G. (2011). The N-terminal part of Als1 protein from *Candida albicans* specifically binds fucose-containing glycans. *Molecular Microbiology*, *80*(6), 1667–1679. <https://doi.org/10.1111/j.1365-2958.2011.07676.x>
- Dube, D. H., & Bertozzi, C. R. (2005). Glycans in cancer and inflammation—Potential for therapeutics and diagnostics. *Nature Reviews Drug Discovery*, *4*(6), 477–488. <https://doi.org/10.1038/nrd1751>
- Feng, Q., Summers, E., Guo, B., & Fink, G. (1999). Ras signaling is required for serum-induced hyphal differentiation in *Candida albicans*. *Journal of Bacteriology*, *181*(20), 6339–6346. <https://doi.org/10.1128/JB.181.20.6339-6346.1999>
- Ganguly, S., & Mitchell, A. P. (2011). Mucosal biofilms of *Candida albicans*. *Current Opinion in Microbiology*, *14*(4), 380–385. <https://doi.org/10.1016/j.mib.2011.06.001>
- Giancetti, E., Arena, A., & Fierabracci, A. (2021). Sialic Acid-Siglec Axis in Human Immune Regulation, Involvement in Autoimmunity and Cancer and Potential Therapeutic Treatments. *International Journal of Molecular Sciences*, *22*(11), 5774. <https://doi.org/10.3390/ijms22115774>

- Granger, B. L., Flenniken, M. L., Davis, D. A., Mitchell, A. P., & Cutler, J. E. (2005). Yeast wall protein 1 of *Candida albicans*. *Microbiology (Reading, England)*, *151*(Pt 5), 1631–1644. <https://doi.org/10.1099/mic.0.27663-0>
- Han, T.-L., Cannon, R. D., & Villas-Bôas, S. G. (2011). The metabolic basis of *Candida albicans* morphogenesis and quorum sensing. *Fungal Genetics and Biology*, *48*(8), 747–763. <https://doi.org/10.1016/j.fgb.2011.04.002>
- Hevey, R. (2019a). Strategies for the Development of Glycomimetic Drug Candidates. *Pharmaceuticals*, *12*(2), 55. <https://doi.org/10.3390/ph12020055>
- Hevey, R. (2019b). Bioisosteres of Carbohydrate Functional Groups in Glycomimetic Design. *Biomimetics*, *4*(3), 53. <https://doi.org/10.3390/biomimetics4030053>
- Hogan, D. A., & Kolter, R. (2002). *Pseudomonas-Candida* Interactions: An Ecological Role for Virulence Factors. *Science*, *296*(5576), 2229–2232. <https://doi.org/10.1126/science.1070784>
- Huang, Y., Mechref, Y., & Novotny, M. V. (2001). Microscale nonreductive release of O-linked glycans for subsequent analysis through MALDI mass spectrometry and capillary electrophoresis. *Analytical Chemistry*, *73*(24), 6063–6069. <https://doi.org/10.1021/ac015534c>
- Jin, C., Kenny, D. T., Skoog, E. C., Padra, M., Adamczyk, B., Vitizeva, V., Thorell, A., Venkatakrishnan, V., Lindén, S. K., & Karlsson, N. G. (2017). Structural Diversity of Human Gastric Mucin Glycans. *Molecular & Cellular Proteomics: MCP*, *16*(5), 743–758. <https://doi.org/10.1074/mcp.M116.067983>
- Kavanaugh, N. L., Zhang, A. Q., Nobile, C. J., Johnson, A. D., & Ribbeck, K. (2014). Mucins Suppress Virulence Traits of *Candida albicans*. *MBio*, *5*(6), e01911-14. <https://doi.org/10.1128/mBio.01911-14>
- Kennedy, M. J., & Volz, P. A. (1985). Ecology of *Candida albicans* gut colonization: Inhibition of *Candida* adhesion, colonization, and dissemination from the gastrointestinal tract by bacterial antagonism. *Infection and Immunity*, *49*(3), 654–663. <https://doi.org/10.1128/IAI.49.3.654-663.1985>
- Krupa, L., Bajka, B., Staroń, R., Dupont, D., Singh, H., Gutkowski, K., & Macierzanka, A. (2020). Comparing the permeability of human and porcine small intestinal mucus for

- particle transport studies. *Scientific Reports*, 10(1), 20290.
<https://doi.org/10.1038/s41598-020-77129-4>
- Kudelka, M. R., Ju, T., Heimburg-Molinaro, J., & Cummings, R. D. (2015). Simple Sugars to Complex Disease—Mucin-Type O-Glycans in Cancer. *Advances in Cancer Research*, 126, 53–135. <https://doi.org/10.1016/bs.acr.2014.11.002>
- Law, C. W., Chen, Y., Shi, W., & Smyth, G. K. (2014). voom: Precision weights unlock linear model analysis tools for RNA-seq read counts. *Genome Biology*, 15(2), R29.
<https://doi.org/10.1186/gb-2014-15-2-r29>
- Lee, K. L., Buckley, H. R., & Campbell, C. C. (1975). An amino acid liquid synthetic medium for the development of mycelial and yeast forms of *Candida Albicans*. *Sabouraudia*, 13(2), 148–153. <https://doi.org/10.1080/00362177585190271>
- Leuker, C. E., Sonneborn, A., Delbrück, S., & Ernst, J. F. (1997). Sequence and promoter regulation of the PCK1 gene encoding phosphoenolpyruvate carboxykinase of the fungal pathogen *Candida albicans*. *Gene*, 192(2), 235–240. [https://doi.org/10.1016/s0378-1119\(97\)00069-3](https://doi.org/10.1016/s0378-1119(97)00069-3)
- Liao, Y., Smyth, G. K., & Shi, W. (2013). The Subread aligner: Fast, accurate and scalable read mapping by seed-and-vote. *Nucleic Acids Research*, 41(10), e108.
<https://doi.org/10.1093/nar/gkt214>
- Liao, Y., Smyth, G. K., & Shi, W. (2014). featureCounts: An efficient general purpose program for assigning sequence reads to genomic features. *Bioinformatics*, 30(7), 923–930.
<https://doi.org/10.1093/bioinformatics/btt656>
- Lieleg, O., Lieleg, C., Bloom, J., Buck, C. B., & Ribbeck, K. (2012). Mucin biopolymers as broad-spectrum antiviral agents. *Biomacromolecules*, 13(6), 1724–1732.
<https://doi.org/10.1021/bm3001292>
- Lindén, S. K., Sheng, Y. H., Every, A. L., Miles, K. M., Skoog, E. C., Florin, T. H. J., Sutton, P., & McGuckin, M. A. (2009). MUC1 limits *Helicobacter pylori* infection both by steric hindrance and by acting as a releasable decoy. *PLoS Pathogens*, 5(10), e1000617.
<https://doi.org/10.1371/journal.ppat.1000617>
- Liu, Y., McBride, R., Stoll, M., Palma, A. S., Silva, L., Agravat, S., Aoki-Kinoshita, K. F., Campbell, M. P., Costello, C. E., Dell, A., Haslam, S. M., Karlsson, N. G., Khoo, K.-H., Kolarich, D., Novotny, M. V., Packer, N. H., Ranzinger, R., Rapp, E., Rudd, P. M., ...

- Smith, D. F. (2017). The minimum information required for a glycomics experiment (MIRAGE) project: Improving the standards for reporting glycan microarray-based data. *Glycobiology*, *27*(4), 280–284. <https://doi.org/10.1093/glycob/cww118>
- Lohse, M. B., Gulati, M., Johnson, A. D., & Nobile, C. J. (2018). Development and regulation of single- and multi-species *Candida albicans* biofilms. *Nature Reviews Microbiology*, *16*(1), 19–31. <https://doi.org/10.1038/nrmicro.2017.107>
- Love, M. I., Huber, W., & Anders, S. (2014). Moderated estimation of fold change and dispersion for RNA-seq data with DESeq2. *Genome Biology*, *15*(12), 550. <https://doi.org/10.1186/s13059-014-0550-8>
- Lu, Y., Su, C., & Liu, H. (2014). *Candida albicans* hyphal initiation and elongation. *Trends in Microbiology*, *22*(12), 707–714. <https://doi.org/10.1016/j.tim.2014.09.001>
- Mehta, A. Y., & Cummings, R. D. (2020). GlycoGlyph: A glycan visualizing, drawing and naming application. *Bioinformatics (Oxford, England)*, *36*(11), 3613–3614. <https://doi.org/10.1093/bioinformatics/btaa190>
- Mi, H., Muruganujan, A., Huang, X., Ebert, D., Mills, C., Guo, X., & Thomas, P. D. (2019). Protocol Update for large-scale genome and gene function analysis with the PANTHER classification system (v.14.0). *Nature Protocols*, *14*(3), 703–721. <https://doi.org/10.1038/s41596-019-0128-8>
- Morales, D. K., & Hogan, D. A. (2010). *Candida albicans* interactions with bacteria in the context of human health and disease. *PLoS Pathogens*, *6*(4), e1000886. <https://doi.org/10.1371/journal.ppat.1000886>
- Nobile, C. J., Fox, E. P., Nett, J. E., Sorrells, T. R., Mitrovich, Q. M., Hernday, A. D., Tuch, B. B., Andes, D. R., & Johnson, A. D. (2012). A Recently Evolved Transcriptional Network Controls Biofilm Development in *Candida albicans*. *Cell*, *148*(1–2), 126–138. <https://doi.org/10.1016/j.cell.2011.10.048>
- Nobile, C. J., & Johnson, A. D. (2015). *Candida albicans* Biofilms and Human Disease. *Annual Review of Microbiology*, *69*, 71–92. <https://doi.org/10.1146/annurev-micro-091014-104330>
- Pappas, P. G., Lionakis, M. S., Arendrup, M. C., Ostrosky-Zeichner, L., & Kullberg, B. J. (2018). Invasive candidiasis. *Nature Reviews Disease Primers*, *4*(1), 1–20. <https://doi.org/10.1038/nrdp.2018.26>

- Perlin, D. S. (2015). Antifungals: From Genomics to Resistance and the Development of Novel Agents. *Clinical Infectious Diseases*, 61(7), 1213–1214.
<https://doi.org/10.1093/cid/civ548>
- Ritchie, M. E., Phipson, B., Wu, D., Hu, Y., Law, C. W., Shi, W., & Smyth, G. K. (2015). Limma powers differential expression analyses for RNA-sequencing and microarray studies. *Nucleic Acids Research*, 43(7), e47. <https://doi.org/10.1093/nar/gkv007>
- Robinson, M. D., & Oshlack, A. (2010). A scaling normalization method for differential expression analysis of RNA-seq data. *Genome Biology*, 11(3), R25.
<https://doi.org/10.1186/gb-2010-11-3-r25>
- Shapiro, R. S., Robbins, N., & Cowen, L. E. (2011). Regulatory Circuitry Governing Fungal Development, Drug Resistance, and Disease. *Microbiology and Molecular Biology Reviews : MMBR*, 75(2), 213–267. <https://doi.org/10.1128/MMBR.00045-10>
- Sudbery, P. E. (2011). Growth of *Candida albicans* hyphae. *Nature Reviews Microbiology*, 9(10), 737–748. <https://doi.org/10.1038/nrmicro2636>
- Tabak, L. A. (2010). The role of mucin-type O-glycans in eukaryotic development. *Seminars in Cell & Developmental Biology*, 21(6), 616–621.
<https://doi.org/10.1016/j.semcdb.2010.02.001>
- Tailford, L. E., Crost, E. H., Kavanaugh, D., & Juge, N. (2015). Mucin glycan foraging in the human gut microbiome. *Frontiers in Genetics*, 6.
<https://doi.org/10.3389/fgene.2015.00081>
- Turner, B. S., Bhaskar, K. R., Hadzopoulou-Cladaras, M., & LaMont, J. T. (1999). Cysteine-rich regions of pig gastric mucin contain von Willebrand factor and cystine knot domains at the carboxyl terminal. *Biochimica et Biophysica Acta (BBA) - Gene Structure and Expression*, 1447(1), 77–92. [https://doi.org/10.1016/S0167-4781\(99\)00099-8](https://doi.org/10.1016/S0167-4781(99)00099-8)
- Valle Arevalo, A., & Nobile, C. J. (2020). Interactions of microorganisms with host mucins: A focus on *Candida albicans*. *FEMS Microbiology Reviews*, 44(5), 645–654.
<https://doi.org/10.1093/femsre/fuaa027>
- Wagner, C. E., Turner, B. S., Rubinstein, M., McKinley, G. H., & Ribbeck, K. (2017). A rheological study of the association and dynamics of MUC5AC gels. *Biomacromolecules*, 18(11), 3654–3664. <https://doi.org/10.1021/acs.biomac.7b00809>

- Wang, B. X., Wu, C. M., & Ribbeck, K. (2021). Home, sweet home: How mucus accommodates our microbiota. *The FEBS Journal*, *288*(6), 1789–1799. <https://doi.org/10.1111/febs.15504>
- Watanabe, Y., Aoki-Kinoshita, K. F., Ishihama, Y., & Okuda, S. (2021). GlycoPOST realizes FAIR principles for glycomics mass spectrometry data. *Nucleic Acids Research*, *49*(D1), D1523–D1528. <https://doi.org/10.1093/nar/gkaa1012>
- Wheeler, K. M., Cárcamo-Oyarce, G., Turner, B. S., Dellos-Nolan, S., Co, J. Y., Lehoux, S., Cummings, R. D., Wozniak, D. J., & Ribbeck, K. (2019). Mucin glycans attenuate the virulence of *Pseudomonas aeruginosa* in infection. *Nature Microbiology*, *4*(12), 2146–2154. <https://doi.org/10.1038/s41564-019-0581-8>
- Zheng, X., Wang, Y., & Wang, Y. (2004). Hgc1, a novel hypha-specific G1 cyclin-related protein regulates *Candida albicans* hyphal morphogenesis. *The EMBO Journal*, *23*(8), 1845–1856. <https://doi.org/10.1038/sj.emboj.7600195>

Acknowledgments

The authors thank B. Wang and V.P. Patil for comments on the manuscript. This research was supported by The NIH NIBIB award R01EB017755-04 (OSP 6940725) (to K.R.), the MRSEC Program of the National Science Foundation under award DMR-1419807 (to K.R.), the National Science Foundation Career award PHY1454673 (to K.R.), the U.S. Army Research Office under cooperative agreement W911NF-19-2-0026 for the Institute for Collaborative Biotechnologies (to K.R.), the core center grant P30-ES002109 from the National Institute of Environmental Health Sciences P30-ES002109 (to K.R.), the Toxicology Training Grant support T32-ES007020 (to J.T), the National Center for Functional Glycomics Grant P41GM103694 (to R.D.C.), the Swiss National Science Spark Grant Foundation CRSK-3_196773 (to R.H), and the NIH NIGMS award R35GM124594 (to C.J.N.), by the Kamangar family in the form of an endowed chair (to C.J.N.). The content is the sole responsibility of the authors and does not represent the views of the funders. The funders had no role in the design of the study; in the collection, analyses, or interpretation of data; in the writing of the manuscript; or in the decision to publish the results.

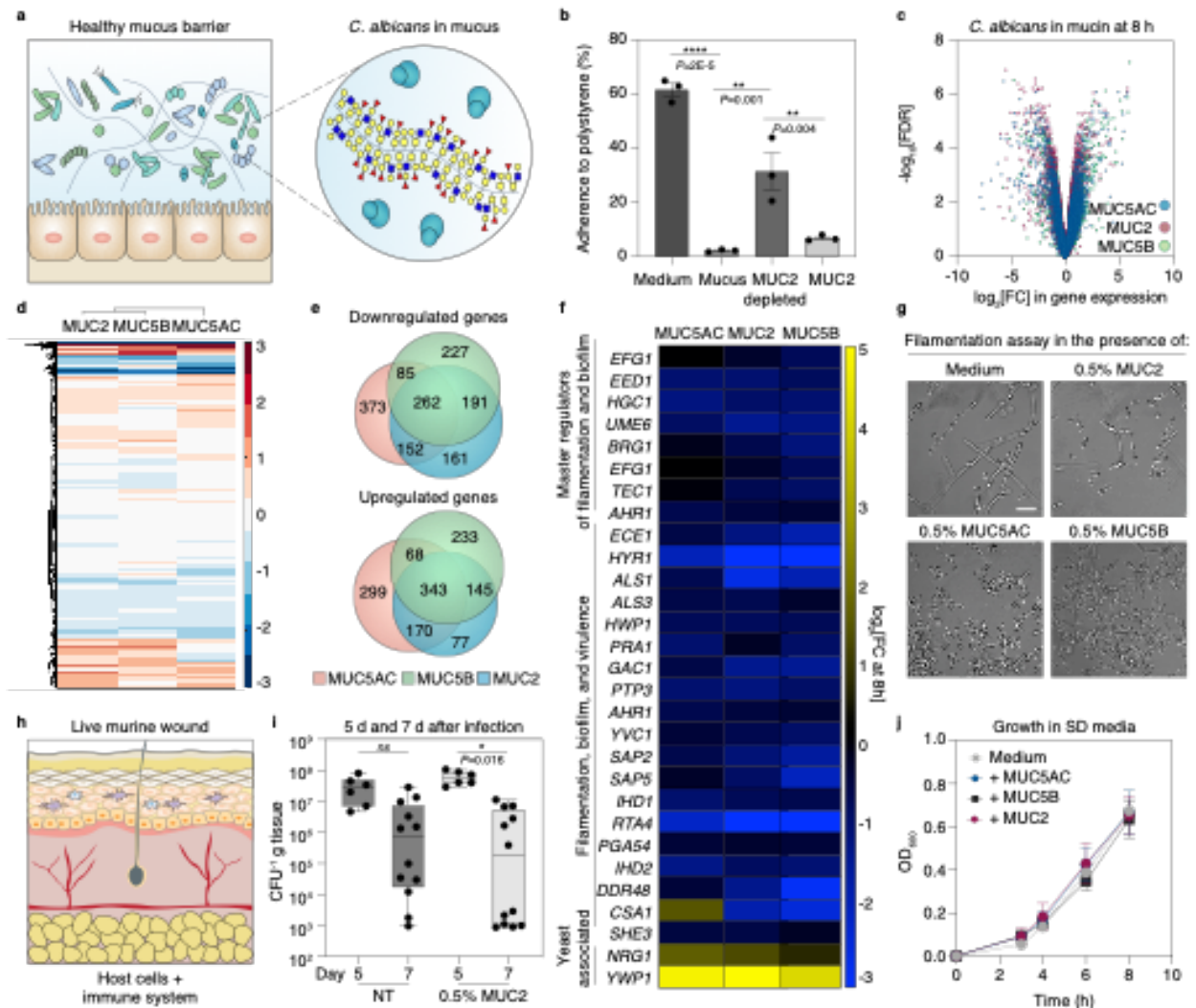


Figure 2.1: Mucins across major mucosal surfaces share a conserved function in attenuating *C. albicans* virulence *in vitro* and *in vivo*

a) The mucus barrier hosts a diverse range of microorganisms while limiting infections. *Candida albicans*, an opportunistic fungal pathogen, resides within the mucosa.

b) Native mucus suppresses fungal adherence to polystyrene wells. The depletion of intestinal mucus components increases fungal adherence. Supplementation of mucus filtrates with purified MUC2 results in reduced adherence. Bars indicate mean \pm SEM from $n=3$ biologically independent replicates using fluorescence images. Significance was assessed using one-way ANOVA followed by Dunnett's multiple comparisons test; **** $P < 0.0001$ ** $P < 0.01$.

c) MUC5AC, MUC5B, and MUC2 elicit global transcriptional responses in *C. albicans*.

d) Dendrogram and hierarchical clustering heat map of genome-wide expression profiles from MUC5AC, MUC2, and MUC5B. Clustering was performed first along the sample dimension and

then along the individual gene dimension using the Matlab clustergram function with Euclidean distances and Ward's linkage method. Color scale bar units are in SDs.

e) Venn diagrams indicate the number of genes differentially expressed (FDR-adjusted $P < 0.05$) after exposure to mucins.

f) RNA sequencing data for selected genes belonging to filamentation, biofilm formation, and pathogenesis.

g) Mucins across three mucosal surfaces suppress filamentation. Phase-contrast images of SC5314 cells grown in RPMI medium with or without mucins at 37 °C for 8 h. Scale bar, 20 μm .

h) Fungal viability was monitored in a live dermal wound model.

i) Fungal burden on murine puncture wounds at 5 and 7 d after treatment with MUC2 or a mock-treatment (NT) control. Symbols represent colony-forming units from $n=6$ biologically independent replicates. The center bars indicate the median, the box limits indicate the upper and lower quartiles and the whiskers indicate the minimum and maximum values. Significance was assessed using Welch and Brown-Forsythe ANOVA (assumes unequal variance) followed by Dunnett T3 multiple comparisons test; $*P=0.016$.

j) Growth is not altered by mucins in the synthetic defined medium (SD). Data are the mean optical density at 600 nm (OD_{600}) \pm SEM; $n=4$ (MUC5B, MUC5AC), $n=6$ (Medium, MUC2) biologically independent replicates.

For **c,d,e,f**, a complete list of FC values and FDR-adjusted P values is provided in Supplementary Data 1. P values were FDR-adjusted using Benjamini–Hochberg correction for multiple comparisons. Data are from $n=3$ biologically independent replicates.

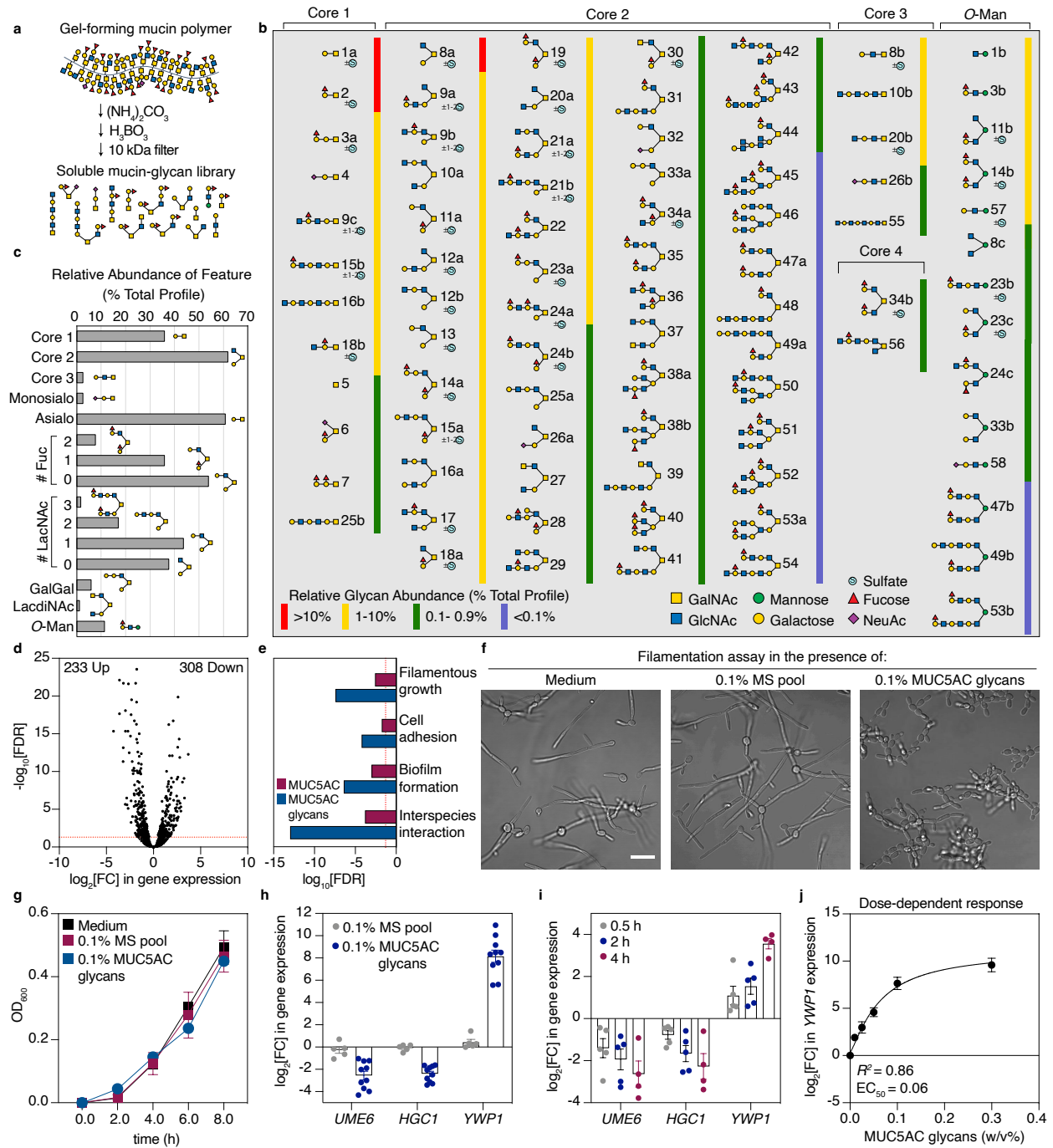


Figure 2.2: Mucin glycans potentially inhibit filamentation in a time- and dose-dependent manner

a) Mucin glycans were isolated (Methods) from the protein backbone using alkaline β -elimination.

b) Structural diversity and relative abundances of MUC5AC glycans analyzed by NSI-MS (Methods). The complete list of structures is listed in Supplementary Table 2.1. Negative mode

NSI-MS detected sulfation on a subset of *O*-glycans, indicated with the letter S in a cyan circle (Supplementary Table 2.2). Neu5Ac, *N*-acetylneuraminic acid.

c) Relative abundances of glycan features in the MUC5AC glycan pool. LacNAc, *N*-acetyllactosamine or Gal β 1-3/4GlcNAc; GalGal, Gal α 1-3Gal; LacdiNAc, GalNAc β 1-4GlcNAc; O-Man, mannose linked α 1 to serine or threonine.

d) MUC5AC glycans elicit global transcriptional responses in *C. albicans*.

e) Functional enrichment analyses reveal key virulence pathways among downregulated genes. Significance of enrichment was calculated using Mann-Whitney *U* test based on mean log₂-transformed FCs from *n*=3 biologically independent replicates. The dotted line represents the threshold for significance (FDR-adjusted *P*<0.05).

f) MUC5AC glycans inhibit filamentation. Phase-contrast images of *C. albicans* SC5314 cells grown in RPMI medium alone, the monosaccharide pool or mucin glycans at 37 °C for 8 h. Scale bar, 20 μ m.

g) Growth is not altered in the presence of the MS pool or mucin glycans in synthetic defined medium (SD). Data are mean OD₆₀₀ \pm SEM for *n*=3 biologically independent replicates.

h) Mucin glycans, unlike their monosaccharide components, downregulate signature virulence genes. Bars indicate mean \pm SEM from *n*=5 (MS pool), *n*=10 (MUC5AC glycans) biologically independent replicates.

i) MUC5AC glycans downregulate virulence gene expression over a prolonged time course. Bars indicate mean \pm SEM from *n*=5 (0.5 h, 2 h), *n*=4 (4 h) biologically independent replicates.

j) Mucin glycans regulate *YWPI* expression in a concentration-dependent manner. Dotted lines indicate the 95% confidence interval from *n*=3 (0.01%, 0.025%, and 0.3% MG), *n*=5 (0.05% and 0.1% MG) biologically independent replicates.

For **d,e**, a complete list of FC values and FDR-adjusted *P*-values is provided in Supplementary Data 3 from *n*=3 biologically independent replicates. *P* values were FDR-adjusted using Benjamini–Hochberg correction for multiple comparisons.

For **h,i,j**, data are log₂-transformed qPCR measurements normalized to a control gene (*ACT1*).

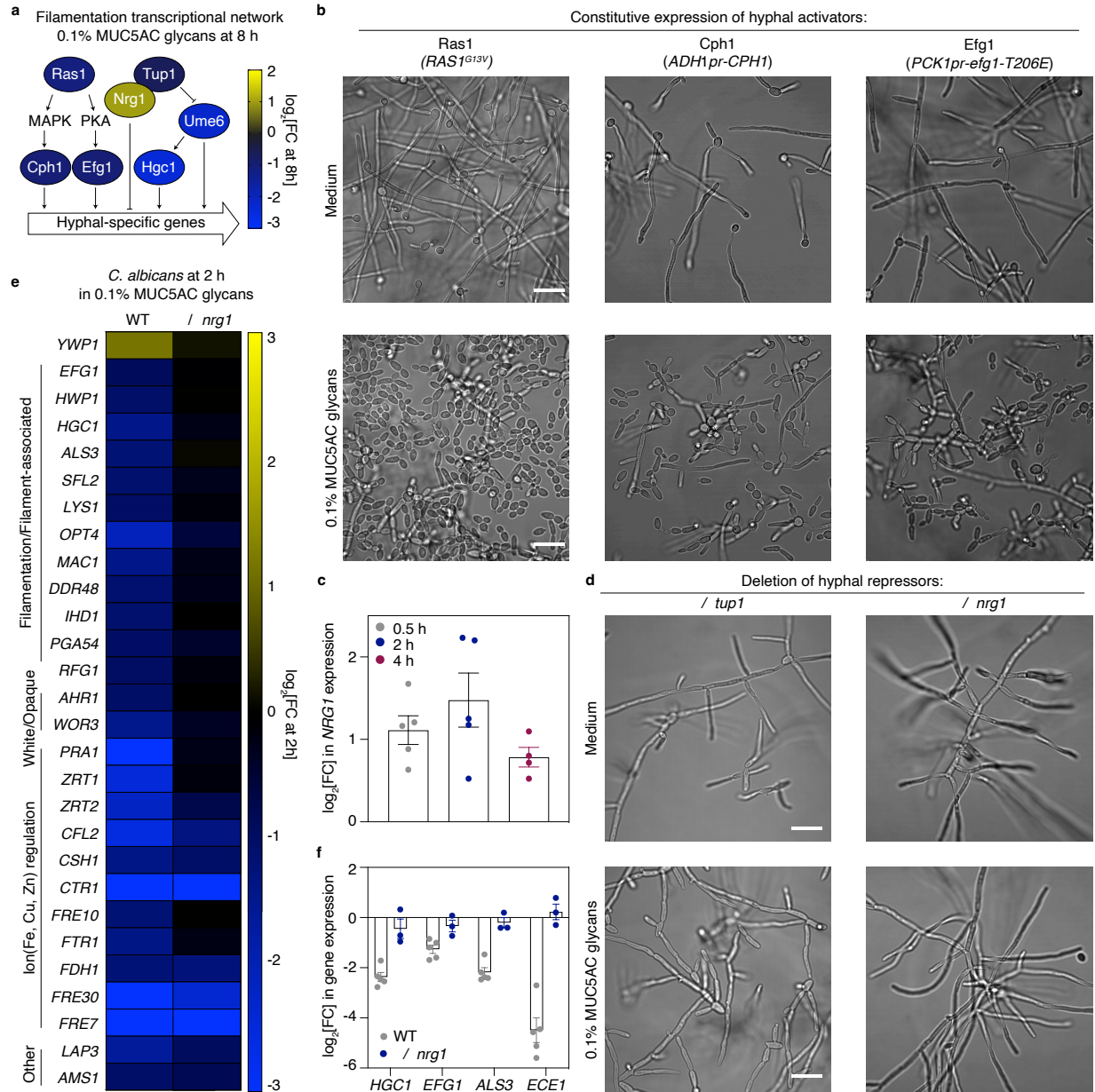


Figure 2.3: Mucin glycans act via Nrg1 to prevent filamentation and hyphal gene expression

a) MUC5AC glycans suppress the expression of key activators of the filamentation pathway. RNA sequencing data for selected genes that are differentially regulated in the presence of MUC5AC glycans from $n=3$ biologically independent replicates (Supplementary Data 3). P values were adjusted for multiple comparisons using Benjamini–Hochberg correction to obtain FDR-adjusted P values.

b) MUC5AC glycans inhibit filamentation in strains hyperactivating the cAMP and MAPK pathways. Phase-contrast images of cells of the indicated genotype were grown in the presence or

absence of MUC5AC glycans in Spider medium (*PCKpr-efg1-T206E*) or RPMI medium (*prADHI-CPHI, RAS1^{G13V}*) at 37 °C for 4 h. Scale bar, 20 μm.

c) Expression of *NRG1* in wild-type (WT) SC5314 cells after 0.5 h, 2 h, or 4 h in 0.1% MUC5AC glycans (versus growth in medium alone). Gene expression was measured with qRT-PCR and normalized to a control gene (*ACT1*). Bars indicate the mean ± SEM from $n=5$ (0.5 h, 2 h), $n=4$ (4 h) biologically independent replicates.

d) Loss of *NRG1* or *TUP1* leads to hyperfilamentation in the presence or absence of mucin glycans. Phase-contrast images of cells of the indicated genotype were grown in the presence or absence of MUC5AC glycans in RPMI medium at 37 °C for 4 h. Scale bar, 20 μm.

e) FC values for gene-expression changes in WT SC5314 or $\Delta/\Delta nrg1$ mutant cells after 2 h in MUC5AC glycans (versus growth in medium alone). Complete lists of FC values and FDR-adjusted P values from $n=2$ biologically independent replicates are provided in Supplementary Data 5 and 6. P values were adjusted for multiple comparisons using Benjamini–Hochberg correction to obtain FDR-adjusted P values.

f) FC values for gene-expression changes in WT SC5314 or $\Delta/\Delta nrg1$ cells after 2 h in 0.1% MUC5AC glycans (versus growth in RPMI medium alone). Gene expression was measured with qRT-PCR and normalized to a control gene (*ACT1*). Bars indicate the mean ± SEM from $n=5$ (WT), $n=3$ ($\Delta/\Delta nrg1$) biologically independent replicates.

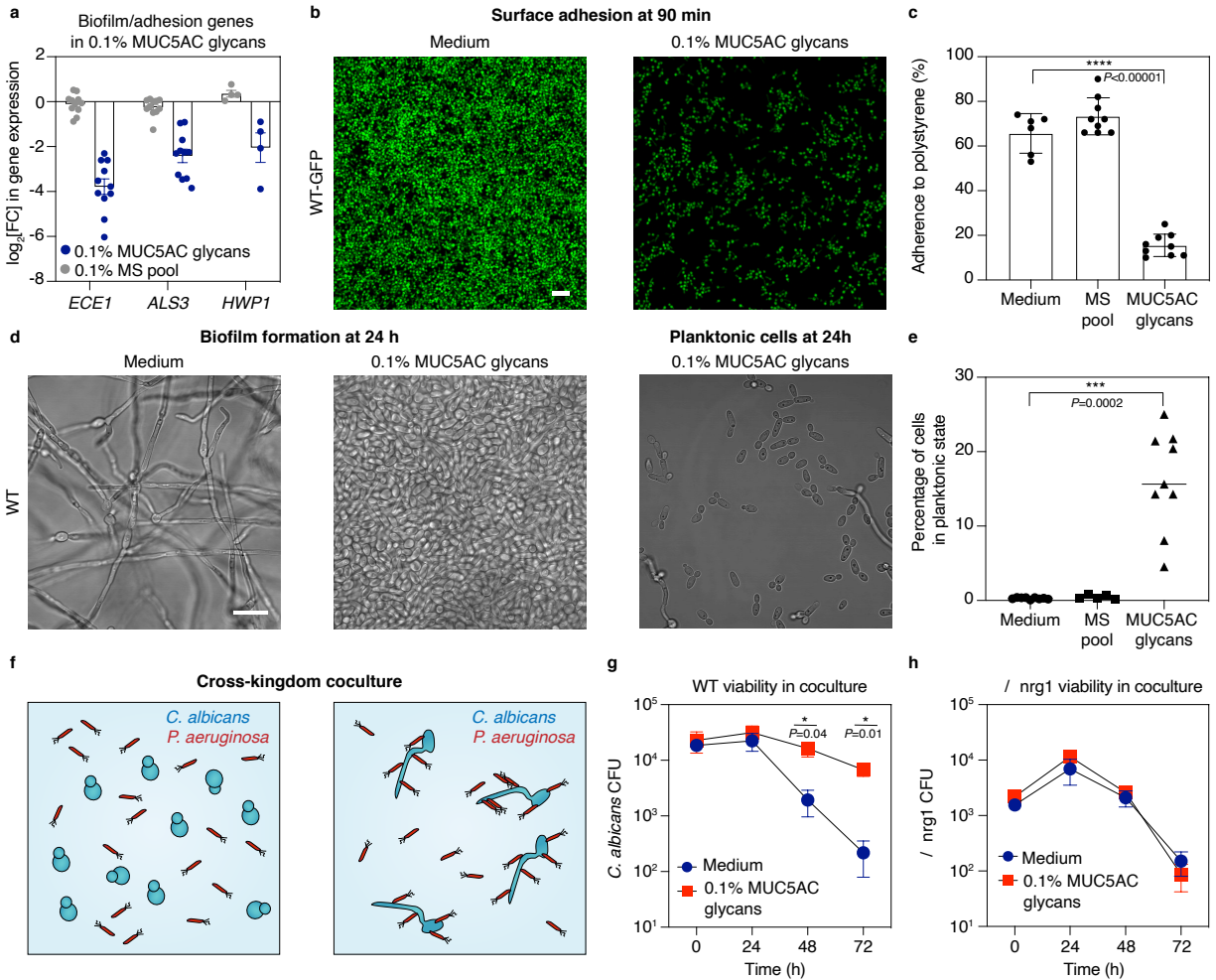


Figure 2.4: Mucin glycans downregulate virulence cascades and mediate fungal-bacterial dynamics

a) Mucin glycans downregulate the expression of adhesion-related genes. Gene expression was measured by qRT-PCR from $n=11$ (*ECE1*, *ALS3*), $n=4$ (*HWP1*) biologically independent replicates. Bars indicate mean \pm SEM. MS, monosaccharide.

b) Fluorescence microscopy images assaying adhesion of wild-type (WT) *C. albicans* expressing green fluorescent protein (GFP) at 90 min in the presence or absence of MUC5AC glycans. Scale bar, 50 μ m.

c) Quantification of adhesion to polystyrene wells using fluorescence images from $n=9$ (MS pool, MUC5AC glycans), $n=6$ (Media) biologically independent replicates. Bars indicate mean \pm SEM. Significance was assessed using ordinary one-way ANOVA followed by Dunnett's multiple comparisons test; **** $P<0.0001$.

- d) Phase-contrast images of (left, middle) biofilm and (right) planktonic WT cells grown for 24 h in the (left) absence or (middle, right) presence of MUC5AC glycans. Non-adhered (planktonic) cells in the MUC5AC glycan-exposed biofilms were imaged (right). Scale bar, 20 μ m.
- e) Quantification of CFUs in the supernatant (planktonic cells) relative to total CFU from adhered cells in the biofilm from $n=9$ (Media, MUC5AC glycans) and $n=5$ (MS pool) biologically independent replicates. Significance was assessed using Brown-Forsythe and Welch ANOVA tests (assumes unequal variance) followed by Dunnett T3 multiple comparisons test; *** $P=0.0002$.
- f) Schematics of *in vitro* *P. aeruginosa* (bacteria) and *C. albicans* (yeast) interactions. Left: *P. aeruginosa* does not effectively kill yeast form *C. albicans*. Right: In contrast, *P. aeruginosa* adheres to *C. albicans* hyphae and secretes toxins, leading to fungal death.
- g) *C. albicans* yeast cells were diluted into RPMI medium with or without MUC5AC glycans for 4 h. *P. aeruginosa* cells ($OD_{600}=0.25$) in spent LB were added to the *C. albicans* cells with or without MUC5AC glycans and cocultured at 37 °C for 72 h. Data are mean \pm SEM; $n=5$ biologically independent replicates. Significance was assessed using two-tailed Student's *t*-tests with Welch's correction; $P=0.04$ (48 h) $P=0.014$ (72 h).
- h) Cultures of $\Delta/\Delta nrg1$ cells were treated as in (h) with or without MUC5AC glycans and cocultured with *P. aeruginosa* at 37 °C for 72 h; $n=5$ biologically independent replicates.
- For **g,h**, the fungal viable cell population was determined daily by plating.

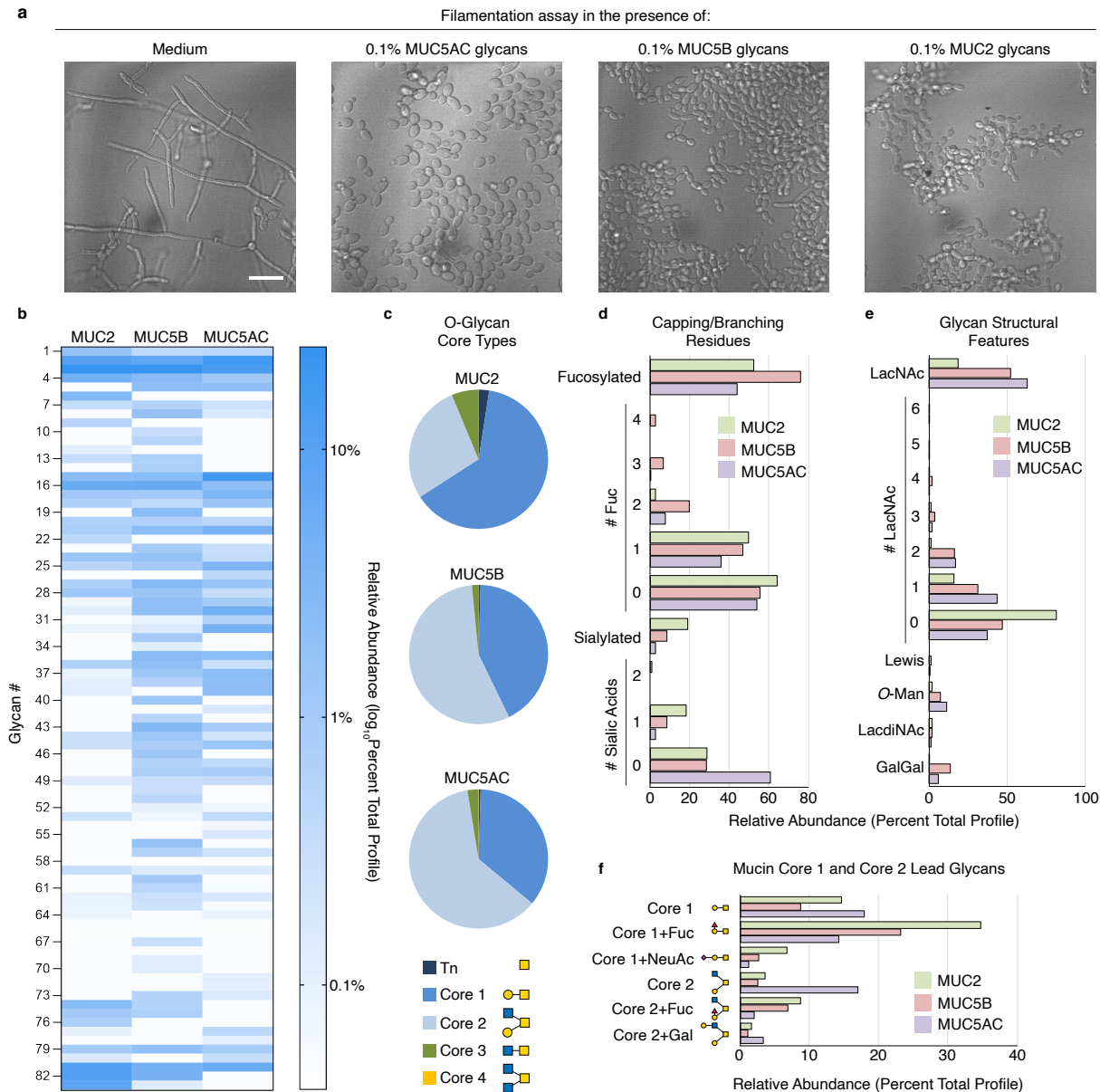


Figure 2.5: Native mucins across microbial niches display a plethora of complex glycan structures with regulatory potential

a) Wild-type *C. albicans* SC5314 cells were diluted into RPMI medium with or without mucin glycan libraries purified from MUC5AC, MUC2, and MUC5B and cultured at 37 °C for 8 h. Phase-contrast images of *C. albicans* revealed that mucin glycans across three mucin types suppress filamentation. Scale bar, 20 μm.

b) Heatmap presenting log₁₀ values for the relative abundances of individual glycans released from the three mucins and detected by NSI-MS as permethylated derivatives (Supplementary

Table 2). MUC2, MUC5B, and MUC5AC are dominated by *O*-GalNAc Core 1 (glycans #3, 4, 5) and Core 2 derived glycan structures (glycans #15, 16, 17). Glycans #81, 82, and 83 represent non-reducing terminal disaccharides of incomplete core structures likely generated through peeling reactions during preparation.

c) Distribution of *O*-glycans by GalNAc-initiated core type on each mucin. Minimal core structures are shown in the legend. The relative abundances of each glycan containing a minimal core structure was summed for comparison.

d) The relative abundances of glycans carrying capping/branching fucose or sialic acid residues were summed for comparison across the three mucins. Glycans with between 0 and 4 fucose residues or between 0 and 2 sialic acid residues were detected. The relative abundances of sialylated and fucosylated glycans was calculated based on the total glycan profile, while the relative abundances of glycans lacking sialic acid or fucose was calculated based on the subset of glycans in the total profile that are structurally amenable to sialylation or fucosylation.

e) The relative abundances of glycans that possess the indicated structural features or motifs were summed for comparison across the three mucins. Abbreviations for the features are as previously described (Fig. 2). The Lewis designation refers to the detection of a fucosylated LacNAc residue.

f) The relative abundance of the six most prevalent Core 1 and Core 2 glycans shared across all three mucins is presented. These mucin-derived glycans defined structures that served as synthetic targets for generating lead compounds for subsequent functional analysis (Fig. 6).

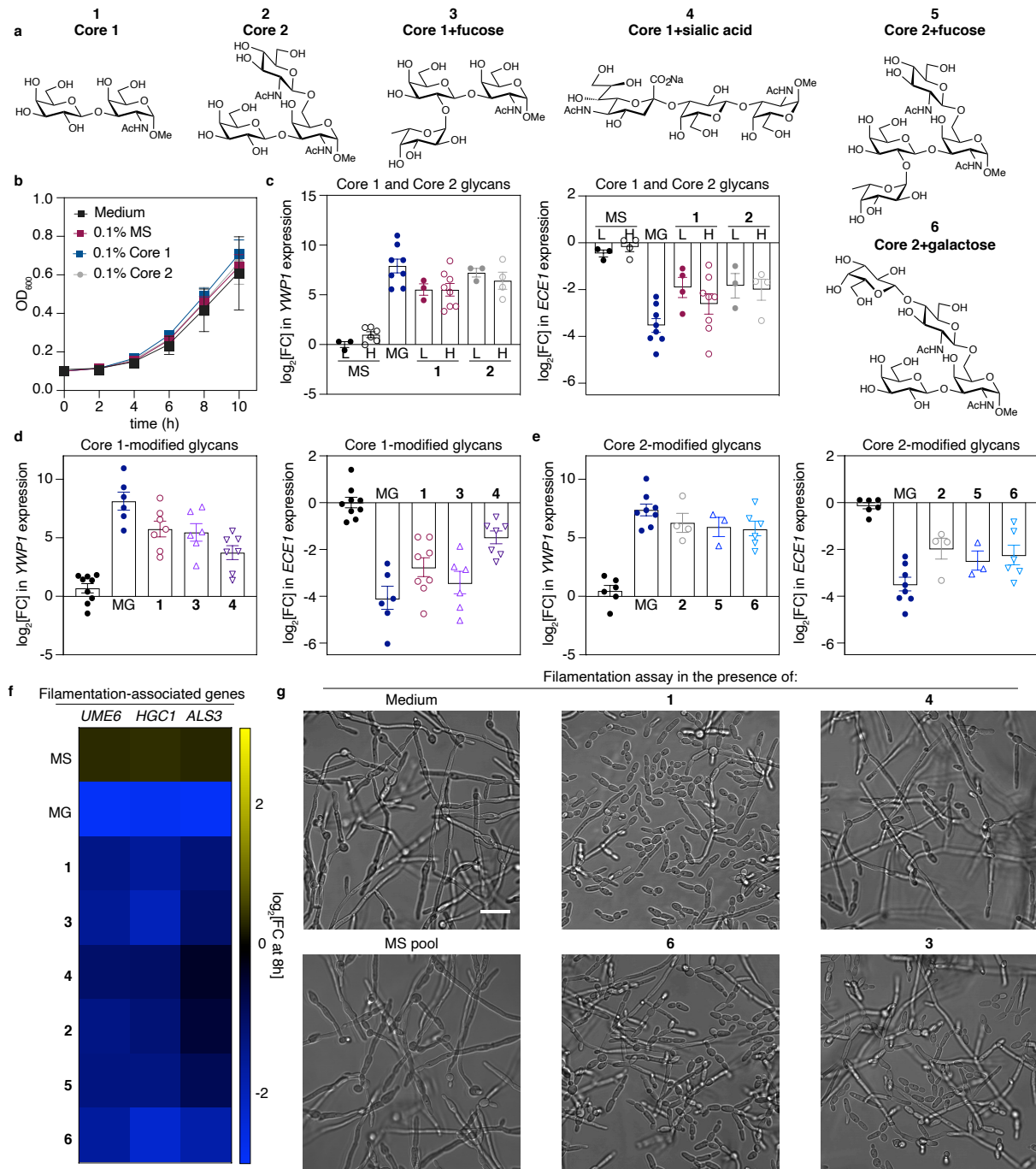


Figure 2.6: Synthetic Core 1- and Core 2-modified glycans are sufficient to suppress *C. albicans* filamentation

a) Depiction of synthesized mucin glycan structures (1-6) that are abundant in the complex mucin glycan pool.

- b) Growth is not altered by the presence of the Core 1 and Core 2 synthesized glycans. Data are the mean optical density at 600 nm ($OD_{600} \pm SEM$; $n=5$ biologically independent replicates. MS, monosaccharide pool.
- c) Exposure to low (L; 0.1% w/v) and high (H; 0.4% w/v) concentrations of synthesized glycan structures (left) increase transcription of the yeast-associated gene *YWPI* and (right) decreases transcription of the filamentation-associated toxin gene *ECE1*. Data from $n=3$ (0.1% MS, **1** and **2**), $n=4$ (0.4% **2**), $n=6$ (0.4% MS) and $n=8$ (0.4% MG and **1**) biologically independent replicates.
- d) Exposure to Core 1-modified glycan structures decreases the expression of virulence-associated gene, *ECE1*, and increases the expression of the yeast-associated gene, *YWPI*. These results are dampened by the addition of sialic acid to Core 1. Data from $n=6$ (MG, **3**), $n=7$ (**4**, **1**) and $n=9$ (MS) biologically independent replicates.
- e) Exposure to Core 2-modified glycan structures decreases the expression of the virulence-associated gene, *ECE1*, and increases the expression of *YWPI*. Data from $n=3$ (**6**), $n=4$ (**2**), $n=6$ (**5**, MS) and $n=8$ (MG) biologically independent replicates.
- f) Expression of filamentation-associated genes in the presence of MS, MG, and synthesized Core 1- and Core 2-modified glycan structures. Data from $n=3$ (**6**), $n=4$ (**3**, **5**), $n=6$ (**2**) and $n=7$ (MS, MG, **1**, **4**) biologically independent replicates.
- g) Phase-contrast images of *C. albicans* SC5314 cells that were grown in RPMI medium alone, 0.4% monosaccharide (MS) pool or the indicated synthetic glycan structure (0.4%) at 37 °C for 8 h. Scale bar, 20 μ m.

For **b,c,d,e**, gene expression was measured with qRT-PCR and normalized to a control gene (*ACT1*). Bars indicate mean \pm SEM. MS, black circles; MG, mucin glycans; FC, fold change.

Chapter 3: Mucin glycans inhibit CTX ϕ -mediated toxigenic conversion and virulence factor production in *Vibrio cholerae*

Work presented in this Chapter is under review:

Wang BX*, Takagi J*, Aoki K, Griffin K, Park JH, Teschler J, Kitts G, Minzer G, Tiemeyer M, Hevey R, Yildiz F, Ribbeck K. Host-derived *O*-glycans inhibit toxigenic conversion by a virulence-encoding phage in *Vibrio cholerae*.

*Contributed equally

Abstract

Pandemic and endemic strains of *Vibrio cholerae* arise from toxigenic conversion by the CTX ϕ bacteriophage, a process by which CTX ϕ infects non-toxigenic strains of *V. cholerae* that are naturally part of normal aquatic flora. CTX ϕ encodes the cholera toxin, an enterotoxin that is responsible for the watery diarrhea associated with cholera infections. Despite the critical role that CTX ϕ plays during infections, signals that affect CTX ϕ -driven toxigenic conversion or influence the expression of the CTX ϕ -encoded cholera toxin remain poorly characterized, particularly in the context of the gut mucosa. Here, we characterized the biochemical mechanisms by which mucin glycoproteins interfere with CTX ϕ -driven pathogenicity in *V. cholerae*. We determined that mucins and their associated glycans block toxigenic conversion by CTX ϕ . Further, we found that mucin glycans directly suppress the expression of CTX ϕ -encoded cholera toxin through a ToxT-dependent mechanism. By synthesizing individual mucin glycan structures *de novo*, we identified the Core-2 motif as the critical structure responsible for this observed virulence attenuation. Overall, our results highlight a novel mechanism by which mucins and their associated *O*-glycan structures affect CTX ϕ -mediated evolution and pathogenicity of *V. cholerae*, which underscores the potential regulatory power that is housed within mucus.

Introduction

Vibrio cholerae is the causative agent of cholera, an acute dehydrating diarrheal disease that infects millions of people each year. While this microbe naturally inhabits brackish water and estuaries (Reidl & Klose, 2002), *V. cholerae* can also transform into a hyper-virulent enteric pathogen through a process known as toxigenic conversion, in which the CTX ϕ prophage infects non-toxigenic strains of *V. cholerae* (Waldor & Mekalanos, 1996). CTX ϕ encodes both subunits of the

cholera toxin, a potent enterotoxin that triggers the massive and watery diarrhea that is the hallmark of cholera infections (Waldor & Mekalanos, 1996). While toxigenic conversion is thought to occur in both natural aquatic habitats and within the gastrointestinal tracts of hosts during infection (Faruque et al., 1999; Faruque & Nair, 2002; Reidl & Klose, 2002; Waldor & Mekalanos, 1996), the signals that affect CTX ϕ toxigenic conversion or impact the expression of the CTX ϕ -encoded cholera toxin have remained largely unclear.

Mucus is an ecological niche that *V. cholerae* colonizes during human infection. *V. cholerae* encounters a multitude of host-derived signals during infection of the gut mucosa, including oxygen limitation (Liu et al., 2011), bile salts (Hung & Mekalanos, 2005), and small molecules produced by the host microbiota (Qin et al., 2020). While each of these signals impacts the virulence program of *V. cholerae*, one set of molecules in the host mucosa that is often overlooked in studies of host-pathogen interactions are mucin glycoproteins, the major gel-forming units of mucus. These abundant molecules, which can reach millimolar concentrations in mucus, play a multi-faceted role in the gut, providing nutrients and attachment sites for the microbiota while simultaneously protecting the body from invading enteric pathogens (Wagner et al., 2018). Recent work in an infant mouse model of infection has shown that *V. cholerae* preferentially colonizes regions of the gut that produce lower amounts of mucin. It has also been reported that the destruction of mucins with the mucolytic agent N-acetyl-L-cysteine (NAC) in infant mice leads to a dramatic increase in *V. cholerae* burden in the small intestines (Millet et al., 2014). Together, these observations strongly suggest that mucins normally play a critical role in protecting the gut from *V. cholerae* infections. However, the molecular mechanisms by which mucins exert these protective effects have not yet been fully explored.

Here, we show that mucins and their associated glycans inhibit toxigenic conversion by the CTX ϕ prophage, likely by downregulating the expression of the toxin co-regulated pilus (TCP), which serves as the receptor for the CTX ϕ phage. In addition, we find that mucin glycans directly suppress the expression of the CTX ϕ -encoded cholera toxin through a ToxT-dependent mechanism, which we support with ELISA-based protein assays and using *in vitro* infection assays. We also synthesize individual mucin glycan structures *de novo* and find that the Core-2 glycan motif, which is abundantly found in mucus, is sufficient for this virulence attenuation. Overall, our results shed light on a novel mechanism by which mucins and their associated glycans may hinder CTX ϕ -mediated evolution and pathogenicity of toxigenic *V. cholerae*.

Results

Mucins and their associated glycans inhibit toxigenic conversion by the CTX ϕ prophage

Although toxigenic conversion by CTX ϕ transforms *V. cholerae* into a hyper-virulent pathogen (Fig. 3.1a), the signals that influence this process have not been well-documented, particularly in the context of the host mucosa. Given the abundance of mucin glycoproteins in mucus, as well as the protective effects of mucins that have recently been observed in an infant mouse model of cholera, we hypothesized that mucins interfere with CTX ϕ -mediated toxigenic conversion. To test this hypothesis, we first natively purified MUC5AC and MUC2 mucins from porcine gastrointestinal tracts. Porcine mucus represents a commonly used model system to study the mucosal niche in higher vertebrates due to strong similarities between human and porcine-derived mucin structure and glycosylation (Celli et al., 2005; Jin et al., 2017; Turner et al., 1999). CTX ϕ encodes for repressors of CTX ϕ replication, conferring protection from secondary infection (Kim et al., 2017; Kimsey & Waldor, 1998). Thus, to test phage transduction, we measured the ability of CTX ϕ harboring a kanamycin-resistance cassette to infect a susceptible *V. cholerae* strain lacking the CTX ϕ phage repressor (Gallego-Hernandez et al., 2020), in the presence or absence of purified mucins (Kimsey & Waldor, 1998). Strikingly, we found that purified MUC5AC and MUC2 completely ablated the ability of CTX ϕ to infect the susceptible *V. cholerae* strain compared to a media control (Fig. 3.1b), suggesting that mucins strongly block toxigenic conversion by CTX ϕ .

We next sought to identify the molecular motif(s) in mucins that suppress CTX ϕ -mediated toxigenic conversion. Mucin glycans, which comprise 50-90% of the molecular mass of mucins, are promising molecules for regulating host-microbe interactions (Jin et al., 2017; Robbe et al., 2004). We chemically isolated mucin glycans via non-reductive, alkaline β -elimination yielding a library of structurally intact glycans released from the MUC5AC polymer (Fig. 3.1c). We then repeated this CTX ϕ transduction assay in the presence or absence of purified MUC5AC glycans and found that these glycans were also sufficient to decrease CTX phage transduction.

We sought to better understand the mechanisms by which mucins and their associated glycans block CTX ϕ transduction. CTX ϕ uses the toxin co-regulated pilus (TCP) as its receptor, and previous work has shown that toxigenic conversion is largely ablated in strains that lack the TCP (Waldor & Mekalanos, 1996). In turn, we hypothesized that mucin glycans block CTX phage

transduction by downregulating TCP expression. To test this hypothesis, we incubated *V. cholerae* with whole intestinal mucus, purified MUC5AC and MUC2 mucin, or with pool of isolated mucin glycans, and then used qRT-PCR to measure the levels of TCP-encoding genes. We found that mucins and their associated glycans downregulated the expression of the TCP by ~4-30 fold relative to a media only control (Fig. 3.1e). Together, these results suggest that one mechanism by which mucins block toxigenic conversion by the CTX ϕ prophage is by downregulating the TCP phage receptor.

Mucin O-glycans suppress the activity of cholera toxin and toxin co-regulated pilus through ToxT

Given the significant downregulation of the TCP by mucins and mucin glycans, we reasoned that mucin glycans may also trigger the differential expression of other *V. cholerae* genes. To determine if mucin glycans induce changes in gene expression beyond the TCP, we performed RNA sequencing of *V. cholerae* in AKI medium with or without 0.1% w/v MUC5AC glycans and assessed the extent to which glycans alter the global transcriptome of *V. cholerae*. A pooled library of MUC5AC glycans triggered global changes in gene expression, significantly upregulating 57 genes and downregulating 95 genes (Fig. 3.2a) compared to cells grown in media alone (Supplementary Table 3.1) without altering growth (Fig. 3.2b). Pathways associated with pathogenesis, ribonucleotide (purine & pyrimidine) metabolism, auxiliary type VI secretion system (T6SS) were downregulated while pathways encoding biofilm-related genes were upregulated. In agreement with our previous qRT-PCR experiment (Fig. 3.1e), our RNA-seq dataset showed that the TCP-encoding operon was significantly downregulated. Strikingly, our transcriptome analysis also indicated that both subunits of the CTX ϕ -encoded cholera toxin were significantly downregulated by mucin glycans (Fig. 3.2d). Additionally, cholera toxin was also downregulated in gastrointestinal mucins (Fig. 3.3a). Using qRT-PCR, we confirmed that mucin glycans potently suppress the expression of both the TCP and the cholera toxin across three different media types (Fig. 3.3b). The addition of a pool of monosaccharides found in mucins did not alter the expression of virulence genes (Fig. 3.1c), suggesting the complex structure of mucin glycans is critical to their function. Furthermore, we found that mucin glycans downregulated virulence genes in a dose-dependent manner, with potent suppression occurring at concentrations below those found in mucosal surfaces (Fig. 3.3d) (Bansil & Turner, 2018). Together, these results

suggest that the complex glycan structures found in the mucus barrier are sufficient for the downregulation of CTX ϕ -related virulence genes.

To further confirm that mucin glycans suppress cholera toxin production, we used ELISA-based assays to directly measure the levels of cholera toxin protein produced in the supernatant of *V. cholerae* grown in the presence and absence of mucin glycans. Strikingly, exposure to mucin glycans resulted in a nearly 100-fold reduction of cholera toxin production relative to a media only control, while equivalent concentrations of monosaccharide (MS) had no effect (Fig. 3.3e).

We also sought to better understand the mechanisms by which mucin glycans downregulate cholera toxin and TCP. Two membrane-localized complexes (TcpP/H and ToxR/S) have been shown to promote the transcription of *toxT*, a potent activator of cholera toxin and TCP expression (Yoon & Waters, 2019). Our RNA-seq results indicate that mucin glycans downregulate the expression of *toxT* to a modest but statistically significant extent (fold change ~ 1.5 fold, $p=0.03$) (Figure 3.3f). To determine if mucin glycans depend on ToxT for the downregulation of CTX ϕ -related virulence genes, we incubated mucin glycans with a *V. cholerae* mutant in which the native promoter for *toxT* was replaced with an IPTG-inducible promoter, which allows for its constitutive expression (Gallego-Hernandez et al., 2020). Using this strain, we found that the ability of mucin glycans (MG) to downregulate the cholera toxin and the toxin-coregulated pilus was completely ablated when constitutively inducing *toxT* expression using 1 mM IPTG (Fig. 3.3g), strongly indicating that the virulence-suppressing effects of mucin glycans are dependent on their ability to suppress *toxT* expression.

Mucin glycans suppress cAMP production in tissue culture infection assays

Cholera toxin binds and enters intestinal epithelial cells to activate its target, adenylate cyclase, which then elevates cyclic AMP levels within host cells (Fig. 3.4a). This then triggers a rapid efflux of chloride and a decreased uptake of sodium ions, leading to massive water secretion through the intestinal cells and causing severe diarrhea, which is the hallmark of cholera infections (Haan & Hirst, 2004). In turn, we hypothesized that the decreased toxin production observed in *V. cholerae* grown in the presence of mucin glycans should also reduce cAMP levels in epithelial cells. To test this hypothesis, we grew *V. cholerae* in the presence or absence of mucin glycans, incubated the supernatant of these samples with HT29 human epithelial cells for four hours, and then analyzed cAMP levels using an ELISA assay. As a control, we first found that HT29 cells did

not produce cAMP when exposed to a media control not treated (NT) with *V. cholerae*. In contrast, addition of *V. cholerae* supernatant from cells grown in the absence of mucin glycans (MG) strongly stimulated cAMP production in HT29 cells (Fig. 3.4b). Strikingly, we found that supernatant from *V. cholerae* grown in the presence of mucin glycans significantly decreased cAMP levels relative to *V. cholerae* grown in the absence of mucin glycans, while monosaccharides had no effect relative to this same control (Fig. 3.4b).

Synthetic mucin O-glycans reveal individual glycans possessing the Core 2 motif are sufficient for virulence attenuation

We next sought to identify specific glycan motifs that were responsible for the downregulation of the CTX ϕ -related virulence genes in *V. cholerae*. Using nanospray ionization multi-dimensional mass spectrometry (NSI-MSn, ThermoFisher Orbitrap Discovery), we characterized >80 glycan structures in our collection of purified mucin glycans, including isobaric glycans with distinct structural characteristics (glycans with identical mass but different isomeric configurations) (Fig. 3.5a). Overall, the MUC5AC glycan pool was dominated by Core 1- and Core 2-type O-glycan structures that were partially modified by fucose (Fig. 3.5b) and sparsely sialylated (Fig. 3.5b). In particular, six glycan structures (Core 1, Core 1+fucose, Core 1+sialic acid (Neu5Ac), Core 2, Core 2+fucose, and Core 2+galactose) represented >40% of the total glycan profile and were thus identified as candidates for virulence-attenuating activity (Fig. 3.5c).

Rather than fractionating glycan pools down to the single-glycan level, which poses technical challenges, we instead chemically synthesized these six highly abundant mucin glycans *de novo*. We first focused on Core 1 and Core 2, the two most abundant core structures, which are the foundation for which more complex glycans are built upon. To determine whether Core 1 and Core 2 could have a similar regulatory capacity as the complex glycan pool, we incubated each of these individual structures with *V. cholerae* and used qRT-PCR to measure the expression of CTX ϕ -related virulence genes. Strikingly, we found that the synthetic Core 2 structure downregulated the expression of these virulence genes to a similar degree as the complex glycan pool, while the Core 1 structure was comparatively less potent (Fig. 3.5d). Moreover, the addition of fucose, galactose, and sialic acid onto these Core 1 (Fig. 3.5e) and Core 2 structures (Fig. 3.5f) did not significantly alter the observed changes in gene expression, suggesting that the underlying Core 2 motif is sufficient for virulence downregulation.

To further probe the importance of the Core 2 motif, we performed an ELISA assay to measure the levels of secreted cholera toxin in *V. cholerae* cultures incubated in the presence or absence of unmodified Core 1 and Core 2. We found that Core 2 reduced cholera toxin production by nearly 10-fold, while Core 1 glycans reduced toxin production by only 2-fold in this same assay (Fig. 3.5g). We also repeated our tissue culture infection assays and found that supernatant taken from *V. cholerae* incubated with the Core 2 structure decreased the levels of cAMP production in HT29 cells by 60% relative to supernatant taken from *V. cholerae* grown in media alone, while there were no significant changes in cAMP production when using the Core 1 structure in these same experiments (Fig. 3.5h). Together, these results suggest that the downregulation of cholera toxin and the TCP are specific to the Core 2 motif.

Discussion

The pathogenicity of *V. cholerae* can largely be attributed to toxigenic conversion by the CTX ϕ bacteriophage, which encodes the cholera toxin and uses the TCP as its phage receptor. In this work, we determined that natively purified mucins and their associated glycans inhibit toxigenic conversion by the CTX ϕ phage, likely by suppressing the expression of the TCP phage receptor. In addition, we found that mucin glycans downregulate the CTX ϕ -encoded cholera toxin through a ToxT-dependent mechanism. By synthesizing individual mucin glycan structures *de novo*, we further determined that the Core-2 glycan structure is specifically responsible for this observed virulence attenuation. Together, our results identify a novel mechanism by which mucins may help the body defend against CTX ϕ -driven virulence of toxigenic *V. cholerae*.

As *V. cholerae* infects the gut mucosa, this pathogen will undoubtedly encounter mucins and their associated glycans during intestinal colonization, which are present at millimolar concentrations in the gastrointestinal tract. Interestingly, our RNA-seq results suggest that *V. cholerae* dramatically rewires its transcriptome in response to mucin glycans, with over 200 genes that exhibit significant changes in gene expression. While our experiments here focused on the CTX ϕ -related TCP and cholera toxin genes, we also observed that mucin glycans trigger gene expression changes in other pathways including biofilm formation, type VI secretion, and ribonucleotide metabolism. Future work that characterizes the molecular details of these gene expression changes may shed more light on how *V. cholerae* alters behavior in mucus.

A few other recent studies have recently investigated how mucins impact *V. cholerae* physiology. For examples, these studies have reported that mucins activate the type VI secretion system (T6SS) and alter motility in this pathogen (Bachmann et al., 2015; Frederick et al., n.d.; Liu et al., 2008, 2015). However, these studies utilized commercially available mucin that is subject to harsh chemical treatments, resulting in mucins that are partially degraded and de-glycosylated (Lieleg et al., 2012; Wagner et al., 2018). Some of these studies have also used commercial mucins collapsed onto 2D agar surfaces, which does not recapitulate the normal 3D structure of mucus. Our work is the first to use natively purified mucins to study *V. cholerae* physiology, which preserves the native structure and function of these large glycoproteins. In addition, we observed that whole-length mucins, isolated mucin glycans, and chemically synthesized Core-2 structures all downregulated the cholera toxin and the TCP, which strengthens our conclusions regarding the virulence-attenuating properties of mucins reported in this work.

Our results are generally consistent with recent work in murine models of infection that have highlighted the protective roles of mucins *in vivo*. Interestingly, over 50% of cholera infections in humans are asymptomatic, suggesting that mucus may also actively suppress the CTX ϕ -mediated pathogenicity of *V. cholerae* during humans infections (Baker-Austin et al., 2018). As mucin glycans suppress the pathogenicity of *V. cholerae* without affecting its viability, these glycans may serve as host-derived, anti-virulence candidates for treating cholera infections that do not select for drug resistance. Overall, our results highlight the potential role that mucins play in altering CTX ϕ -mediated evolution and pathogenicity of *V. cholerae* and underscore the wealth of biochemical information and regulatory power that is housed within mucus.

Methods

Mucin purification

This study used native porcine gastric mucins (MUC5AC). Mucus was scraped from fresh pig stomachs and solubilized in sodium chloride buffer with protease inhibitors. Insoluble material was removed by low speed centrifugation for 1 h at 6,000 g and ultracentrifugation at 190,000 g for 1 hr at 4 °C (40,000 rpm, Beckman 50.2 Ti rotor with polycarbonate bottles). Mucins were purified using size-exclusion chromatography on a Sepharose CL-2B column. Mucin fractions were identified based on absorbance at 280 nm, then desalted and concentrated with an Amicon stirred cell pressure-based concentrator (Sigma) with an Omega ultrafiltration 100 kDa membrane disc filter (Pall). Purified mucins were then lyophilized for storage at -80 °C and reconstituted by shaking them gently at 4 °C overnight in the desired medium.

Mucin glycan isolation

This study applied non-reductive alkaline β -elimination ammoniolysis to dissociate non-reduced glycans from MUC5AC. Mucins were added to 1x PBS at a ratio of 30 mg per mL and insoluble material was removed by low-speed centrifugation, 8000 x g, (7,000 rpm Sorvall GS-3 rotor), for 20 minutes at 4 °C. Mucins were then precipitated with 60% (v/v) ethanol, collected by centrifugation, and dissolved in water. Dissolved mucin was then desalted and concentrated with an Amicon stirred cell pressure-based concentrator (Sigma) with 100 kDa membrane filter disc (Pall), and lyophilized. Lyophilized mucins were dissolved in ammonium hydroxide saturated with ammonium carbonate and incubated at 60°C for 48 h to release oligosaccharide glycosylamines and partially deglycosylated mucins. Volatile salts were removed via repeated centrifugal evaporation and the oligosaccharide glycosylamines were separated from residual deglycosylated mucins via centrifugal filtration through 10 kDa molecular weight cut-off membranes in accordance with the manufacturer's instructions (Amicon Ultracel). The resulting oligosaccharide glycosylamines were converted to reducing oligosaccharide hemiacetals via treatment with boric acid. Residual boric acid was removed via repeated centrifugal evaporation from methanol.

Glycans were analyzed using matrix-assisted laser desorption/ionization time-of-flight (MALDI-TOF). β -eliminated glycans were permethylated and analyzed at the Glycomics Core at Beth Israel Deaconess Medical Center. Mass spectrometry data were acquired on an UltraFlex II MALDI-TOF Mass Spectrometer (Bruker Daltonics). Reflective positive mode was used, and data were

recorded between 500 m/z and 6000 m/z. The mass spectrometry O-glycan profile was acquired by aggregating at least 20,000 laser shots. Mass peaks were manually annotated and assigned to a particular O-glycan composition based on known core structures.

Glycan synthesis and analysis

All commercial reagents were used as supplied unless otherwise stated, and solvents were dried and distilled using standard techniques. Thin layer chromatography was performed on silica-coated glass plates (TLC Silica Gel 60 F₂₅₄, Merck) with detection by fluorescence, charring with 5% H₂SO_{4(aq)}, or staining with a ceric ammonium molybdate solution. Organic solutions were concentrated and/or evaporated to dry under vacuum in a water bath (<50 °C). Molecular sieves were dried at 400 °C under vacuum for 20-30 minutes prior to use. Amberlite IR-120H resin was washed extensively with MeOH and dried under vacuum prior to use. Medium-pressure liquid chromatography (MPLC) was performed using a CombiFlash Companion equipped with RediSep normal-phase flash columns, and solvent gradients refer to sloped gradients with concentrations reported as % v/v. NMR spectra were recorded on a Bruker Avance DMX-500 (500 MHz) spectrometer, and assignments achieved with the assistance of 2D gCOSY, 2D gTOCSY, 2D gHSQC, and 2D gHMBC; chemical shifts are expressed in ppm and referenced to either Si(CH₃)₄ (for CDCl₃), residual CHD₂OD (for CD₃OD), or a MeOH internal standard (for D₂O). Low resolution electron-spray ionization mass spectrometry (ESI-MS) was performed using a Waters micromass ZQ. High resolution mass spectrometry was performed using an Agilent 1100 LC equipped with a photodiode array detector, and a Micromass QTOF I equipped with a 4 GHz digital-time converter. Optical rotation was determined in a 10 cm cell at 20 °C using a Perkin-Elmer Model 341 polarimeter. HPLC analysis was performed using an Agilent 1100 LC equipped with an Atlantis T3 (3 mm, 2.1x100 mm) C18 column and ELSD detection.

Transduction Assays.

CTX-kanamycin (Km) Φ was isolated by growing *V. cholerae* O395 (pCTX-Km) overnight in 5 mL LB with kanamycin (50 μ g/mL), pH 8.5 at 37 °C and filtering supernatant fluid through 0.22- μ m filters (Millipore). The CTX Φ Δ VC1464 repressor was deleted in order to eliminate phage immunity. Δ VC1464 was grown anaerobically in 37 °C in planktonic conditions. Harvested cells were normalized to an OD₅₆₀ of 1.0 and mixed with CTX-Km Φ cells for 1 h at 37 °C. After 1 h, cells were plated on LB plates and LB plates containing Km (50 μ g/mL) plates. Three biological

replicates were analyzed for mucin glycans and two biological replicates were used for mucins with three technical replicates. Two-tailed unpaired Student's t-tests were used for statistical analyses for all experiments using the Prism 8 software (GraphPad Software, Inc.).

RNA extraction for qRT-PCR and RNA-seq experiments

50 μ L of cells grown with or without mucin glycans were pelleted at max speed in a tabletop centrifuge for 2 minutes. Cell pellets were resuspended in 300 μ L of 2x Tissue and Cell Lysis Buffer (Lucigen) with 2 μ L of proteinase K. Samples were incubated at 65 $^{\circ}$ C to aid in cell lysis. 175 μ L of MPC Protein Precipitation Reagent (Lucigen) were added to samples and spun for 10 minutes at max speed in a tabletop centrifuge to precipitate out proteins. The supernatant was then mixed with 500 μ L of isopropanol, and spun down for 15 minutes at max speed. The resulting pellet of RNA was washed 2 times with 70% ethanol and centrifuged for 15 minutes at max speed following each wash. The RNA was then air-dried for 5 minutes and dissolved in 50 μ L of nuclease free water. To remove contaminating DNA from the RNA prep, each sample was incubated with 5 μ L of Ambion RNA turbo buffer and 2 μ L of Turbo DNase (ThermoFisher) for 30 minutes at 37 $^{\circ}$ C. Next, 5 μ L of Ambion reaction inactivator was added to each sample to remove DNase. Samples were spun at max speed for 2 minutes, and then supernatant containing purified RNA was collected and stored at -20 $^{\circ}$ C until use.

qRT-PCR protocols

To prepare cDNA for qRT-PCR samples, approximately 500 ng of purified RNA was combined with 1 μ L of random hexamers (NEB), 10 μ L of ProtoScript II reaction mix (NEB), and 2 μ L of ProtoScript enzyme mix (NEB). Samples were then incubated at 25 $^{\circ}$ C for 5 minutes and then 42 $^{\circ}$ C for 1 hour to generate cDNA.

The Sybr Fast qPCR 2x master Mix (Roche) was used to perform qRT-PCR experiments. Briefly, ~20 ng of cDNA was incubated with 5 μ L of 2x Sybr (Roche), a final concentration of 300 nM of each primer, and nuclease free water. qRT-PCR experiments were done in 384 well plate format on a LightCycler 480 system (Roche). The thermocycling program was 95 $^{\circ}$ C for 10 minutes, 95 $^{\circ}$ C for 15 seconds, 60 $^{\circ}$ C for 30 seconds, and 72 $^{\circ}$ C for 30 seconds, with 40 cycles of steps 2-4. Fold changes were then calculated using the ddCT method, and calculated relative to the housekeeping gene, *gyrA*

RNA-seq protocols

Purified RNA was depleted of rRNA using the Illumina RiboZero depletion kit. Depleted RNA was submitted to the MIT BioMicro center for strand-specific library preparation. Libraries were then run on a HiSeq2000 with paired-end reads and a read length of 40 nucleotides. BWA was used to map the reads to the *V. cholerae* type strain, and uniquely mapping reads were used. Any read that overlapped with any region of a gene was counted as a read. DEseq analysis was then used to identify significant changes in gene expression between cells grown in the presence and absence of mucin glycans.

Cholera toxin ELISA assays

GM1 ganglioside enzyme-linked immunosorbent CT assays were performed as previously described (*Laboratory Testing for Cholera | Cholera | CDC, 2021*) on supernatants from *V. cholerae* grown in media, mucin glycans, and synthetic glycans. Briefly, a 96-well polystyrene microtiter plates was coated with GM1 ganglioside overnight. The plates were washed three times with phosphate-buffered-saline (PBS; pH 7.4)–0.2% BSA–0.05% Tween 20 and then 1% (wt/vol) bovine serum albumin (BSA) was used to block the GM1-coated plates for 30 min at room temperature. The plates were washed three times. Next, supernatant was added to the wells and incubated for 1 h at 37 C. Then, 1% BSA was used to block the wells for 30 min at room temperature and the wells were washed three times thereafter. Subsequently, a goat anti-CT polyclonal antibody (1:1,000) and then an AP-linked rabbit anti-goat IgG antibody (1:1,000) were added to the wells and allowed to incubate for 1 h at room temperature each; the plates were washed following each step. For development of the CT-antibody complex, *p*-nitrophenyl phosphate substrate solution (Invitrogen) was used according to the manufacturer's protocol. The color intensity in each well was measured at 405 nm in a plate reader. CT amounts in the samples were estimated by comparison to a standard curve.

cAMP ELISA assays

HT-29 cells were incubated for 4 h at 37 °C with supernatants from *V. cholerae* cells grown in AKI media with or without mucin glycans for 3-4 h (OD₆₀₀=0.5) at 37 °C in anaerobic conditions. HT-29 cells were subsequently processed according to the manufacturer's protocol to quantify the cAMP level in cellular lysate using the cAMP activity assay kit (Abcam).

References

- Bachmann, V., Kostiuk, B., Unterweger, D., Diaz-Satizabal, L., Ogg, S., & Pukatzki, S. (2015). Bile Salts Modulate the Mucin-Activated Type VI Secretion System of Pandemic *Vibrio cholerae*. *PLOS Neglected Tropical Diseases*, 9(8), e0004031. <https://doi.org/10.1371/journal.pntd.0004031>
- Baker-Austin, C., Oliver, J. D., Alam, M., Ali, A., Waldor, M. K., Qadri, F., & Martinez-Urtaza, J. (2018). *Vibrio* spp. Infections. *Nature Reviews Disease Primers*, 4(1), 1–19. <https://doi.org/10.1038/s41572-018-0005-8>
- Bansil, R., & Turner, B. S. (2018). The biology of mucus: Composition, synthesis and organization. *Advanced Drug Delivery Reviews*, 124, 3–15. <https://doi.org/10.1016/j.addr.2017.09.023>
- Celli, J., Gregor, B., Turner, B., Afdhal, N. H., Bansil, R., & Erramilli, S. (2005). Viscoelastic Properties and Dynamics of Porcine Gastric Mucin. *Biomacromolecules*, 6(3), 1329–1333. <https://doi.org/10.1021/bm0493990>
- Faruque, S. M., & Nair, G. B. (2002). Molecular ecology of toxigenic *Vibrio cholerae*. *Microbiology and Immunology*, 46(2), 59–66. <https://doi.org/10.1111/j.1348-0421.2002.tb02659.x>
- Faruque, S. M., Rahman, M. M., Asadulghani, Islam, K. M. N., & Mekalanos, J. J. (1999). Lysogenic Conversion of Environmental *Vibrio mimicus* Strains by CTX Φ . *Infection and Immunity*, 67(11), 5723–5729. <https://doi.org/10.1128/IAI.67.11.5723-5729.1999>
- Frederick, A., Huang, Y., Pu, M., & Rowe-Magnus, D. A. (n.d.). *Vibrio cholerae* Type VI Activity Alters Motility Behavior in Mucin. *Journal of Bacteriology*, 202(24), e00261-20. <https://doi.org/10.1128/JB.00261-20>
- Gallego-Hernandez, A. L., DePas, W. H., Park, J. H., Teschler, J. K., Hartmann, R., Jeckel, H., Drescher, K., Beyhan, S., Newman, D. K., & Yildiz, F. H. (2020). Upregulation of virulence genes promotes *Vibrio cholerae* biofilm hyperinfectivity. *Proceedings of the National Academy of Sciences*, 117(20), 11010–11017. <https://doi.org/10.1073/pnas.1916571117>

- Haan, L. de, & Hirst, T. R. (2004). Cholera toxin: A paradigm for multi-functional engagement of cellular mechanisms (Review). *Molecular Membrane Biology*, 21(2), 77–92. <https://doi.org/10.1080/09687680410001663267>
- Hung, D. T., & Mekalanos, J. J. (2005). Bile acids induce cholera toxin expression in *Vibrio cholerae* in a ToxT-independent manner. *Proceedings of the National Academy of Sciences*, 102(8), 3028–3033. <https://doi.org/10.1073/pnas.0409559102>
- Jin, C., Kenny, D. T., Skoog, E. C., Padra, M., Adamczyk, B., Vitizeva, V., Thorell, A., Venkatakrishnan, V., Lindén, S. K., & Karlsson, N. G. (2017). Structural Diversity of Human Gastric Mucin Glycans. *Molecular & Cellular Proteomics: MCP*, 16(5), 743–758. <https://doi.org/10.1074/mcp.M116.067983>
- Kim, E. J., Yu, H. J., Lee, J. H., Kim, J.-O., Han, S. H., Yun, C.-H., Chun, J., Nair, G. B., & Kim, D. W. (2017). Replication of *Vibrio cholerae* classical CTX phage. *Proceedings of the National Academy of Sciences of the United States of America*, 114(9), 2343–2348. <https://doi.org/10.1073/pnas.1701335114>
- Kimsey, H. H., & Waldor, M. K. (1998). CTX ϕ immunity: Application in the development of cholera vaccines. *Proceedings of the National Academy of Sciences of the United States of America*, 95(12), 7035–7039.
- Laboratory Testing for Cholera | Cholera | CDC*. (2021, November 4). <https://www.cdc.gov/cholera/laboratory.html>
- Lieleg, O., Lieleg, C., Bloom, J., Buck, C. B., & Ribbeck, K. (2012). Mucin Biopolymers As Broad-Spectrum Antiviral Agents. *Biomacromolecules*, 13(6), 1724–1732. <https://doi.org/10.1021/bm3001292>
- Liu, Z., Miyashiro, T., Tsou, A., Hsiao, A., Goulian, M., & Zhu, J. (2008). Mucosal penetration primes *Vibrio cholerae* for host colonization by repressing quorum sensing. *Proceedings of the National Academy of Sciences*, 105(28), 9769–9774. <https://doi.org/10.1073/pnas.0802241105>
- Liu, Z., Wang, Y., Liu, S., Sheng, Y., Rueggeberg, K.-G., Wang, H., Li, J., Gu, F. X., Zhong, Z., Kan, B., & Zhu, J. (2015). *Vibrio cholerae* Represses Polysaccharide Synthesis To

- Promote Motility in Mucosa. *Infection and Immunity*, 83(3), 1114–1121.
<https://doi.org/10.1128/IAI.02841-14>
- Liu, Z., Yang, M., Peterfreund, G. L., Tsou, A. M., Selamoglu, N., Daldal, F., Zhong, Z., Kan, B., & Zhu, J. (2011). *Vibrio cholerae* anaerobic induction of virulence gene expression is controlled by thiol-based switches of virulence regulator AphB. *Proceedings of the National Academy of Sciences*, 108(2), 810–815.
<https://doi.org/10.1073/pnas.1014640108>
- Millet, Y. A., Alvarez, D., Ringgaard, S., Andrian, U. H. von, Davis, B. M., & Waldor, M. K. (2014). Insights into *Vibrio cholerae* Intestinal Colonization from Monitoring Fluorescently Labeled Bacteria. *PLOS Pathogens*, 10(10), e1004405.
<https://doi.org/10.1371/journal.ppat.1004405>
- Qin, Z., Yang, X., Chen, G., Park, C., & Liu, Z. (2020). Crosstalks Between Gut Microbiota and *Vibrio Cholerae*. *Frontiers in Cellular and Infection Microbiology*, 10.
<https://www.frontiersin.org/article/10.3389/fcimb.2020.582554>
- Reidl, J., & Klose, K. E. (2002). *Vibrio cholerae* and cholera: Out of the water and into the host. *FEMS Microbiology Reviews*, 26(2), 125–139. <https://doi.org/10.1111/j.1574-6976.2002.tb00605.x>
- Robbe, C., Capon, C., Coddeville, B., & Michalski, J.-C. (2004). Structural diversity and specific distribution of O-glycans in normal human mucins along the intestinal tract. *Biochemical Journal*, 384(Pt 2), 307–316. <https://doi.org/10.1042/BJ20040605>
- Turner, B. S., Bhaskar, K. R., Hadzopoulou-Cladaras, M., & LaMont, J. T. (1999). Cysteine-rich regions of pig gastric mucin contain von Willebrand factor and cystine knot domains at the carboxyl terminal. The sequences described in this paper have been submitted to the GenBank Nucleotide Sequence Database, and have been assigned the GenBank accession number AF054583 for mucin clone PGM-2X and GenBank accession number AF054584 for clone PGM-Z13.1. *Biochimica et Biophysica Acta (BBA) - Gene Structure and Expression*, 1447(1), 77–92. [https://doi.org/10.1016/S0167-4781\(99\)00099-8](https://doi.org/10.1016/S0167-4781(99)00099-8)

- Wagner, C. E., Wheeler, K. M., & Ribbeck, K. (2018). Mucins and Their Role in Shaping the Functions of Mucus Barriers. *Annual Review of Cell and Developmental Biology*, 34, 189–215. <https://doi.org/10.1146/annurev-cellbio-100617-062818>
- Waldor, M. K., & Mekalanos, J. J. (1996). Lysogenic conversion by a filamentous phage encoding cholera toxin. *Science (New York, N.Y.)*, 272(5270), 1910–1914. <https://doi.org/10.1126/science.272.5270.1910>
- Yoon, S. hun, & Waters, C. M. (2019). *Vibrio cholerae*. *Trends in Microbiology*, 27(9), 806–807. <https://doi.org/10.1016/j.tim.2019.03.005>

Acknowledgments

This research was supported by The NIH NIBIB award R01EB017755-04 (OSP 6940725) (to K.R.), the MRSEC Program of the National Science Foundation under award DMR-1419807 (to K.R.), the National Science Foundation Career award PHY1454673 (to K.R.), the core center grant P30-ES002109 from the National Institute of Environmental Health Sciences P30-ES002109 (to K.R.), the Toxicology Training Grant support T32-ES007020 (to J.T), the National Center for Functional Glycomics Grant P41GM103694 (to R.D.C.), the National Institute of Health NIAID-R01AI114261 to FHY, the Swiss National Science Spark Grant Foundation CRSK-3_196773 (to R.H).

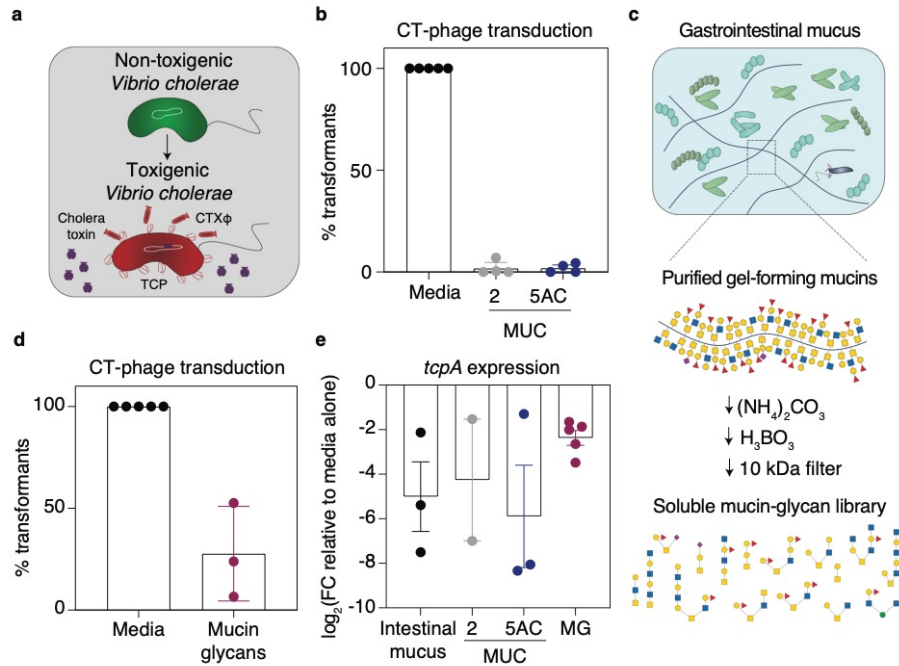


Figure 3.1: Mucins and their associated glycans inhibit toxigenic conversion and downregulate the major toxin coregulated pili, *tcpA*

k) Schematic of *Vibrio cholerae* toxigenic conversion by CTX ϕ

l) The presence of mucins reduce CTX-Km ϕ transduction. Bars indicate mean \pm SEM, with individual measurements shown.

m) Mucins were purified from intestinal and gastric mucus. Complex mucin glycans were isolated from the mucin polymer gels using alkaline β -elimination (Methods), leaving their reducing ends intact.

n) The presence of mucin glycans reduce CTX-Km ϕ transduction. Bars indicate mean \pm SEM, with individual measurements shown.

o) Intestinal mucus, mucins, and mucin glycans downregulate the expression of toxin coregulated pilus A (*tcpA*) relative to media alone. Gene expression measured by qRT-PCR and normalized to a control gene (*gyrA*). Bars indicate mean \pm SEM, with individual measurements shown.

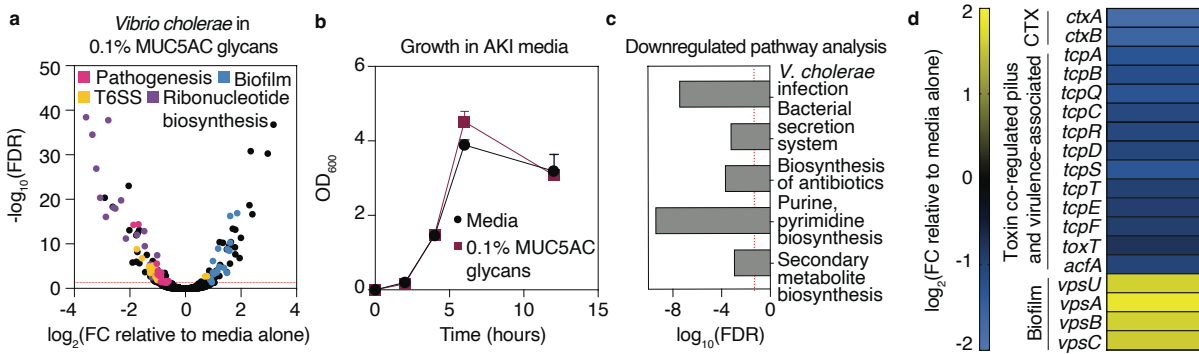


Figure 3.2: Mucin glycans downregulate pathways in *V. cholerae* infection

a) MUC5AC glycans elicit a global transcriptional response in *Vibrio cholerae*. A complete list of FC values and FDR-adjusted *P*-values is provided in Supplementary Table 1. FC data are average measurements from *n*=2 biologically independent replicates. FDR-adjusted *P*-values were determined using the Benjamini–Hochberg *P*-value adjustment method. The dotted line represents the threshold for significance (FDR adjusted *P*<0.05).

b) Growth is not altered by the presence mucin glycans in AKI medium. Data are mean optical density at 600 nm ($OD_{600} \pm SEM$) for *n*=3 biologically independent replicates.

c) Functional enrichment analyses reveal key virulence pathways among downregulated genes. Significance of enrichment was calculated from the Mann-Whitney U test followed by a Benjamini-Hochberg procedure for multiple corrections, for mean \log_2 -transformed FCs from *n*=2 biologically independent replicates. The dotted line represents the threshold for significance (FDR adjusted *P*<0.05).

d) RNA sequencing data for selected genes belonging to *Vibrio cholerae* pathogenesis and biofilm formation. A complete list of FC values and FDR-adjusted *P* values is provided in Supplementary Table 1. FC data are average measurements from *n*=2 biologically independent replicates.

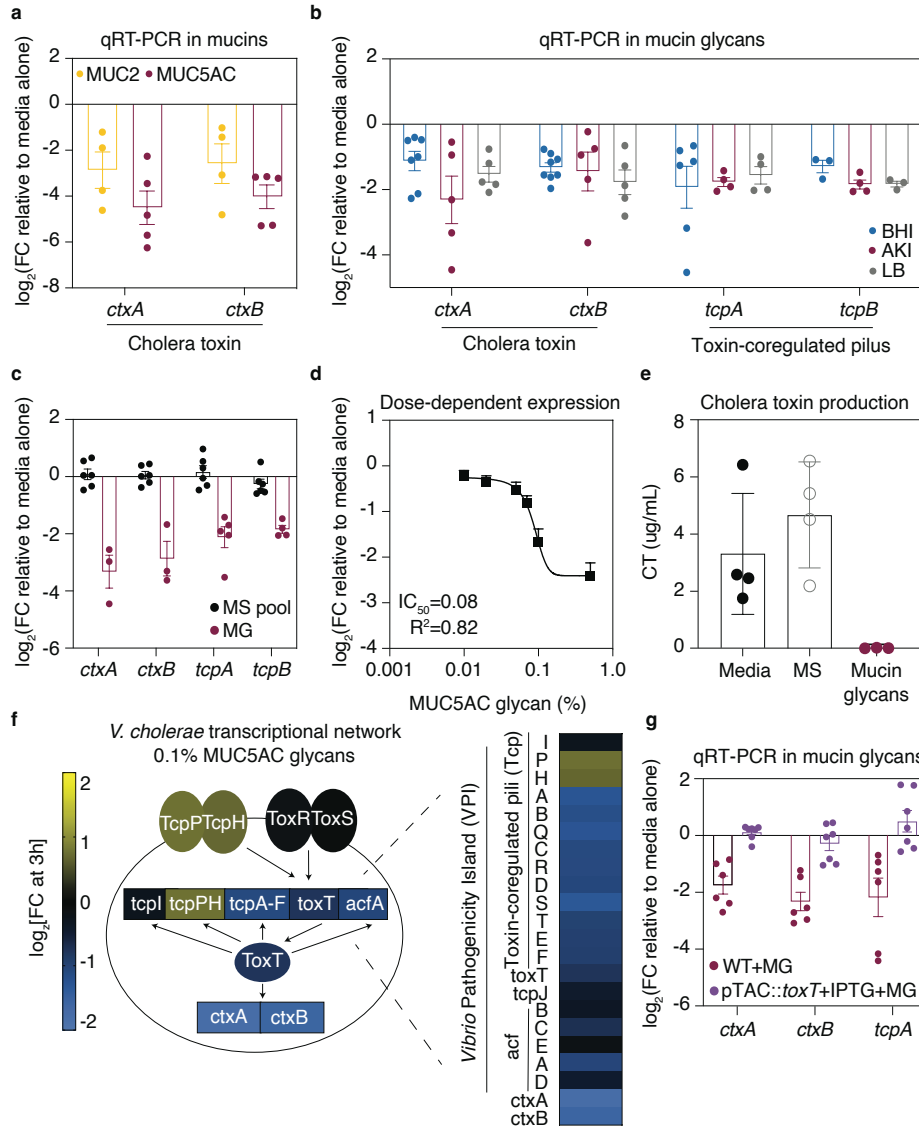


Figure 3.3: Mucin glycans downregulate the expression and production of cholera toxin

a) Full-length mucins downregulate the expression of cholera toxin relative to media alone. Gene expression measured by qRT-PCR and normalized to a control gene (*gyrA*). Bars indicate mean \pm SEM, with individual measurements shown.

b) Mucin glycans downregulate the expression of cholera toxin and TCP-encoding genes in three different media conditions. Gene expression measured by qRT-PCR and normalized to a control gene (*gyrA*). Bars indicate mean \pm SEM, with individual measurements shown.

c) Complex mucin glycans (MG), but not their monosaccharide components (MS pool), induce expression changes in CTX ϕ -associated virulence genes relative to media (AKI) alone. Gene

expression measured by qRT-PCR and normalized to a control gene (*gyrA*). Bars indicate mean \pm SEM, with individual measurements shown.

d) Mucin glycans regulate *ctxA* expression in a dose-dependent manner. Gene expression was measured by qRT-PCR and normalized to a control gene (*gyrA*). Bars indicate mean \pm SEM, with individual measurements shown. A nonlinear antagonist binding best-fit curve finds that the half-maximum inhibitory concentration (IC_{50}) is 0.087 wt% ($R^2 = 0.82$).

e) Complex mucin glycans, but not their monosaccharide (MS) components, suppress cholera toxin production. Bars indicate mean \pm SEM, with individual measurements shown. MS, monosaccharides.

f) Schematic overview of the regulation of cholera toxin (*ctxAB*) expression in *V. cholerae*, with each component colored according to its relative fold change in the presence of mucin glycans. Genes on the VPI are specifically highlighted. A complete list of FC values and FDR-adjusted P values is provided in Supplementary Table 1. FC data are average measurements from $n=2$ biologically independent replicates.

g) Mucin glycans (MG) are unable to downregulate the expression of CTX ϕ -associated virulence genes when *toxT* is constitutively expressed in a strain in which the native promoter for *toxT* has been replaced with an IPTG-inducible promoter. Gene expression measured by qRT-PCR and normalized to a control gene (*gyrA*). Bars indicate mean \pm SEM, with individual measurements shown. MG, mucin glycans.

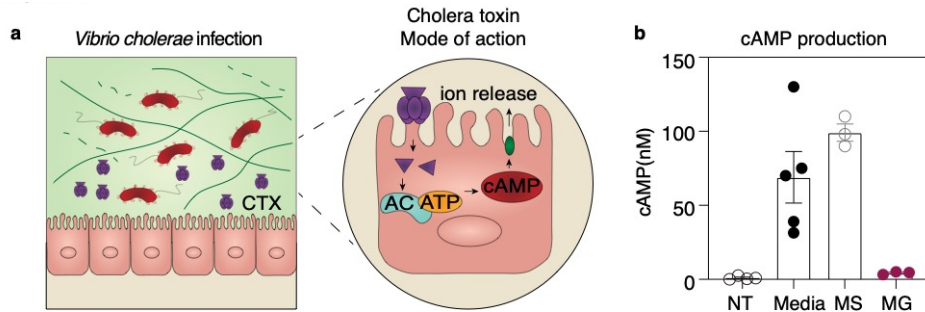


Figure 3.4: Mucin glycans reduce cAMP production

a) Schematic of cholera toxin mode of action. Cholera toxin activates adenylate cyclase activity leading to elevated cAMP levels and activation of cytosolic PKA. Active PKA leads to ATP-mediated efflux of ions and water from enterocytes.

b) cAMP levels decrease in HT29 cells exposed to supernatant grown in the presence of mucin glycans compared to the supernatant of cells grown in media alone or monosaccharides. Bars indicate mean \pm SEM, with individual measurements shown. NT, no treatment; MS, monosaccharides; MG, mucin glycans.

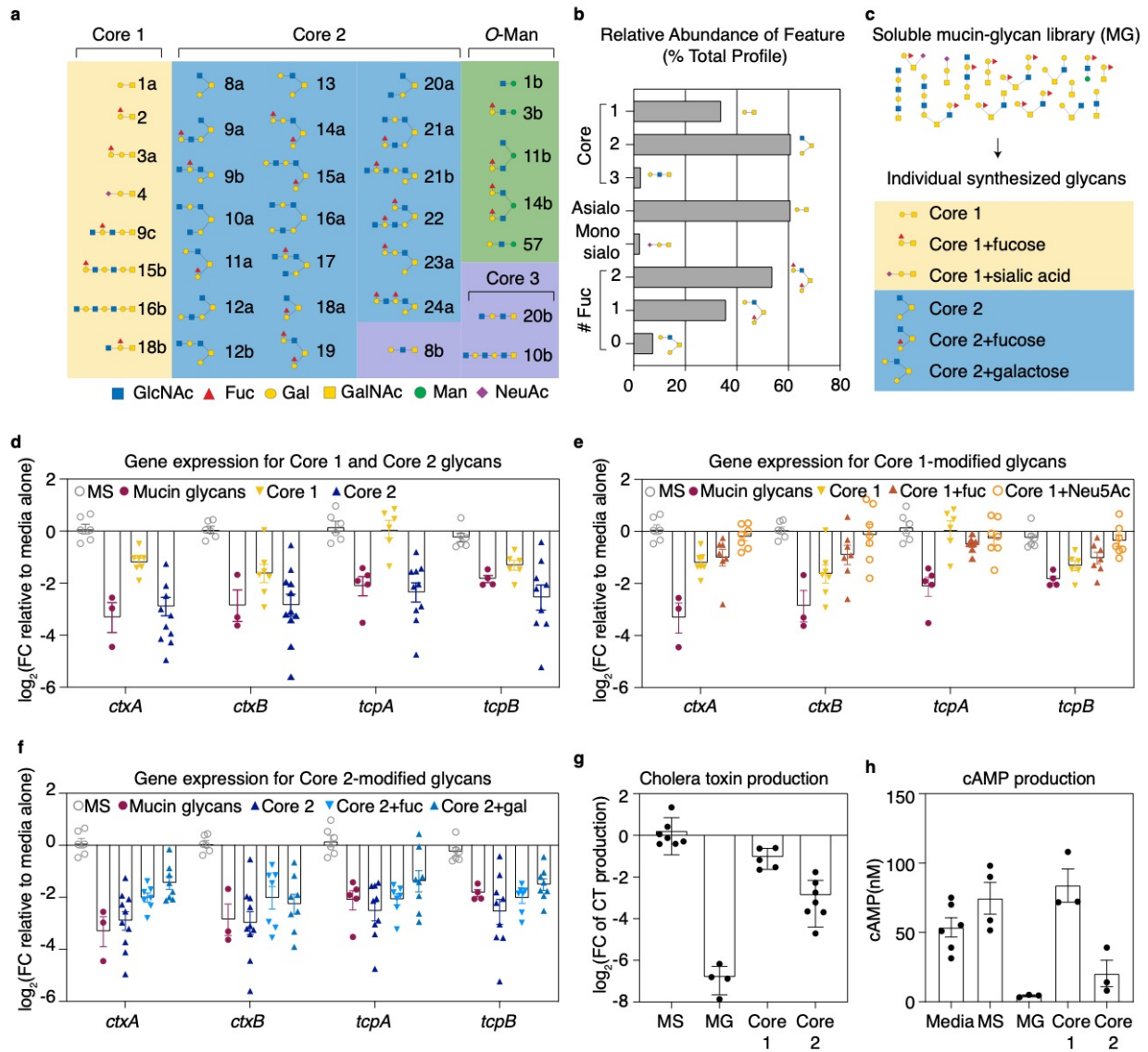


Figure 3.5: Synthesized Core 2 glycan structures recapitulate the mucin-attenuating response

a) O-Glycan structural diversity detected by NSI-MS (Methods) analysis of the O-linked glycans released from MUC5AC glycans. Glycan structures depicted are over >1% of the relative abundance of the glycan pool. GalNAc, *N*-acetylgalactosamine; GlcNAc, *N*-acetylglucosamine; Man, mannose; Fuc, fucose; NeuAc, *N*-acetylneuraminic acid; Gal, galactose.

b) Relative abundances of Core structural features in the MUC5AC glycan pool. The complex mucin glycan pool is dominated by Core 1 and Core 2-derived glycan structures that are heavily fucosylated and sparsely sialylated.

- c) Depiction of synthesized mucin glycan structures that are abundant in the complex mucin glycan pool.
- d) Exposure to the Core 2 glycan structures decreases the expression of cholera toxin, while Core 1 elicits a dampened effect. Gene expression was measured by qRT-PCR and normalized to a control gene (*gyrA*). Bars indicate mean \pm SEM, with individual measurements shown. MS, monosaccharides.
- e) Addition of fucose or sialic acid to Core 1 does not measurably alter the expression of cholera toxin and toxin coregulated pili production. Gene expression was measured by qRT-PCR and normalized to a control gene (*gyrA*). Bars indicate mean \pm SEM, with individual measurements shown. MS, monosaccharides.
- f) Addition of fucose or galactose to Core 2 does not alter the expression of cholera toxin and toxin co-regulated pili relative to Core 2 alone. Gene expression was measured by qRT-PCR and normalized to a control gene (*gyrA*). Bars indicate mean \pm SEM, with individual measurements shown. MS, monosaccharides.
- g) Core 2 glycans reduce cholera toxin production by nearly 10-fold, while Core 1 glycans reduce toxin production by 2-fold. Cholera toxin production was measured using a GM1-ELISA based assay. Bars indicate mean \pm SEM, with individual measurements shown. MS, monosaccharides; MG, mucin glycans.
- h) cAMP levels are decreased in HT29 cells exposed to supernatant grown in the presence of Core 2 compared to the supernatant of cells grown in Core 1, media alone or monosaccharides (MS). Bars indicate mean \pm SEM, with individual measurements shown. MS, monosaccharides; MG, mucin glycans.

Chapter 4: Conclusions and Future Directions

Conclusions

In this thesis, I analyzed the role of mucins on regulating microbial virulence, host-pathogen interactions, and cross-kingdom competition. In Chapter 2, I isolated and catalogued >100 mucin *O*-glycans from three major mucosal surfaces and established that they suppress filamentation and related phenotypes relevant to *Candida albicans* infection, including surface adhesion, biofilm formation, and interspecies interactions between *C. albicans* and the bacterium *Pseudomonas aeruginosa*. Using synthetic *O*-glycans, I identified three synthesized structures that recapitulate the mucin glycan response and inhibit filamentation with potency comparable to the complex *O*-glycan pool. In Chapter 3, I determined that mucins and their associated glycans block toxigenic conversion by CTX ϕ suggesting that mucus prevents the evolution of hypervirulent strains. Further, I found that mucin glycans directly suppress the expression of CTX ϕ -encoded cholera toxin and toxin-coregulated pili through a ToxT-dependent mechanism. By synthesizing individual mucin glycan structures *de novo*, I identified the Core-2 motif as the critical structure responsible for this observed virulence attenuation. Collectively, the projects in my thesis established that mucins display an abundance of virulence-attenuating molecules in the form of mucin *O*-glycans, which serve a multifaceted role in preserving host health, and thus opens many avenues of future research that I detail in this chapter.

Future directions

Glycan-responsive receptors

The complexity and diversity of mucin glycans makes them ideal for encoding potential regulatory information with a high degree of specificity. In Chapter 2, I determined that the transcriptional regulator, Nrg1, is crucial in mucin glycan-mediated virulence suppression in *Candida albicans*. Despite elucidating the pathways in which mucin glycans act by, the receptors involved in sensing mucin glycans leading to *NRG1* upregulation remain unknown. Although extensive studies have recognized an increasing number of genes regulating the yeast-hyphal transition, the early stages of inducer sensing are not well understood in *C. albicans*, confounding our ability to screen and identify mucin glycan receptors. Nrg1 regulation is temporally coordinated by two central signaling pathways mediating cell growth (Y. Lu et al., 2011). Upon hyphal induction, Nrg1 is

transiently transcriptionally downregulated and degraded leading to its dissociation from the promoters of hyphal-specific genes and initiating the downstream filamentation pathways. The transcriptional downregulation of *NRG1* occurs via the cAMP-PKA pathway, while Nrg1 degradation depends on the release of the quorum sensing molecule, farnesol, from hyphal promoters using a cAMP-PKA independent pathway (Y. Lu et al., 2014). In a preliminary screen using a transcription factor deletion library, deletion of *SFL1* led to *C. albicans* filamentation in the presence or absence of mucin glycans. Sfl1 inhibits Brg1 and Efg1 upon cAMP-PKA pathway activation, suggesting that mucin glycans may act during the initial activation to prevent hyphal-gene expression (Znaidi et al., 2013). However, we observed that in the presence of mucins glycans, expression of filamentation and/or yeast-associated genes continued to be differentially regulated (*NRG1*, *YWP1*), despite the lack of filamentation-suppression, while expression in other genes was completely or partially ablated (*HGC1*, *UME6*, *ECE1*) (Fig. 4.1). These results indicate that mucin glycans likely act through multiple pathways to downregulate sets of virulence-associated genes. This is consistent with recent work in *Pseudomonas aeruginosa*, which established that mucin glycans act through RetS to inhibit Type VI Secretion. Meanwhile, other virulence-associated pathways, such as quorum sensing, biofilm, and siderophore production, acted via a RetS-independent mechanism (Wang, Wheeler, et al., 2021) highlighting that mucin glycans act through multiple distinct pathways to control microbial virulence.

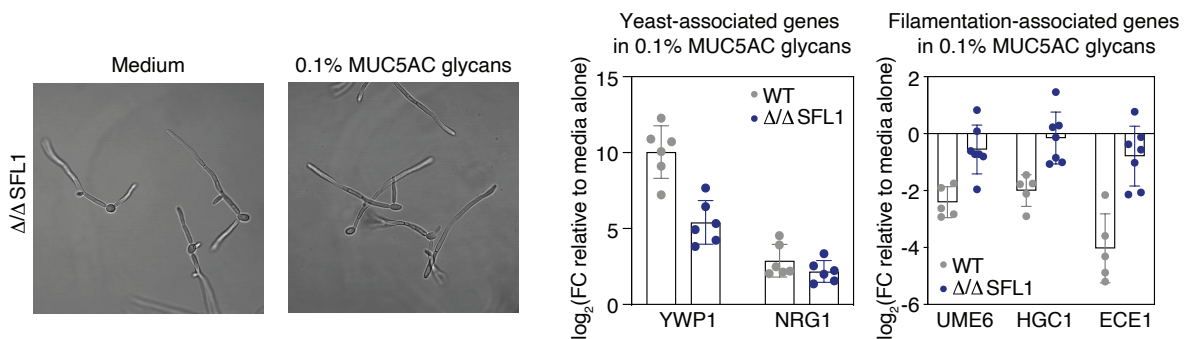


Fig. 4.1 Mucin glycans do not suppress filamentation in a $\Delta/\Delta sfl1$ mutant. Phase-contrast images of *C. albicans* WT and $\Delta/\Delta sfl1$ were acquired after 8 h in the presence or absence of mucin glycan libraries purified from MUC5AC (left). RT-qPCR for yeast and filamentation-associated genes in the presence or absence of mucin glycans in *C. albicans* WT and $\Delta/\Delta sfl1$ cells.

After hyphal initiation, Nrg1 levels gradually increase to those in yeast cells (Y. Lu et al., 2011). Thus, for sustained hyphal formation, cells must actively sense their environment triggering Nrg1 exclusion from hyphal-specific genes or reduced *NRG1* expression. Nutrient-poor environment and certain environmental factors, such as serum or bacterial peptidoglycan, sustain hyphal development (Y. Lu et al., 2011). Inhibition of Tor1, the central regulator of cell growth and nutrient availability in *C. albicans*, through sub-lethal doses of rapamycin, leads to robust hyphal elongation in rich medium (Y. Lu et al., 2014). The transcriptional regulator, Brg1, is a sensitive readout to Tor1 signaling (Y. Lu et al., 2012; Su et al., 2013). Overexpression of Brg1 activates *UME6* expression, which leads to sustained hyphal development by inhibiting Nrg1 binding of hyphal promoters (Cleary et al., 2012). Preliminary data suggest that *C. albicans* remains filamentous in the presence of sub-lethal doses of rapamycin implying that mucin-glycans act through modulating nutritional cues. However, downregulation of filamentation-genes was observed both in the presence and absence of mucin glycans under these conditions, suggesting that gene regulation may be more complex (data not shown).

Understanding how external signals are sensed and how these sensors activate these signal transduction pathways remains relatively unknown in *C. albicans*. Mucin glycans may be directly sensed by microbial receptors, such as the membrane bound histidine kinases, second messenger systems, nutritional sensors, or sugar binding cell-wall proteins. Additionally, mucin glycans may function as ligands to mimic nutrient signaling pathways, thus inhibiting hyphal maintenance pathways. Many open questions need to be addressed to gain a detailed understanding on the mucin glycan-mediated responses. For example, it remains unclear whether mucin glycans are sensed via direct interaction with cell wall, membrane-bound proteins, or if mucin glycans enter intracellularly and contribute to virulence-attenuation without altering cell growth. Additionally, it is unclear whether mucin glycans act through multiple mechanisms and/or if individual glycan structures can modulate specific pathways. Screening libraries with individual glycan structure may be able to elucidate the signaling pathways and receptors involved in the mucin-glycan response and their contribution in mucin glycan-mediated virulence suppression; however, these may be limited by the functional redundancy of gene families in *C. albicans*. Despite these limitations, uncovering the receptors involved in sensing mucin glycans and the pathways regulated by glycans will elucidate how *C. albicans* senses its host environment and how these cues regulate the morphologic transition between commensalism and pathogenicity.

Expanding the repertoire of synthetic glycan library

Given the tremendous complexity and diversity of mucin glycans, along with the dynamic changes in glycosylation according to disease state and immunoregulatory responses (Jiang et al., 2018; Reily et al., 2019; Tian & Ten Hagen, 2009), it is anticipated that mucin-glycans possess a myriad of specific functions to host-microbe interactions. In Chapter 2, I test six distinct glycan structures for biological activity in *Candida albicans* and in Chapter 3 for *Vibrio cholerae*. In *C. albicans*, I observe a sliding scale of bioactivity for each glycan structure instead of an on-off switch. Meanwhile, in *V. cholerae*, the mucin glycan virulence-suppression seems dependent on glycan identity and structure. By screening prominent glycan structures shared across three mucin species, my work has provided the foundation for probing the role and function mucin glycans.

The structural diversity across the three glycan pools can exceed to several hundred glycan structures when isomeric forms and modification such as sulfation are considered, suggesting glycan diversity has evolved to be functionally important. Key questions remain including the function of larger, branched structures that may be specific to a mucin-type whether glycan structures have synergistic effects when combined. Limitations to probing these questions include the synthesis of individual glycans, which is time-consuming and technically difficult, as glycan structures become longer and more complex. Advancements in glycan synthesis methods would allow us to screen a larger library of glycans, individually and in combination, to help identify structural features required for activity and address synergistic effects. In conjunction with the synthetic approach, optimization procedures for fractionating the purified glycan pool using a combination of mixed-mode hydrophilic interaction liquid chromatography/anion exchange chromatography (HILIC/AEX), which separates glycans based on length and number of negative charges (Deguchi et al., 2008), and PGC chromatography, which separates glycans based on hydrophobic interactions and hydroxyl orientations (Abrahams et al., 2018) could identify specific structural features required for activity. Systematically identifying the glycan-code underlying mucin glycan virulence-attenuation may provide a platform for discovery of novel therapeutic and diagnostic strategies for mucosal disease.

Evolution of pathogenicity

In Chapter 3, I report that in the presence of mucins *V. cholerae* shows a striking reduction in CTX ϕ transduction efficiency relative to media alone. The emergence of toxigenic *Vibrio cholerae*

serotypes is driven by the evolution of nonpathogenic environmental strains acquiring virulence genes with pandemic potential (Mavian et al., 2020; Nelson et al., 2009). The acquisition of these virulence genes occurs via horizontal gene transfer events, which allows the uptake and integration of genes through three main mechanisms: transformation, transduction, and conjugation. In *V. cholerae*, the major virulence factors, cholera toxin and toxin coregulated pili (TCP), are encoded by a filamentous bacteriophage and a pathogenicity island respectively, suggesting that the generation of toxigenic strains occurred primarily through phage transduction and conjugation events (Baker-Austin et al., 2018; Herrington et al., 1988; Nelson et al., 2009). Besides cholera toxin and TCP, *Vibrio cholerae* has acquired several other mobile genetic elements from prophages (GJ Φ , RS1, TLC Φ), pathogenicity islands (VPI-2, VSP-1 & VSP-2) and integrative conjugative elements (ICEs) that have been implicated in enhancing *V. cholerae* fitness (Kumar et al., 2020; J. F. Miller, 2003; Rajanna et al., 2003; Sarkar et al., 2019). The frequent acquisition of novel genes has allowed *V. cholerae* to rapidly adapt to adverse environmental conditions driving multidrug resistance to treatment and the evolution of novel pathogenic isolates (De, 2021). For example, unlike its predecessors, the seventh pandemic strain of *V. cholerae* horizontally acquired two genomic islands (VSP-1 and VSP-II) and a resistance marker to the antimicrobial agent, polymyxin B, augmenting its pathogenicity (Imamura et al., 2017, 2017; Murphy et al., 2021). While mucins and their associated glycans have been shown to decrease CTX ϕ transduction, it remains unknown if this effect observed in *V. cholerae* is a general phenomenon extending to other phage types and other modes of horizontal gene transfer. Understanding signals that influence the acquisition and evolution of new pathogenic strains in both the natural aquatic habitats and within the gastrointestinal tracts of hosts during infection is crucial.

Metabolic role of commensals

While much of my thesis has focused on mucin glycans modulating virulence behaviors in pathogens, the mucus barrier houses trillions of commensal microbes which perform essential functions for host health (Wang, Wu, et al., 2021). There has been a great deal of research on the roles of these commensals and their ability to degrade mucins in the absence of another carbon source; however, an understanding on how mucins modulate their physiology is largely lacking. For most commensals, mucin glycans are not a preferred carbon source and are utilized when host dietary carbohydrates are depleted (Nicholson et al., 2012). Despite not being utilized as a primary nutritional source, mucin glycans play an important role in shaping the microbiota (Sonnenburg et

al., 2005). For example, animal studies have demonstrated that mice that received orally administered mucin glycans exhibit a reduction in bacterial burden of, *C. difficile*, a delay in diet-induced obesity, and an increase in the mucolytic commensal, *A. muciniphila*, which is associated with increased intestinal barrier function (Pruss et al., 2021). A mechanistic understanding on how mucin glycans underly this response remains unclear, but it is likely through both metabolic and regulatory functions.

To understand the role of mucin glycans on influencing host commensals, I grew the commensals, *Escherichia coli*, *Enterococcus faecalis*, and *Bacteroides fragilis*, anaerobically with or without mucin glycans in a rich medium (BHI+vitamin K+hemin). Of note, the growth rate of these strains did not change in the presence or absence of mucin glycans, suggesting that these microbes are not utilizing mucin glycans as a major carbon source (Fig. 4.2). However, using RNA-Sequencing revealed that over a hundred genes were differentially regulated in each of microbes demonstrating that mucin glycans can affect the physiology of these microbes in conditions where they are not serving as a primary nutrient source (Fig. 4.3a). Interestingly, many of the pathways regulated by mucin glycans were involved in metabolism, suggesting mucin glycans may modulate metabolism independent of growth. As a commensal, these microbes have evolved and adapted to the host mucus environment; however, future work aims to have a more detailed understand on how these commensals sense and respond to mucin glycans as well as how these responses impact resident commensals and the broader microbial community.

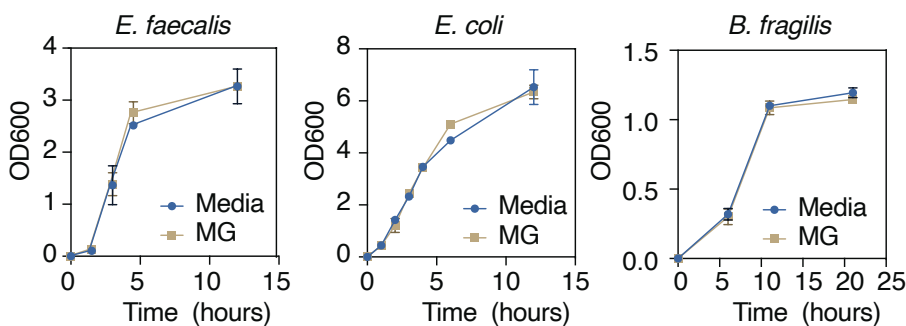


Fig. 4.2 Mucin glycans do not alter the growth of intestinal commensal microbes. Growth of *E. faecalis*, *E. coli*, and *B. fragilis* in BHI+hemin+Vitamin K media with or without mucin glycans.

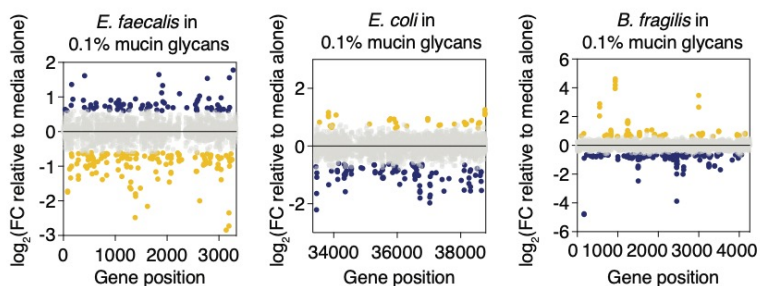


Fig. 4.3 Plots summarizing RNA-Seq profiling of *E. faecalis*, *E. coli*, and *B. fragilis* in 0.1% MUC5AC glycans in BHI+hemin+Vitamin K media. In yellow are significantly upregulated genes and in blue are significantly downregulated genes.

Designing glycomimetic therapeutics

Antifungal resistance is an emerging problem worldwide. Clinical antifungal agents available are somewhat limited with azoles, echinocandins and polyenes as the three main types of antifungal classes. However, about 7% of all *Candida* blood samples tested at the Center for Disease Control and Prevention (CDC) are resistant to the azole, fluconazole, and an increasing resistance to echinocandins is particularly concerning (*Antifungal Resistance in Candida | Fungal Diseases | CDC, 2020*). Patients with *Candida* infections that are resistant to both fluconazole and echinocandin drugs have limited treatment options (Pemán et al., 2009). Collectively, the limited efficacy, toxicity, and the development of resistance contribute to a high mortality rate of ~40% in deep-seated candidiasis (Robbins et al., 2017), highlighting an urgent need for alternative treatments to fungal infections. In Chapter 2, I identify mucin *O*-glycans as potent host molecules with untapped therapeutic potential to manage fungal infection through targeting virulence pathways. Mucin glycans attenuate virulence in *C. albicans* without killing, thus abolishing the selective pressure that drives resistance with antifungal usage. Beyond the issue of resistance, antifungal agents can have off-target consequences on the composition and function of the microbiota, making the host more susceptible to bacterial overgrowth and dysbiosis. Therefore, the discovery of *O*-glycans that can control virulence traits without killing the microbe may lead to the development novel glycan-based or glycan-mimetic therapeutics that enhance, or potentially replace, current antifungals. By harnessing naturally occurring host-derived virulence-attenuating molecules, I anticipate that soluble mucin glycans will have fewer off-target side effects than

traditional treatment, evade the evolution of resistance and, in conjunction with treating infection, may promote a healthy microbiota.

Many well-known small-molecule drugs, such as antibiotics and anticancer agents, naturally contain glycans as part of their core structure and/or sugar side chain and several classes of therapeutics are based on isolated or synthetic glycans (Ernst & Magnani, 2009). Currently, most biotherapeutic products are glycoproteins, including cytokines, antibodies, glycosyltransferases, and glycosidases (Ernst & Magnani, 2009). Glycosylation provides a crucial role in the activity and stability of these therapeutics in the body (Seeberger & Cummings, 2015). For example, the glycoprotein erythropoietin is a circulating cytokine, containing both sialylated *N*-glycans and *O*-glycans that bind to the erythropoietin receptor, leading to the proliferation of red blood cells, providing an effective treatment to those with anemia (Falck et al., 2017). Deglycosylation of erythropoietin leads to rapid clearance by filtration in the kidney reducing its efficacy by ~90%, demonstrating the crucial role of glycosylation in function (Delorme et al., 1992).

Native glycans, which are unconjugated to larger macromolecules, are generally ineffective as small-molecule pharmaceuticals due to their inherently poor pharmacokinetic properties, poor oral absorption, and low-affinity interactions with drug targets (Hevey, 2019). Some successful glycan drugs, include heparin, a glycosaminoglycan that serves as an anticoagulant to prevent blood clots by binding to the enzyme, antithrombin, via a pentasaccharide sulfation sequence (Ernst & Magnani, 2009). Other glycan-inspired drugs include the antiviral treatment, zanamivir (Relenza) and oseltamivir (Tamiflu) which are glycomimetics that competitively interfere with the activity of neuraminidase, thus inhibiting the release and propagation of the influenza virus from host cells (Seeberger & Cummings, 2015).

By identifying the most bioactive mucin *O*-glycans, we can establish the precise glycan epitopes required for activity to design glycomimetic structures that retain activity while exhibiting improved drug-like properties for fungal and bacterial infections. Modification such as multivalent glycan presentation can lead to conjugates with enhanced efficacies and improved pharmacokinetic properties (Hevey, 2019). Beyond treatment for infection, these glycan components can be more broadly utilized to create mucin-inspired mimetics. Mucin mimetics, such as artificial saliva and eyedrops, have typically focused on the lubricating and hydrating properties of the mucin gel without addressing the virulence-attenuating activity embedded in mucins (Werlang et al., 2019).

In xerostomic patients, there is an increased susceptibility to microbial colonization leading to oral infections (e.g., candidiasis), highlighting a need for mucin mimetic therapeutics with microbe virulence-attenuating capacity (Nadig et al., 2017; Tarapan et al., 2019). By identifying glycan structures that are important in suppressing microbial virulence, we can engineer synthetic mucins with the identified structures grafted to a backbone which may recapitulate both the physical and biological properties of the mucus gel.

References

- Abrahams, J. L., Campbell, M. P., & Packer, N. H. (2018). Building a PGC-LC-MS N-glycan retention library and elution mapping resource. *Glycoconjugate Journal*, 35(1), 15–29. <https://doi.org/10.1007/s10719-017-9793-4>
- Antifungal Resistance in Candida | Fungal Diseases | CDC*. (2020, May 18). <https://www.cdc.gov/fungal/diseases/candidiasis/antifungal-resistant.html>
- Baker-Austin, C., Oliver, J. D., Alam, M., Ali, A., Waldor, M. K., Qadri, F., & Martinez-Urtaza, J. (2018). *Vibrio* spp. Infections. *Nature Reviews Disease Primers*, 4(1), 1–19. <https://doi.org/10.1038/s41572-018-0005-8>
- Cleary, I. A., Lazzell, A. L., Monteagudo, C., Thomas, D. P., & Saville, S. P. (2012). BRG1 and NRG1 form a novel feedback circuit regulating *Candida albicans* hypha formation and virulence: *C. albicans* mRNA stability and virulence. *Molecular Microbiology*, 85(3), 557–573. <https://doi.org/10.1111/j.1365-2958.2012.08127.x>
- De, R. (2021). Mobile Genetic Elements of *Vibrio cholerae* and the Evolution of Its Antimicrobial Resistance. *Frontiers in Tropical Diseases*, 2. <https://www.frontiersin.org/article/10.3389/fitd.2021.691604>
- Deguchi, K., Keira, T., Yamada, K., Ito, H., Takegawa, Y., Nakagawa, H., & Nishimura, S.-I. (2008). Two-dimensional hydrophilic interaction chromatography coupling anion-exchange and hydrophilic interaction columns for separation of 2-pyridylamino derivatives of neutral and sialylated N-glycans. *Journal of Chromatography A*, 1189(1), 169–174. <https://doi.org/10.1016/j.chroma.2007.09.028>
- Delorme, E., Lorenzini, T., Giffin, J., Martin, F., Jacobsen, F., Boone, T., & Elliott, S. (1992). Role of glycosylation on the secretion and biological activity of erythropoietin. *Biochemistry*, 31(41), 9871–9876. <https://doi.org/10.1021/bi00156a003>
- Ernst, B., & Magnani, J. L. (2009). From carbohydrate leads to glycomimetic drugs. *Nature Reviews Drug Discovery*, 8(8), 661–677. <https://doi.org/10.1038/nrd2852>
- Falck, D., Habegger, M., Plomp, R., Hook, M., Bulau, P., Wuhler, M., & Reusch, D. (2017). Affinity purification of erythropoietin from cell culture supernatant combined with MALDI-TOF-MS analysis of erythropoietin N-glycosylation. *Scientific Reports*, 7(1), 5324. <https://doi.org/10.1038/s41598-017-05641-1>

- Herrington, D. A., Hall, R. H., Losonsky, G., Mekalanos, J. J., Taylor, R. K., & Levine, M. M. (1988). Toxin, toxin-coregulated pili, and the *toxR* regulon are essential for *Vibrio cholerae* pathogenesis in humans. *The Journal of Experimental Medicine*, *168*(4), 1487–1492. <https://doi.org/10.1084/jem.168.4.1487>
- Hevey, R. (2019). Strategies for the Development of Glycomimetic Drug Candidates. *Pharmaceuticals (Basel, Switzerland)*, *12*(2), E55. <https://doi.org/10.3390/ph12020055>
- Imamura, D., Morita, M., Sekizuka, T., Mizuno, T., Takemura, T., Yamashiro, T., Chowdhury, G., Pazhani, G. P., Mukhopadhyay, A. K., Ramamurthy, T., Miyoshi, S., Kuroda, M., Shinoda, S., & Ohnishi, M. (2017). Comparative genome analysis of VSP-II and SNPs reveals heterogenic variation in contemporary strains of *Vibrio cholerae* O1 isolated from cholera patients in Kolkata, India. *PLoS Neglected Tropical Diseases*, *11*(2), e0005386. <https://doi.org/10.1371/journal.pntd.0005386>
- Jiang, Y., Liu, Z., Xu, F., Dong, X., Cheng, Y., Hu, Y., Gao, T., Liu, J., Yang, L., Jia, X., Qian, H., Wen, T., & An, G. (2018). Aberrant O-glycosylation contributes to tumorigenesis in human colorectal cancer. *Journal of Cellular and Molecular Medicine*, *22*(10), 4875–4885. <https://doi.org/10.1111/jcmm.13752>
- Kumar, A., Das, B., & Kumar, N. (2020). *Vibrio* Pathogenicity Island-1: The Master Determinant of Cholera Pathogenesis. *Frontiers in Cellular and Infection Microbiology*, *10*. <https://www.frontiersin.org/article/10.3389/fcimb.2020.561296>
- Lu, Y., Su, C., & Liu, H. (2012). A GATA Transcription Factor Recruits Hda1 in Response to Reduced Tor1 Signaling to Establish a Hyphal Chromatin State in *Candida albicans*. *PLOS Pathogens*, *8*(4), e1002663. <https://doi.org/10.1371/journal.ppat.1002663>
- Lu, Y., Su, C., & Liu, H. (2014). *Candida albicans* hyphal initiation and elongation. *Trends in Microbiology*, *22*(12), 707–714. <https://doi.org/10.1016/j.tim.2014.09.001>
- Lu, Y., Su, C., Wang, A., & Liu, H. (2011). Hyphal Development in *Candida albicans* Requires Two Temporally Linked Changes in Promoter Chromatin for Initiation and Maintenance. *PLOS Biology*, *9*(7), e1001105. <https://doi.org/10.1371/journal.pbio.1001105>
- Mavian, C., Paisie, T. K., Alam, M. T., Browne, C., Beau De Rochars, V. M., Nembrini, S., Cash, M. N., Nelson, E. J., Azarian, T., Ali, A., Morris, J. G., & Salemi, M. (2020). Toxigenic *Vibrio cholerae* evolution and establishment of reservoirs in aquatic

- ecosystems. *Proceedings of the National Academy of Sciences*, 117(14), 7897–7904.
<https://doi.org/10.1073/pnas.1918763117>
- Miller, J. F. (2003). Bacteriophage and the Evolution of Epidemic Cholera. *Infection and Immunity*, 71(6), 2981–2982. <https://doi.org/10.1128/IAI.71.6.2981-2982.2003>
- Murphy, S. G., Johnson, B. A., Ledoux, C. M., & Dörr, T. (2021). *Vibrio cholerae*'s mysterious Seventh Pandemic island (VSP-II) encodes novel Zur-regulated zinc starvation genes involved in chemotaxis and cell congregation. *PLOS Genetics*, 17(6), e1009624.
<https://doi.org/10.1371/journal.pgen.1009624>
- Nadig, S. D., Ashwathappa, D. T., Manjunath, M., Krishna, S., Annaji, A. G., & Shivaprakash, P. K. (2017). A relationship between salivary flow rates and *Candida* counts in patients with xerostomia. *Journal of Oral and Maxillofacial Pathology : JOMFP*, 21(2), 316.
https://doi.org/10.4103/jomfp.JOMFP_231_16
- Nelson, E. J., Harris, J. B., Glenn Morris, J., Calderwood, S. B., & Camilli, A. (2009). Cholera transmission: The host, pathogen and bacteriophage dynamic. *Nature Reviews Microbiology*, 7(10), 693–702. <https://doi.org/10.1038/nrmicro2204>
- Nicholson, J. K., Holmes, E., Kinross, J., Burcelin, R., Gibson, G., Jia, W., & Pettersson, S. (2012). Host-Gut Microbiota Metabolic Interactions. *Science*, 336(6086), 1262–1267.
<https://doi.org/10.1126/science.1223813>
- Pemán, J., Cantón, E., & Espinel-Ingroff, A. (2009). Antifungal drug resistance mechanisms. *Expert Review of Anti-Infective Therapy*, 7(4), 453–460. <https://doi.org/10.1586/eri.09.18>
- Pruss, K. M., Marcobal, A., Southwick, A. M., Dahan, D., Smits, S. A., Ferreyra, J. A., Higginbottom, S. K., Sonnenburg, E. D., Kashyap, P. C., Choudhury, B., Bode, L., & Sonnenburg, J. L. (2021). Mucin-derived O-glycans supplemented to diet mitigate diverse microbiota perturbations. *The ISME Journal*, 15(2), 577–591.
<https://doi.org/10.1038/s41396-020-00798-6>
- Rajanna, C., Wang, J., Zhang, D., Xu, Z., Ali, A., Hou, Y.-M., & Karaolis, D. K. R. (2003). The *Vibrio* Pathogenicity Island of Epidemic *Vibrio cholerae* Forms Precise Extrachromosomal Circular Excision Products. *Journal of Bacteriology*, 185(23), 6893–6901. <https://doi.org/10.1128/JB.185.23.6893-6901.2003>

- Reily, C., Stewart, T. J., Renfrow, M. B., & Novak, J. (2019). Glycosylation in health and disease. *Nature Reviews Nephrology*, *15*(6), 346–366. <https://doi.org/10.1038/s41581-019-0129-4>
- Robbins, N., Caplan, T., & Cowen, L. E. (2017). Molecular Evolution of Antifungal Drug Resistance. *Annual Review of Microbiology*, *71*, 753–775. <https://doi.org/10.1146/annurev-micro-030117-020345>
- Sarkar, A., Morita, D., Ghosh, A., Chowdhury, G., Mukhopadhyay, A. K., Okamoto, K., & Ramamurthy, T. (2019). Altered Integrative and Conjugative Elements (ICEs) in Recent *Vibrio cholerae* O1 Isolated From Cholera Cases, Kolkata, India. *Frontiers in Microbiology*, *10*. <https://www.frontiersin.org/article/10.3389/fmicb.2019.02072>
- Seeberger, P. H., & Cummings, R. D. (2015). Glycans in Biotechnology and the Pharmaceutical Industry. In A. Varki, R. D. Cummings, J. D. Esko, P. Stanley, G. W. Hart, M. Aebi, A. G. Darvill, T. Kinoshita, N. H. Packer, J. H. Prestegard, R. L. Schnaar, & P. H. Seeberger (Eds.), *Essentials of Glycobiology* (3rd ed.). Cold Spring Harbor Laboratory Press. <http://www.ncbi.nlm.nih.gov/books/NBK453070/>
- Sonnenburg, J. L., Xu, J., Leip, D. D., Chen, C.-H., Westover, B. P., Weatherford, J., Buhler, J. D., & Gordon, J. I. (2005). Glycan Foraging in Vivo by an Intestine-Adapted Bacterial Symbiont. *Science*, *307*(5717), 1955–1959. <https://doi.org/10.1126/science.1109051>
- Su, C., Lu, Y., & Liu, H. (2013). Reduced TOR signaling sustains hyphal development in *Candida albicans* by lowering Hog1 basal activity. *Molecular Biology of the Cell*, *24*(3), 385–397. <https://doi.org/10.1091/mbc.e12-06-0477>
- Tarapan, S., Matangkasombut, O., Trachootham, D., Sattabanasuk, V., Talungchit, S., Paemuang, W., Phonyiam, T., Chokchaitam, O., Mungkung, O.-O., & Lam-Ubol, A. (2019). Oral *Candida* colonization in xerostomic postradiotherapy head and neck cancer patients. *Oral Diseases*, *25*(7), 1798–1808. <https://doi.org/10.1111/odi.13151>
- Tian, E., & Ten Hagen, K. G. (2009). Recent insights into the biological roles of mucin-type O-glycosylation. *Glycoconjugate Journal*, *26*(3), 325–334. <https://doi.org/10.1007/s10719-008-9162-4>
- Wang, B. X., Wheeler, K. M., Cady, K. C., Lehoux, S., Cummings, R. D., Laub, M. T., & Ribbeck, K. (2021). Mucin Glycans Signal through the Sensor Kinase RetS to Inhibit

- Virulence-Associated Traits in *Pseudomonas aeruginosa*. *Current Biology*, 31(1), 90-102.e7. <https://doi.org/10.1016/j.cub.2020.09.088>
- Wang, B. X., Wu, C. M., & Ribbeck, K. (2021). Home, sweet home: How mucus accommodates our microbiota. *The FEBS Journal*, 288(6), 1789–1799. <https://doi.org/10.1111/febs.15504>
- Werlang, C., Cárcarmo-Oyarce, G., & Ribbeck, K. (2019). Engineering mucus to study and influence the microbiome. *Nature Reviews Materials*, 4(2), 134–145. <https://doi.org/10.1038/s41578-018-0079-7>
- Znaidi, S., Nesseir, A., Chauvel, M., Rossignol, T., & d'Enfert, C. (2013). A Comprehensive Functional Portrait of Two Heat Shock Factor-Type Transcriptional Regulators Involved in *Candida albicans* Morphogenesis and Virulence. *PLoS Pathogens*, 9(8), e1003519. <https://doi.org/10.1371/journal.ppat.1003519>

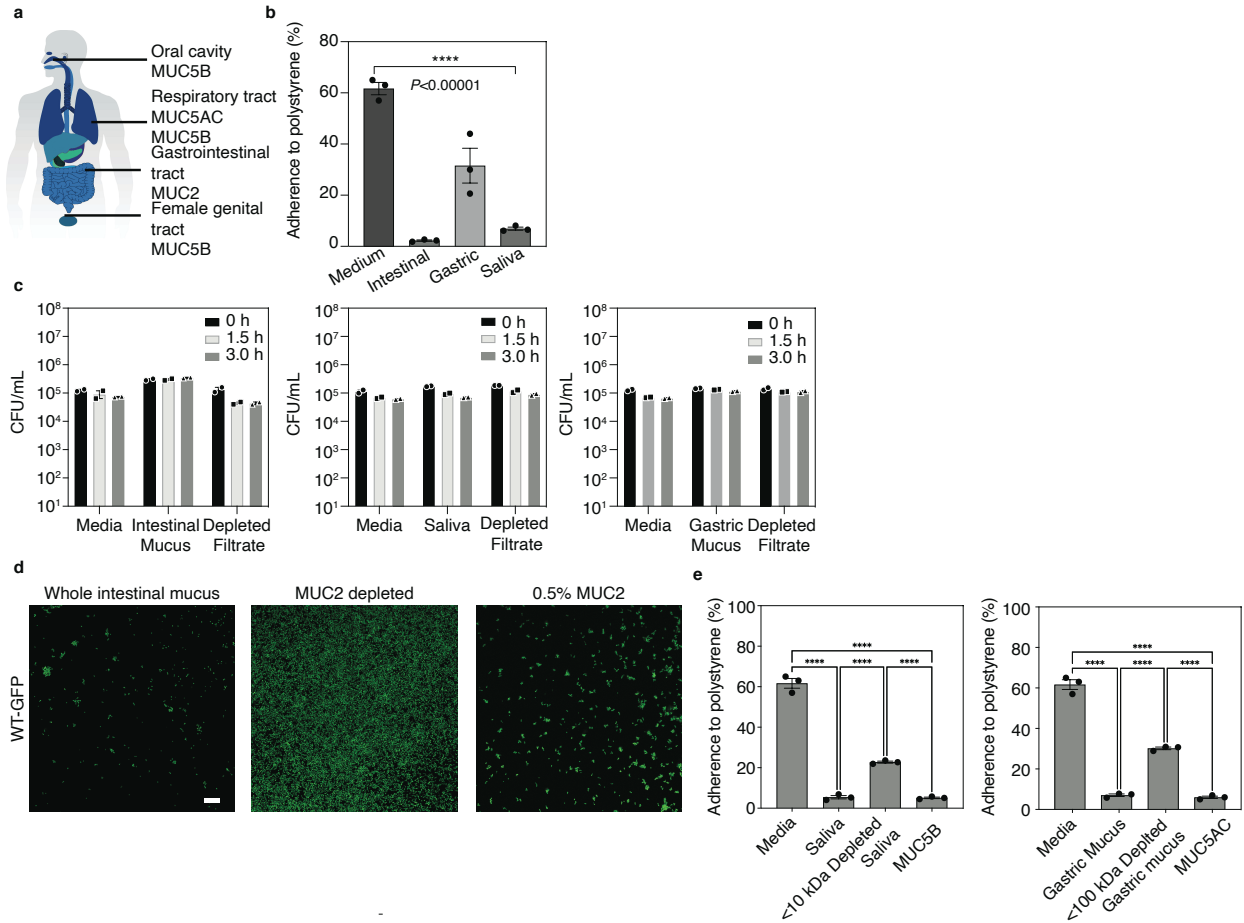
Appendix A: Supplementary Information for Chapter 2

Supplementary materials include:

Figure S2.3 to Figures S2.5

Tables S2.1 to S2.3

Data S2.1 to S2.4



Supplementary Figure 2.1: Mucins are the bioactive components of mucus that suppress adhesion and filamentation in *C. albicans* independent of growth

a) Mucus, which is made of gel-forming mucins (with protein names including MUC), covers all non-keratinized epithelial surfaces of the body. This study investigated MUC5B purified from human saliva and MUC2 and MUC5AC purified from porcine intestinal and gastric mucus respectively.

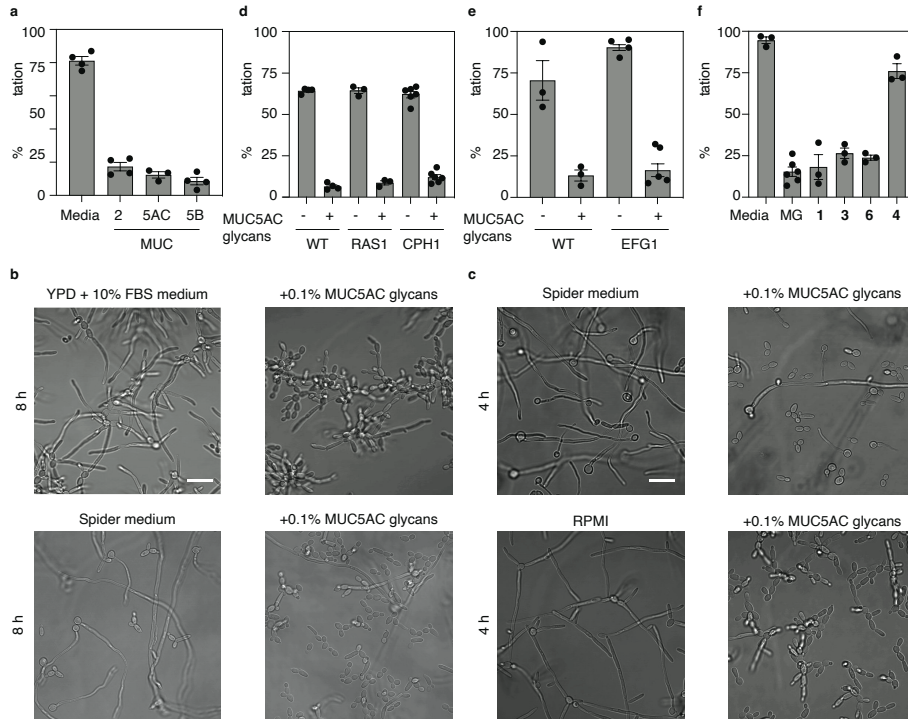
b) Native mucus across the major sources decreases adherence to polystyrene wells. Bars indicate mean \pm SEM from $n=3$ biologically independent replicates using fluorescence images. Significance was assessed using ordinary one-way ANOVA followed by Bonferroni's multiple comparisons; **** $P<0.0001$.

c) *C. albicans* SC5314 cells were diluted into RPMI medium in the presence or absence of mucus or a mucin-depleted filtrate. *C. albicans* colony-forming units (CFUs) were determined via serial

dilutions on YEPD plates. Data are mean CFU \pm standard error; $n=2$ biologically independent replicates.

d) Fluorescence microscopy images assaying adhesion of wild-type (WT) *C. albicans* expressing green fluorescent protein (GFP) at 90 min in mucus, mucus-depleted filtrate, or MUC2. Scale bar, 50 μm .

e) The depletion of mucus components leads to increased fungal adherence. Supplementation of mucus filtrates with exogenous purified mucins lead to decreased adhesion. Bars indicate mean \pm SEM from $n=3$ biologically independent replicates using fluorescence images. Significance was assessed using ordinary one-way ANOVA followed by Dunnett's multiple comparisons test; **** $P<0.0001$.



Supplementary Figure 2.2: Mucin glycan-mediated suppression of virulence pathways is independent of specific experimental conditions, including medium and time point

a) Quantification of *C. albicans* morphology in the presence of mucins at 8 h using phase-contrast images from $n=3$ (MUC5AC) or $n=4$ (Media, MUC5B, MUC2) independent biological replicates.

b) *C. albicans* SC5314 cells were diluted into the specified medium with or without mucin glycans and cultured at 37 °C for 8 h. Phase-contrast images of *C. albicans* were acquired after 8 h in the presence or absence of mucin glycan libraries purified from MUC5AC. Scale bar, 20 μm.

c) *C. albicans* SC5314 cells were diluted into the specified medium with or without mucin glycans and cultured at 37 °C. Phase-contrast images of *C. albicans* were acquired after 4 h in the presence or absence of mucin glycan libraries purified from MUC5AC. Scale bar, 20 μm.

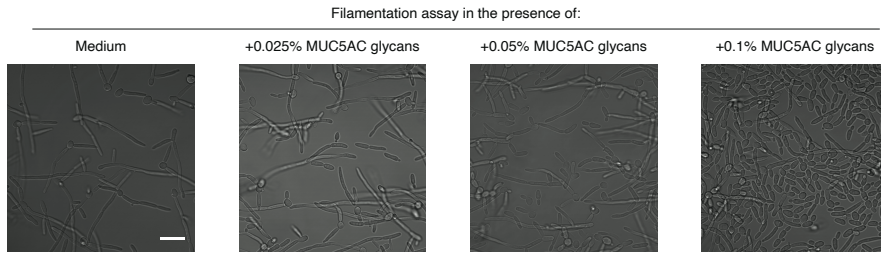
d) Quantification of *C. albicans* morphology in the presence of mucin glycans in RPMI medium at 8 h using phase-contrast images from $n=6$ (CPH1), $n=4$ (WT), $n=3$ (RAS1) independent biological replicates. *prADHI-CPH1* strain abbreviated as CPH1; *RASI^{G13V}* strain abbreviated as RAS1.

e) Quantification of *C. albicans* morphology in the presence of mucin glycans in Spider medium at 8 h using phase-contrast images from $n=3$ (WT), $n=4$ (EFG1-) or $n=5$ (EFG1+) independent biological replicates. *PCKpr-efg1-T206E* strain abbreviated as EFG1.

f) Quantification of *C. albicans* morphology in the presence of synthesized glycans in RPMI medium at 8 h using phase-contrast images from $n=6$ (MG) $n=3$ (Medium, C1, 2F, 2G, 1SA) independent biological replicates. C1, Core 1; 1F, Core 1+fucose; 2G, Core 2+galactose; 1SA, Core 1+sialic acid.

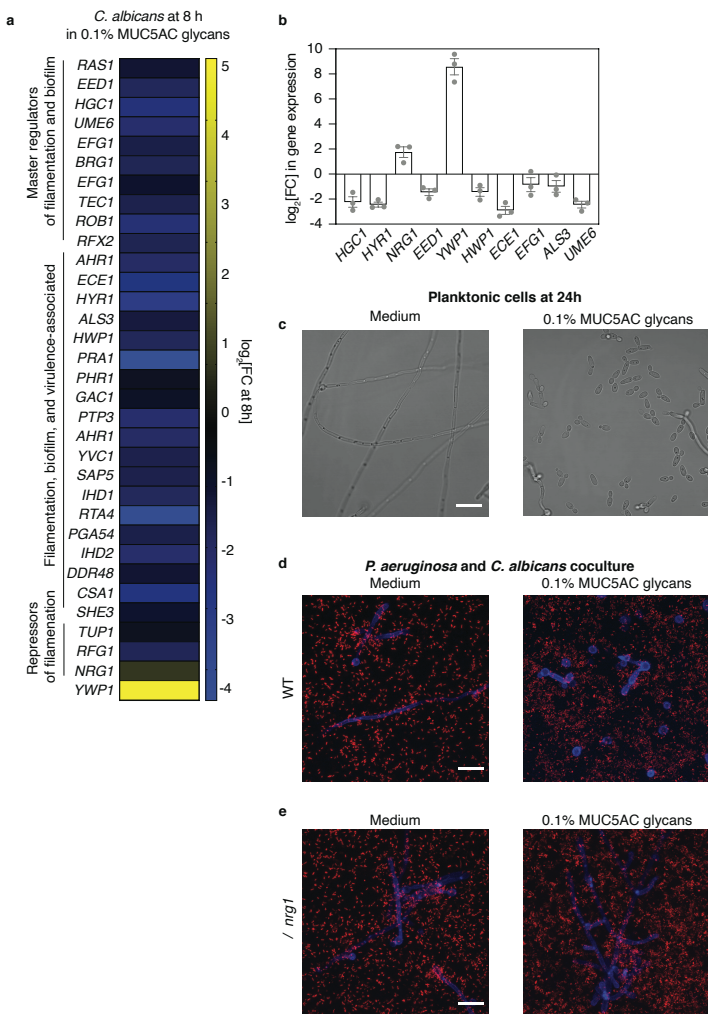
For **b,c**, similar results were observed in different fields of view across three independent replicates.

For **a,d,e,f**, the percentage of hyphae was obtained by dividing the number of hyphae by the total number of cells with $n>100$ cells. Bars indicate mean \pm SEM. MG, mucin glycans.



Supplementary Figure 2.3: Filamentation suppression by mucin glycans occurs in a concentration-dependent manner

C. albicans SC5314 cells were diluted into RPMI medium with or without mucin glycans at the indicated concentrations and cultured at 37°C for 8 h. Phase-contrast images of *C. albicans* were acquired after 8 h in the presence or absence of mucin glycan libraries purified from MUC5AC. Similar results were observed in different fields of view across three independent replicates. Scale bar, 20 μm .



Supplementary Figure 2.4: Mucin glycans downregulate virulence traits and alter fungal-bacterial dynamics

a) RNA sequencing data for selected genes belonging to the filamentation pathway that are differentially regulated in the presence of MUC5AC glycans at 8 h. A complete list of fold-change (FC) values and false discovery rate (FDR)-adjusted P values is provided in Supplementary Data 3. FC data are mean measurements from $n=3$ biologically independent replicates. FDR-adjusted P -values were determined using the Benjamini–Hochberg P -value adjustment method.

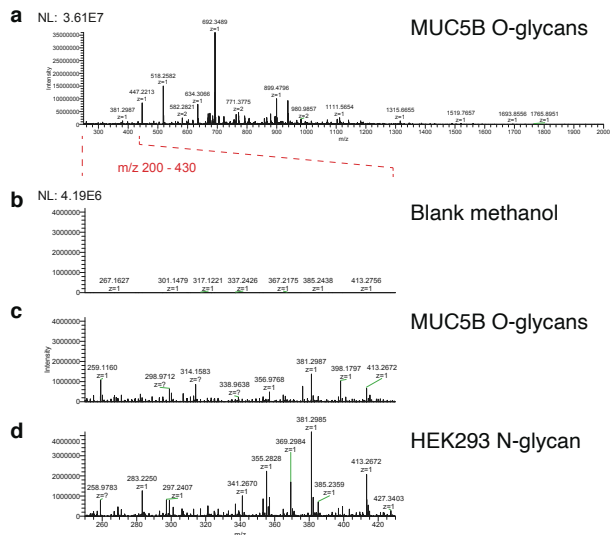
b) qRT-PCR confirms that mucin glycans downregulate the expression of key virulence genes. Exposure to 0.1% MUC5AC glycans decreases the expression of filamentation genes and increases the expression of *YWP1* at 8 h. Data are \log_2 -transformed qPCR measurements of relative gene

expression normalized to a control gene (*ACT1*). Data mean \pm standard error of the mean and were calculated from $n=3$ biologically independent replicates.

c) Phase-contrast images of planktonic cells of biofilms grown in the presence or absence of 0.1% MUC5AC glycans imaged at 24 h. Scale bar, 20 μm .

d) Confocal microscopy of *C. albicans* stained with calcofluor white stain (blue) and *P. aeruginosa-mCherry* (red) cocultured with or without 0.1% MUC5AC glycans at 24 h. Scale bar, 20 μm .

e) Confocal microscopy of $\Delta/\Delta nrg1$ mutant strain cells stained with calcofluor white stain (blue) and *P. aeruginosa-mCherry* (red) cocultured with or without 0.1% MUC5AC glycans at 24 h. Similar results were observed in different fields of view across three independent replicates. Scale bar, 20 μm .






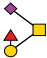
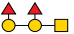



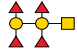




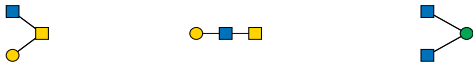

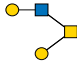


Supplementary Figure 2.5: Analysis of background ions detected in full MS indicates that the mucin glycan pools do not contain detectable peptide contaminants





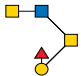

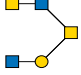
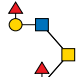
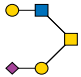
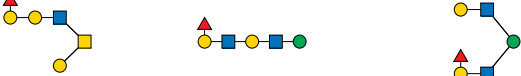
O-glycan pools released (Methods) from mucin glycoproteins (MUC5B is shown as an example) were permethylated and analyzed by NSI-MS following porous graphitized carbon (PGC) clean-up.

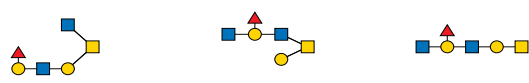


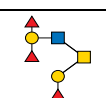




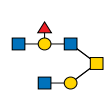
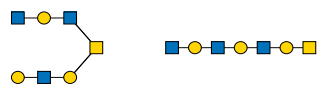
- Full MS profile of a mixture of permethylated MUC5B *O*-glycans. Magnified view of lower mass range ($m/z=200-430$) is highlighted in subsequent panels.
- Ions detected in range $m/z=200-430$ following injection of vehicle (pure methanol) to demonstrate solvent background.
- Ions detected in range $m/z=200-430$ following injection of permethylated MUC5B *O*-glycans (magnification of spectrum in panel a). Note largest peaks in this mass range are less than 5% of the signal intensity of the largest peaks in panel a.
- Ions detected in range $m/z=200-430$ following injection of permethylated N-linked glycans released from a tryptic digest of HEK cell glycoproteins by PNGaseF and subsequent Sep-Pak C18 clean-up, which is unlikely to contain any peptide contamination. The low-abundance contaminant peaks detected in the HEK N-glycan preparation are at m/z values equivalent to those detected in the mucin *O*-glycan preparation and are, therefore, not derived from contaminant peptides or glycopeptides produced by hydrazinolysis. Y-axis is shown as absolute intensity.


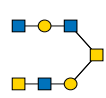

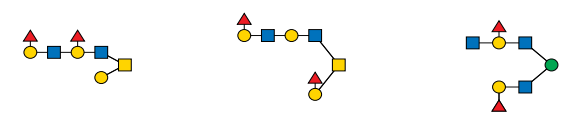
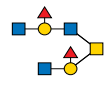

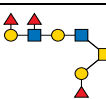

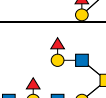
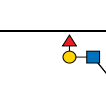
Supplementary Table 2.1: Glycan profiles for MUC2, MUC5B, and MUC5AC

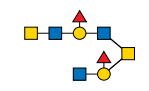
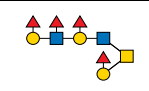
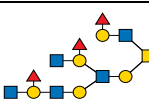
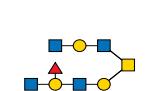
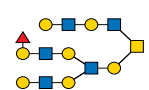
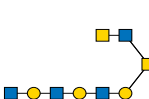
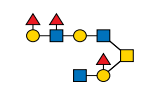
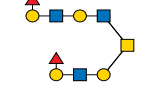
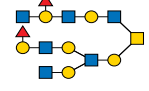
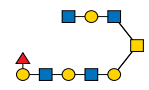
Glycan #	Representative Structure	MUC2	MUC5B	MUC5AC
		% Total Profile	% Total Profile	% Total Profile
1		1.68	0.40	0.46
2	 	10.10	7.90	16.83
3		24.11	21.15	13.40
4		4.65	2.42	1.10
5	 		2.01	1.91
6		3.07		
7		0.34	0.63	0.25
8		0.05	1.51	0.16
9		0.50		

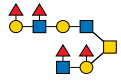


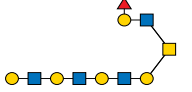
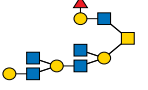
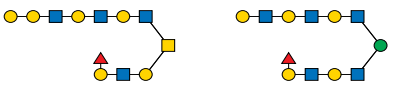
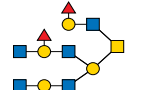
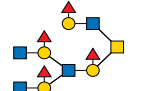
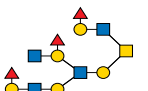

10			0.33	
11			0.48	
12		0.11		
13		0.32	0.73	
14			0.72	
15		2.49	2.35	15.98
16		6.07	6.21	1.86
17		1.13	1.05	3.13
18		0.75	0.40	1.37
19			2.24	

20		0.67	0.67	0.46
21		0.81	2.20	3.83
22		0.42		
23		0.04	0.91	0.29
24		1.31	1.65	0.34
25		0.52	1.03	3.28
26				0.41
27		0.68	2.73	1.46
28		1.23	1.34	0.31
29		0.07	1.82	0.90

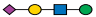



30		0.11	1.88	4.49
31		0.03	0.09	0.60
32		0.09	0.15	4.29
33			0.98	
34			0.12	
35			2.40	2.26
36		0.67	1.88	0.28
37		0.09	1.19	2.24
38		0.11	0.58	1.99
39		0.13	0.03	2.03

40			1.23	
41				0.18
42			0.50	
43			2.89	0.88
44		0.26	1.20	0.22
45		0.28	0.80	1.34
46			1.17	
47			0.63	0.37
48			0.74	0.93
49		0.13	0.32	0.32

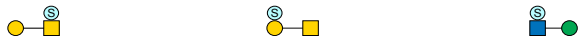

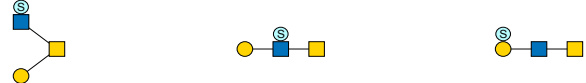



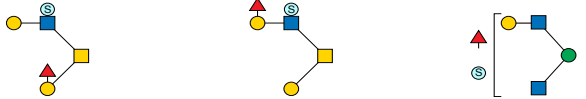

50			0.32	
51			0.47	
52			0.10	0.07
53		0.25	0.07	0.37
54			0.03	0.07
55				0.17
56			1.62	
57			0.62	0.25
58				0.05
59		0.32	0.14	0.15

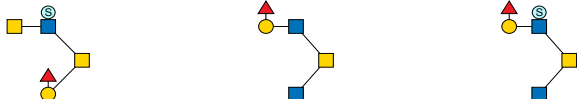

60			0.95	
61			0.46	0.06
62		0.09	0.27	0.17
63		0.09	0.25	0.05
64		0.08		0.09
65				0.05
66		0.05		0.04
67			0.28	
68			0.04	0.03
69			0.12	0.02

70		0.03	0.12	0.02
71				0.12
72				0.10
73			0.59	0.15
74		2.38	0.62	
75		1.03	0.76	
76		0.74		
77		0.10		0.46
78				0.11
79		1.02	1.73	0.88

80		0.16	0.04	0.34
81		10.40	4.23	6.02
82		11.67	4.33	
83		8.59	0.13	
		100.00	100.00	100.00
Note 1: Glycans 81, 82, 83 are the expected products				

Supplementary Table 2.2: Sulfated glycan profiles for MUC2, MUC5B, and MUC5AC preparations

Glycan #	Representative Structure	MUC2		MUC5B		MUC5AC	
		% of Total sulfated glycans	% of Top 5 sulfated glycans	% of Total sulfated glycans	% of Top 5 sulfated glycans	% of Total sulfated glycans	% of Top 5 sulfated glycans
S1				8.36	21.96		
S2				9.67	25.39		
S3		19.68	34.30			6.34	9.97
S4				11.05	29.02	9.55	15.01
S5		13.22	23.05			22.43	35.25
S6		9.37	16.33				
S7				4.51	11.85	17.11	26.88
S8		7.30	12.72				

S9		7.80	13.59				
S10				4.49	11.78	8.20	12.89
			100.00		100.00		100.00
		57.36		38.08		63.64	

Supplementary Table 2.3: Primer sequences

ECE1_F	TGCCATTTGTTGTCAGAGCTG
ECE1_R	TAGCTTGTTGAACAGTTTCCAGG
HWP1_F	GCTGGTTCAGAATCATCCATGC
HWP1_R	AAGGTTCAGTGGCAGGAGCTG
HGC1_F	GTCAGCTTCTGCACCTCATC
HGC1_R	AAACAGCACGAGAACCAGCG
NRG1_F	GGTTGCACGTTGTCGAAACC
NRG1_R	TGTTGCTGCTGCTGCTTGG
ACT1_F	CCCAGGTATTGCTGAACGTA
ACT1_R	GAACCACCAATCCAGACAGA
YWP1_F	TGCTAGTACTGCTAACAAAGTCAC
YWP1_R	CACCATTAACACCACCAGCA
UME6_F	TCATTCAATCCTACTCGTCCACC
UME6_R	CCAGATCCAGTAGCAGTGCTG
RIP1_F	TGCTGACAGAGTCAAGAAACC
RIP1_R	GAACCAACCACCGAAATCAC
EFG1_F	CATCACAACCAGGTTCTACAACCAAT
EFG1_R	CTACTATTAGCAGCACCACCC
18S_F	GGATTTACTGAAGACTAACTACTG
18S_R	GAACAACAACCGATCCCTAGT
ALS3_F	ACTTCCACAGCTGCTTCCACTTCT
ALS3_R	TCCACGGAACCGGTTGTTGCT
HYR1_F	CGGTTCTGGAAGTGGTCATAA
HYR1_R	AGAGTGTGAACCTGCGTTAG
EED1_F	TGCTCTACCACCACAACAAG
EED1_R	TTGCGGTGCTTGCTCATA

Supplementary Data 2.1: Pathway analyses of shared differentially expressed genes across mucin types

Over-representation of biological pathways in cells grown in the presence of mucin was assessed using Fisher's exact test followed by a Benjamini-Hochberg procedure for multiple corrections, for differentially expressed genes from $n=3$ (no mucin treatment), $n=3$ (MUC5AC-treated), $n=3$ (MUC5B-treated), and $n=3$ (MUC2-treated) biologically independent replicates.

Analysis Type:	PANTHER Overrepresentation Test)
Annotation Version and Release Date:	GO Ontology database
Analyzed List:	Client Text Box Input (Candida albicans)
Reference List:	Candida albicans (all genes in database)
Test Type:	FISHER
Correction:	FDR
GO biological process complete	FDR value
biological_process (GO:0008150)	1.67E-09
Unclassified (UNCLASSIFIED)	3.35E-09
growth (GO:0040007)	2.58E-03
filamentous growth (GO:0030447)	3.05E-03
cellular process (GO:0009987)	4.23E-03
aggregation of unicellular organisms (GO:0098630)	6.87E-03
cell aggregation (GO:0098743)	7.63E-03
intraspecies interaction between organisms (GO:0051703)	7.82E-03
interspecies interaction between organisms (GO:0044419)	8.05E-03
biofilm formation (GO:0042710)	8.58E-03
pathogenesis (GO:0009405)	9.40E-03
developmental process (GO:0032502)	9.66E-03
biological adhesion (GO:0022610)	9.87E-03
fungal-type cell wall organization or biogenesis (GO:0071852)	1.62E-02
biological regulation (GO:0065007)	1.72E-02
cell wall organization or biogenesis (GO:0071554)	1.94E-02
single-species biofilm formation (GO:0044010)	3.59E-02
amino sugar biosynthetic process (GO:0046349)	3.83E-02

Supplementary Data 2.2: Functional enrichment analyses identify key virulence pathways among downregulated genes in MUC5AC glycans

Significance of enrichment was calculated from a two-sided Mann-Whitney *U* test followed by a Benjamini-Hochberg procedure for multiple corrections, for mean log₂-transformed FCs from *n*=3 biologically independent replicates.

Analysis Type: PANTHER Enrichment Test (release 20200728)
 GO Ontology database DOI: 10.5281/zenodo.4033054 Released 2020-09-10
 Annotation Version and Release Date:
 Analyzed List: 8h-panther.txt (Candida albicans)
 Correction: FDR

GO biological process complete	number	overUnder	pvalue	fdr
filamentous growth (GO:0030447)	535	-	1.37E-14	4.12E-12
signal transduction (GO:0007165)	208	-	3.55E-13	9.66E-11
cell communication (GO:0007154)	423	-	9.03E-13	2.13E-10
intracellular signal transduction (GO:0035556)	149	-	2.93E-12	5.89E-10
hyphal growth (GO:0030448)	89	-	5.05E-10	6.87E-08
cellular ion homeostasis (GO:0006873)	121	-	1.04E-09	1.32E-07
cellular metal ion homeostasis (GO:0006875)	94	-	1.71E-09	1.93E-07
pathogenesis (GO:0009405)	251	-	2.11E-09	2.20E-07
single-species biofilm formation on inanimate substrate (GO:0044011)	106	-	2.11E-06	8.77E-05
intraspecies interaction between organisms (GO:0051703)	129	-	2.24E-06	9.21E-05
response to starvation (GO:0042594)	236	-	2.72E-06	1.04E-04
aggregation of unicellular organisms (GO:0098630)	134	-	1.01E-05	3.12E-04
rRNA processing (GO:0006364)	128	+	0.00E+00	0.00E+00
ncRNA metabolic process (GO:0034660)	203	+	0.00E+00	0.00E+00
cellular nitrogen compound biosynthetic process (GO:0044271)	507	+	0.00E+00	0.00E+00
nitrogen utilization (GO:0019740)	15	+	3.28E-06	1.23E-04
biosynthetic process (GO:0009058)	908	+	8.88E-12	1.66E-09

Supplementary Data 2.3: Complete fold changes (FCs) and false discovery rates (FDRs) for RNA-sequencing experiments in MUC5AC glycans at 2 h in WT

FCs are relative to *C. albicans* grown in medium alone. Experiments were performed in RPMI medium supplemented in the presence or absence of 0.1% MUC5AC ($n=2$) at 2 h with the SC5314 strain grown under shaking conditions. *P* values were adjusted for multiple comparisons using Benjamini–Hochberg correction to obtain FDR-adjusted *P* values.

Gene Name	log2FC	p-value	adj p-value
POL93	-4.0696629	2.21E-47	7.75E-44
C1_00270W_A	-3.8652886	1.35E-45	2.37E-42
FRE7	-3.9775907	5.84E-41	6.82E-38
CTR1	-3.485706	1.38E-36	1.21E-33
FRE30	-3.5024474	2.01E-31	1.41E-28
PRA1	-3.4512862	6.59E-26	3.85E-23
CFL2	-2.562312	1.77E-18	8.85E-16
ZRT2	-2.1635578	1.18E-15	5.16E-13
ZRT1	-2.4612652	1.73E-13	6.72E-11
OPT4	-2.0646418	9.91E-12	3.47E-09
C5_04980W_A	1.86087807	2.22E-11	7.06E-09
SOD1	1.73282982	1.17E-10	3.41E-08
C3_03370C_A	-1.7860535	5.48E-10	1.48E-07
LAP3	-1.6321758	7.28E-10	1.82E-07
WOR3	-1.4436968	7.24E-09	1.69E-06
CSH1	-1.379441	1.18E-08	2.59E-06
MAC1	-1.4068485	2.83E-08	5.83E-06
C1_06340W_A	-1.6340338	1.92E-07	3.73E-05
FTR1	-1.3652296	4.01E-07	7.38E-05
YWP1	1.17727959	1.68E-06	0.00029459
RPS21	1.01977507	8.76E-06	0.00146017
HGC1	-1.3990302	1.04E-05	0.00166318
RPL18	1.01925642	1.15E-05	0.00175704
AMS1	-0.9952898	1.31E-05	0.00191812
FDH1	-1.1716575	1.77E-05	0.00247509
RPS10	0.98639207	2.32E-05	0.00289811
RPL32	0.98580864	2.28E-05	0.00289811
RPS9B	0.97273997	2.28E-05	0.00289811
RME1	1.30411272	2.67E-05	0.0032293

FRE10	-1.1646741	2.77E-05	0.0032293
SHM1	-1.11157	3.97E-05	0.00448063
RPL3	0.96290071	4.25E-05	0.0046557
PGA54	-0.9558758	5.23E-05	0.00554692
DDR48	-1.0785533	6.29E-05	0.00647929
RFG1	-0.9676007	7.44E-05	0.00744348
C4_04390W_A	0.96568553	7.80E-05	0.00759124
LYS1	-0.9593232	8.89E-05	0.00832305
MNN24	-1.0686042	9.03E-05	0.00832305
RPS15	0.934956	9.62E-05	0.00864104
RPL15A	0.89359912	0.000106	0.00908682
FET31	-1.2483654	0.000106	0.00908682
RPS22A	0.90999255	0.000122	0.01014151
C2_05710C_A	0.9367161	0.000149	0.01061864
RPL43A	0.89973937	0.000136	0.01061864
RPL12	0.88925386	0.000135	0.01061864
RPL9B	0.88663278	0.000146	0.01061864
RPL10A	0.8713336	0.000147	0.01061864
HMX1	-0.9850415	0.000139	0.01061864
IHD1	-1.0645951	0.000146	0.01061864
RPS12	0.90020399	0.00018	0.01235576
RPL4B	0.88855008	0.000183	0.01235576
MED16	-1.0402734	0.000181	0.01235576
RPS20	0.9134069	0.000226	0.01342403
RPP2A	0.91284173	0.000212	0.01342403
RPS7A	0.88518952	0.000211	0.01342403
RPL21A	0.84345119	0.000217	0.01342403
AHR1	-0.9855144	0.000225	0.01342403
PLB1	-1.1520654	0.000219	0.01342403
RPL17B	0.90089859	0.000245	0.01382849
RPL2	0.83780244	0.000241	0.01382849
RPL28	0.83555485	0.00024	0.01382849
UBI3	0.85043246	0.000255	0.01415419
RPL20B	0.84701684	0.00028	0.01530358
RPL24A	0.84937288	0.000303	0.01630011
RPS14B	0.87563246	0.000334	0.0171965
RPL30	0.85845727	0.000344	0.0171965
RPL27A	0.83222929	0.000331	0.0171965
RPL25	0.83201958	0.000341	0.0171965
RPL13	0.82393935	0.000325	0.0171965
RPS16A	0.87531001	0.00037	0.01759552
RPL8B	0.86460086	0.000377	0.01759552

RPL35	0.84730786	0.00037	0.01759552
RPL37B	0.84115151	0.000367	0.01759552
ALS3	-1.1661648	0.000375	0.01759552
RPS24	0.82736986	0.00039	0.01776014
C7_00850W_A	0.81907858	0.000391	0.01776014
EFG1	-0.8702502	0.000414	0.01857075
C2_05410W_A	0.8378538	0.000433	0.01919919
RPS19A	0.83191492	0.000469	0.02052837
TMA19	0.80921287	0.000533	0.02302309
HWP1	-1.0110607	0.000586	0.02484012
SFL2	-1.064273	0.000591	0.02484012
ASM3	-1.1130043	0.000596	0.02484012
RPL6	0.82461549	0.000642	0.02524812
RPS5	0.80494314	0.000628	0.02524812
RPL10	0.77722087	0.000642	0.02524812
LYS2	-0.7764211	0.000626	0.02524812
LYS22	-0.8701096	0.000625	0.02524812
RPL16A	0.78196215	0.000661	0.02570324
RPL11	0.8306352	0.000681	0.02622522
RPS27	0.84996342	0.00072	0.02681324
C1_06890C_A	0.82495013	0.000706	0.02681324
RPS25B	0.78671641	0.000717	0.02681324
C1_05720W_A	0.78437576	0.000768	0.02823057
RPS6A	0.7726178	0.000782	0.02823057
RIB3	-0.9498007	0.00078	0.02823057
YVC1	-0.8311406	0.000796	0.02843006
RPL29	0.82828117	0.000912	0.0319393
DUR1,2	-1.0696534	0.000908	0.0319393
PGA6	0.97363978	0.000956	0.03314118
FET34	-0.7653322	0.000999	0.03431029
C1_02330C_A	0.79680992	0.001051	0.0357454
RPS1	0.73701597	0.001091	0.03672945
CR_09530C_A	-1.0116091	0.001226	0.04089513
YST1	0.77589833	0.001271	0.0419816
RPS26A	0.76821516	0.00131	0.0428766
KCH1	0.76200352	0.001329	0.04308884
RPS17B	0.77401694	0.001452	0.04664046
RPL23A	0.87053751	0.000206	0.01342403

Supplementary Data 2.4: Complete fold changes (FCs) and false discovery rates (FDRs) for RNA-sequencing experiments in MUC5AC glycans at 2 h in $\Delta/\Delta nrg1$

FCs are relative to *C. albicans* grown in medium alone. Experiments were performed in RPMI medium supplemented in the presence or absence of 0.1% MUC5AC ($n=2$) at 2 h with the SC5314 strain grown under shaking conditions. *P* values were adjusted for multiple comparisons using Benjamini–Hochberg correction to obtain FDR-adjusted *P* values.

Gene Name	log ₂ FC	p-value	adj p-value
CTR1	-3.863497	1.64E-112	9.90E-109
FRE7	-3.246178	4.51E-66	1.36E-62
FRE30	-2.374854	1.14E-33	2.29E-30
POL93	-1.758926	8.55E-23	1.29E-19
C1_00270W_A	-1.510451	4.29E-16	5.17E-13
RTA4	-1.437765	3.66E-13	3.67E-10
CFL2	-1.294671	6.12E-11	5.27E-08
FDH1	-1.23537	8.05E-10	6.07E-07
CRP1	1.015274	4.63E-09	3.10E-06
CSH1	-0.994026	9.14E-09	5.51E-06
LAP3	-0.888649	5.02E-06	0.002749
AMS1	-0.77494	5.56E-06	0.002789
ASM3	-0.868896	6.85E-06	0.003173
AOX2	-0.806712	7.55E-06	0.003251
C4_06910W_A	0.688879	2.85E-05	0.011449
BLP1	-0.805053	3.52E-05	0.012812
SAP5	0.830269	3.61E-05	0.012812
RIB3	-0.730184	5.26E-05	0.017592
ZRT2	-0.707804	9.33E-05	0.029589
C3_03410C_A	-0.610602	1.22E-04	0.036694
CR_09140C_A	-0.731137	1.29E-04	0.037002
ICL1	-0.699044	1.42E-04	0.03898